

Ministero dell'Istruzione, dell'Università e della Ricerca
PROGRAMMI DI RICERCA SCIENTIFICA DI RILEVANTE INTERESSE NAZIONALE
(PRIN)
Anno 2010-2011 - Progetto GRETA, prot. 2010WHY5PR

ETICHETTE E SENSORI ECO-COMPATIBILI LOCALIZZABILI ED
IDENTIFICABILI CON TECNICHE WIRELESS A BANDA ULTRA LARGA

**GREEN TAGS AND SENSORS WITH UTRAWIDEBAND IDENTIFICATION
AND LOCALIZATION CAPABILITIES (GRETA)**



GRETA

Deliverable Number: D1

Reference Scenarios and Applications Requirements Definition

Date of Delivery: August 2013 (T0+6)

Editor(s): Prof. Luca Roselli

Participating institutions: UNIAQ, UNIBO, UNIFE, UNIPG, UNIPV

Contributors: UNIAQ, UNIBO, UNIFE, UNIPG, UNIPV

Workpackage number: WP1

Nature: R

Dissemination Level: Public

Version: final

Abstract:

The present deliverable describes the project goals, the technologies proposed to aim them and a study of the possible application contexts.

The evolution of the contemporary society and the developments of information technologies are pushing towards the introduction of systems more and more distributed in the environment. In this context we find the paradigms of the Internet of Things, the Ubiquitous Electronics, and the Autonomous Logistics, which are gaining an increasing popularity. The impact of systems composed of a plurality of low-cost nodes (tags) that are spatially distributed, identifiable, localizable, and capable to sense physical parameters, is potentially enormous in fields such as logistics (tracking of goods in the supply and distribution chains), security (localization and tracking of authorized people or goods in some areas), energy (monitoring of environmental parameters and consumptions), and health-care (monitoring of patients, medical or paramedical personnel, medicines, and health-care equipments).

Nowadays, the identification, localization, and sensing functionalities are offered separately by different wireless technologies such as Radio-Frequency IDentification (RFID), Wireless Sensor Networks (WSN), and Real-Time Locating Systems (RTLS).

It is commonly accepted that the integration of the aforementioned functionalities in a unique low-cost device would extend tremendously the range of applications: however, this is not possible with the existing technologies, considerably different from each other. Hence, such an integration requires to identify new technological solutions and an ex-novo system design. Moreover, it is clear that the employed electronic circuits will have to possess a feature so far considered only marginally and usually ex-post, but key in the future: full compatibility with the environment.

Starting from these considerations, the GRETA project (GREen TAgS and sensors with ultra-wide-band identification and localization capabilities) will focus on innovative solutions and disruptive technologies aimed at the realization of a distributed system for identification, localization, tracking and monitoring in indoor scenarios, based on environmentally friendly materials, where the tags must be:

- i. localizable with sub-meter precision even in indoor scenarios and in the presence of obstacles;
- ii. small-sized (flat, with an area in the order of a few square centimeters) and working without cumbersome batteries;
- iii. made with recyclable materials, to be integrated in goods, clothes and packings.

Keyword list: (Please fill in)

CONTENTS

List of acronyms	4
1 Introduction	16
1.1 Notation	16
1.2 Organization of the document	16
2 Reference scenarios	18
2.1 Typical application cases	18
2.2 Variables to be sensed and measurement techniques	19
2.3 UWB backscattering communication techniques	21
2.3.1 Introduction	21
2.3.2 The UWB technology	22
2.3.3 UWB RFID and localization with active tags	27
2.3.4 UWB RFID and localization with (semi-)passive tags	30
2.3.5 Hybrid tags based on UHF and UWB modulations	31
2.3.6 Chipless tags	31
2.3.7 Semi-passive tags based on backscatter modulation	34
2.4 Localization techniques	38
2.5 Multi-reader and multi-tag scenarios	39
3 Architecture and technologies	42
3.1 System tag architecture	42
3.2 Energy harvesting architecture	43
3.3 Sensor architecture	45
3.4 Low power microcontroller	46
3.5 UWB backscatter modulator	47
3.6 Data synchronization architectures	49
3.7 System integration	49
3.8 Antenna system	52
3.8.1 UWB antenna	52
3.8.2 Harvester antenna	54
3.9 Localization and tracking algorithm	57
3.9.1 Localization via parameter estimators	58
3.9.2 Tracking via bayesian filters	60
3.10 Network management protocols	61
3.10.1 Tag-reader	62
3.10.2 Reader-to-reader	62
4 Preliminary link and power budget	63
4.1 Link budget	63
4.2 Power budget	71
4.2.1 RF-to-DC power budget	71
5 Demonstrator definition	76
6 Dissemination plan	78
6.1 University of Bologna	78
6.2 University of Ferrara	78
6.3 University of L'Aquila	78
6.4 University of Pavia	78

6.5 University of Perugia	79
References	79

LIST OF ACRONYMS

ACK	acknowledge
ADC	analog-to-digital converter
AFL	anchor-free localization
AGNSS	assisted-GNSS
AGPS	assisted GPS
AltBOC	alternate binary offset carrier
AOA	angle-of-arrival
AOD	angle of departure
AP	access point
API	application programming interface
ARNS	aeronautical radio navigation services
A-S	anti-spoofing
AS	azimuth spread
ASIC	application specific integrated circuit
AWGN	additive white Gaussian noise
BCH	Bose-Chaudhuri-Hocquenghem
BEP	bit error probability
BLAS	basic linear algebra subprograms
BOC	binary offset carrier
bps	bits per second
BPSK	binary phase shift keying
BPZF	band-pass zonal filter
BS	base station
BSC	binary symmetric channel
C/A	coarse/acquisition
C/NAV	commercial/navigation
CAD	Computer Aided Design
CAP	contention access period
CAWGN	complex additive white Gaussian noise
CBOC	composite binary offset carrier

CC	central cluster
cdf	cumulative distribution function
CDF	cumulative density function
CDMA	code division multiple access
CF	characteristic function
CFP	contention free period
CH	cluster head
CIR	channel impulse response
CKF	cubature Kalman filter
CL	civil-long
CM	civil-moderate
CMOS	Complementary Metal Oxide Semiconductor
Coop-POCS	cooperative projection onto convex sets (POCS)
Coop-OA	cooperative outer-approximation (OA)
COTS	commercial off-the-shelf
CNLS	constrained non-linear least squares (NLS)
CNSS	Compass navigation satellite system
CPR	channel pulse response
cps	chips per second
CRB	Cramér-Rao bound
CRLB	Cramér-Rao lower bound
CRC	cyclic redundancy check
CRPF	cost reference particle filter
CS	control segment/commercial service
CSI	channel state information
CSS	chirp spread spectrum
CTS	clear-to-send
CW	continuos wave
DAA	Detect and Avoid
DC	Direct Current
DGPS	differential GPS

DIFS	DCF inter-frame spacing
DM	data mining
DMLL	distributed maximum log-likelihood
DLL	delay-locked loop
DoA	Direction of Arrival
DoD	Department of Defense
DP	direct path
DPE	direct position estimation
DS	delay spread
DSSS	direct sequence spread spectrum
dwMDS	distributed weighted multidimensional scaling
EB	energy-based
EBG	Electromagnetic Band Gap
ECEF	Earth-centered, Earth-fixed
ED	energy detector
EGNOS	European geostationary navigation overlay system
EIRP	effective isotropic radiated power
EKF	extended Kalman filter
EKFBT	extended Kalman filter with bias tracking
e.m.	electro-magnetic
EPE	Ekahau positioning engine
ERP	Effective Radiated Power
ERQ	enhanced robust quad
ESA	European Space Agency
EU	European Union
F/NAV	freely accessible navigation
FCC	federal communications commission
FDMA	frequency division multiple access
FEC	forward error correction
FFD	full function device
FIM	Fisher information matrix

FLL	Frequency-locked loop
FOC	full operational capability
FOM	figure of merit
FPGA	field programmable gate array
FPK	Flächen-Korrektur-Parameter (area correction parameters)
GAGAN	GPS aided GEO augmented navigation
GANSS	Galileo/Additional navigation satellite systems
GDOP	geometric dilution of precision
GEO	geostationary
GIOVE	Galileo In-Orbit Validation Element
GIS	geographical information system
GLONASS	global orbiting navigation satellite system
GML	generalized maximum likelihood
GNSS	global navigation satellite system
GPRS	general packet radio service
GPS	global positioning system
GS	geodetic system
GSM	Global System for Mobile communications
HB	Harmonic Balance
hdwMDS	hybrid dwMDS
HEO	highly-inclined elliptical orbits
HMM	hidden Markov model
HOW	handover word
HPOCS	hybrid POCS
HW	hardware
i.i.d.	independent,identically distributed
I/NAV	integrity/navigation
ICD	interface control document
ICT	information and communication technologies
ID	IDentification
IE	informative element

IF	intermediated frequency
IGSO	inclined geosynchronous orbit
ILS	instrument landing system
IMU	inertial measurement unit
INS	inertial navigation system
IRNSS	regional navigation satellite system
IR-UWB	impulse radio UWB
ISM	industrial scientific medical
ISRO	Indian space research organization
IST	information society technologies
IVP	inertial virtual platform
JBSF	jump back and search forward
KDD	Knowledge Discovery
KF	Kalman filter
KNN	k-nearest-neighbor
LAAS	local area augmentation system
LAN	local area network
LAPACK	linear algebra package
LBS	location-based services
LCS	location services
LDC	low duty-cycle
LDPC	low density parity check
LDR	low data rate
LEO	Localization Error Outage
LLC	logical link control
LLR	log-likelihood ratio
LLS	linear least squares
LOB	line-of-bearing
LOS	line-of-sight
LR	likelihood ratio
LRT	likelihood ratio test

LS	least-squares
LSE	least squares estimator
MAC	medium access control
MAP	maximum a posteriori
MBOC	multiplexed binary offset carrier
MB-UWB	multi-band UWB
MCRB	modified Cramér–Rao bound
MDS	multi-dimensional scaling
MEMS	micro-electro-mechanical systems
MESS	maximum energy sum selection
MEO	medium earth orbit
MF	matched filter
MGF	moment generating function
MHT	multiple hypotheses testing
MIMO	multiple-input multiple-output
MISO	multiple-input single-output
ML	maximum likelihood
MLE	maximum likelihood estimator
MMSE	minimum mean squared error
MQKF	multiple quadrature Kalman filtering
MRC	maximal ratio combining
MS	mobile station
MSAS	multi-functional satellite augmentation system
MSB	most significant bit
MSE	mean squared error
MSK	Minimum-shift Keying
MST	minimum spanning tree
MTSAT	multi-functional transport satellite
MUI	multi-user interference
N/A	not available
NAV	navigation

NAVSTAR	navigation system for timing and ranging
NB	narrowband
NBI	narrowband interference
NDIS	network driver interface specification
NG	network green
NLOS	non-line-of-sight
NLS	non-linear least squares
NN	neural network
NPE	Navizon positioning engine
NQRT	new quad robustness test
NRZ	non-return to zero
NSI5	non-standard I5
NSQ5	non-standard Q5
NTP	network time protocol
OA	outer-approximation
OCS	operational control segment
OFDM	orthogonal frequency division multiplexing
OMA	open mobile alliance
OOK	on-off keying
O-QPSK	offset quadrature shift keying
OQRT	original quad robustness test
ORQ	original robust quad
OS	open service
OTDOA	observed TDOA
P2P	peer-to-peer
P2PP	P2P-positioning
PAM	pulse amplitude modulation
PAN	personal area network
PDA	personal digital assistant
pdf	probability density function
PDP	power delay profile

PF	particle filter
PHY	physical layer
PLL	phase-locked loop
PMU	Power Management Unit
PN	pseudo-noise
POC	payload operation center
POCS	projection onto convex sets
PN	pseudo-noise
PPM	pulse position modulation
PPS	precise position service
PR	Pseudo-random
PRN	pseudo-random noise
PRS	public regulated service
PRT	partial robustness test
PSD	power spectral density
PSDP	power spatial delay profile
PSK	phase shift keying
pTOA	pseudo time of arrival
PV	position-velocity
PVT	position, velocity, and time
QKF	quadrature Kalman filter
QZSS	quasi-zenith satellite system
RDSS	radio determination satellite service
RF	radio frequency
RFD	reduced function device
RFID	Radio frequency identification
R-GML	reduced complexity generalized maximum likelihood
RIMS	ranging and integrity monitoring stations
RLE	robust location estimation
RMS	root-mean square
RMSE	root mean square error

RMU	remote measurement unit
RNSS	regional navigation satellite system
RQ	robust quadrilateral
RRC	root raised cosine/radio resource control
RRLP	radius resource location protocol
RSMB	root square of mean biased value
RSS	received signal strength
RT	robust trilateration
RTCM	radio technical commission for maritime services
RTLS	real-time locating systems
RTK	real-time kinematic
RTS	ready-to-send
RTT	round-trip time
r.v.	random variable
RV	random variable
SA	selective availability
SAR	search and rescue
SAW	surface acoustic wave
SBAS	satellite-based augmentation system
SBS	serial backward search
SBSMC	serial backward search for multiple clusters
SCKF	square-root cubature Kalman filter
SDR	software defined radio
SDS	symmetric double sided
SET	SUPL enabled terminal
S-GML	soft generalized maximum likelihood
SIR	sequential importance resampling
SLP	SUPL location platform
SIFS	short inter frame spacing
SIMO	single-input multiple-output
SIS	signal-in-space

SISO	single-input single-output
SMD	Surface Mounting Device
SoA	state-of-the-art
SoL	safety-of-life
SMC	sequential Monte Carlo
SNR	signal-to-noise ratio
SNIR	signal-to-noise-plus-interference ratio
SPAWN	sum and product algorithm over a wireless network
SPKF	sigma-point Kalman filter
sps	symbols per second
SPS	standard position service
SQKF	square-root quadrature Kalman filter
SRN	secondary reference nodes
SS	spread spectrum/space segment
ST	simple thresholding
SUPL	secure user-plane location
SV	satellite vehicle
SW	software
TDOA	time difference-of-arrival
TDR	Time-domain reflectometry
TI	trilateration intersection
TFTC	Thin Film Transistor Circuit
TLM	telemetry
TMBOC	time-multiplexed binary offset carrier
TOA	time-of-arrival
TOF	time-of-flight
TOW	time of week
TH	time-hopping
TNR	normalized threshold
TTFF	time-to-first-fix
TW-TOA	two-way-TOA

U.S.	United States
UE	user equipment
UERE	user equivalent range error
UHF	ultra high frequency
UKF	unscented Kalman filter
ULP	user location protocol
UMTS	universal mobile telecommunications system
URE	user range error
US	user segment
UT	user terminal
UTC	coordinated universal time
UTM	universal transverse Mercator
UTRA	UMTS terrestrial radio access
UWB	ultra-wide band
UWB-IR	ultra-wide band impulse radio
VANET	vehicular ad-hoc network
VRS	virtual reference station
WAAS	wide area augmentation system
WADGPS	wide area differential GPS
WARN	wide area reference network
WB	wideband
WE	wireless extensions
WGS84	world geodetic system
WiMAX	worldwide interoperability for microwave access
WLAN	wireless local area network
WLS	weighted least squares
WMAN	wireless metropolitan area network
WPAN	wireless personal area network
WR API	wireless research application programming interface
WSN	wireless sensor network
WT	wireless tools

WWB Weiss-Weinstein bound

ZZB Ziv-Zakai lower bound

ZZBT Ziv-Zakai Bellini-Tartara

1 INTRODUCTION

1.1 Notation

Hereafter the main mathematical notation rules used throughout the text are listed for the reader convenience. Meanings and formats will be maintained along the text, unless otherwise stated.

x, y, z, \dots	scalar variables, either deterministic or stochastic (depending on the context), either real or complex (depending on the context).
$\mathbf{a}, \mathbf{b}, \mathbf{c}, \dots$	vector variables, column-wise defined, either deterministic or stochastic, either real or complex.
$\mathbf{A}, \mathbf{B}, \mathbf{C}, \dots$	matrix variables, either deterministic or stochastic, either real or complex.
\mathbb{R}^M	Field of the real numbers, M -dimensional.
\mathbb{C}^M	Field of the complex numbers, M -dimensional.
$\mathbf{a} \in \mathbb{R}^M$	M -element real vector.
$\mathbf{b} \in \mathbb{C}^N$	N -element complex vector.
$\mathbf{A} \in \mathbb{R}^{M,N}$	Real matrix, with M rows and N columns.
$\Re\{\cdot\}$	Real part.
$\Im\{\cdot\}$	Imaginary part.
$(\cdot)^T$	Transpose operator.
$(\cdot)^*$	Complex conjugate operator.
$(\cdot)^H$	Hermitian operator (transpose, complex conjugate).
$(\cdot)^\dagger$	Moore-Penrose pseudo-inverse.
$\mathbf{A} \succeq \mathbf{B}$	The matrix $(\mathbf{A} - \mathbf{B})$ is nonnegative definite.
$\mathbf{A} \succ \mathbf{B}$	The matrix $(\mathbf{A} - \mathbf{B})$ is positive definite.
$\mathbb{E}\{\cdot\}$	Expected value (stochastic) operator.
\triangleq	Equal by definition.
$\nabla_{\mathbf{x}}(\mathbf{d}(\mathbf{x}))$	Jacobian matrix (partial derivatives of $\mathbf{d}(\mathbf{x})$ w.r.t. \mathbf{x}).
$g(t)$	Function of a continuous variable. E.g., signal or process as a function of the continuous time.
$g[n]$	Function of a discrete variable. E.g., signal or process in the discrete time domain.
f_c	Carrier or central frequency.
B_W	Bandwidth
f_s	Sampling frequency.
T_c	Chip interval.
T_s	Symbol/Pulse interval.
c	Speed of light.
τ_{mean}	Mean excess delay.
σ_τ	Delay spread (RMS).
$P(\cdot)$	Power or Probability (depending on the context).
$p(\cdot)$	Probability density function.
d	Distance (in meters).
(x, y, z)	Cartesian coordinates of a point.

1.2 Organization of the document

This report is organized as follows.

Section 2 describes the reference scenario starting from the application cases and presenting several key technologies. The purpose of the *Section 3* is the identification of the application requirements,

including the viable technologies. *Section 4* provides a preliminary link budget under simplified assumptions. In *Section 5* a preliminary description of the specific case of study and of the demonstrator is provided. Finally, *Section 6* the dissemination plan of each unitity is reported.

2 REFERENCE SCENARIOS

In this section the reference scenario will be defined starting from the application cases and presenting several key technologies.

2.1 Typical application cases

The proposed technology, with its characteristic of eco-compatibility, energy autonomy, and sensing abilities, can be used to implement smart tags in various areas of application:

- **eHealth:** energetically autonomous and not invasive sensors for biomedical (e.g. smart plasters) or drugs monitoring, and in general for efficient hospital management.
- **ICT for food:** on-paper tags with embedded sensors for continuous monitoring of the product along the production and commercial distribution chain (e.g., cold chain).
- **Factories of the future:** goods tracking and monitoring along the industrial process for an advanced logistic management (supply chain management, SCM).

The specific cases of study of this project, chosen within the previously described scenarios, are the *smart band-aid* and the *food monitoring*.

The *smart band-aid* is a band aid with an integrated temperature sensor (thermometer), in continuous contact with the skin of the patient. In such a way, when interrogated the sensor is already at the equilibrium temperature, so the measurement time is only due to the wireless data communication (few ms), and the current drawbacks of mercury or infrared thermometers, such as systematic errors, long measurements duration, use of highly polluting substances, and difficulties in applying to kids patients can be eliminated.

The *blood bags tracker* instead is a device able to track and monitor blood product fluid bags of human nature from production phase (blood donor) to consumer phase (transfusion in a patient). The aim of such a system is to reduce the risk in the clinical transfusion field. Moreover, a temperature sensor is also integrated in order to monitor the temperature of the blood, that is the main parameter to guarantee the good quality of the blood products.

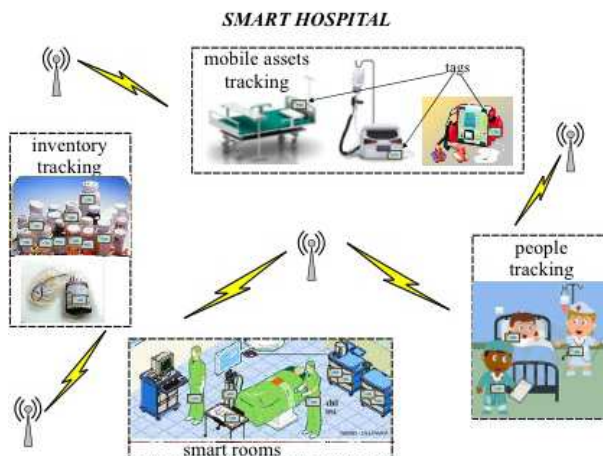


Figure 1: eHealth example application.

In fig. 1 an example of the applications in the area of the eHealth is reported: different objects, such as *smart band-aid* and *blood bags tracker*, are wirelessly communicating information to each other and to the hospital staff in order to guarantee a better service quality.

In the area of the ICT for food the tag might be applied as a label on food (for example fruits and vegetables) in order to continuously collect information about some parameters (for instance temperature, humidity, air composition, ...). In this way the freshness and composition status of the foods can be

monitored constantly reading the tags and therefore the risk of marketing deteriorated food is reduced. Figure 2 illustrates the application in the case of the food quality monitoring.

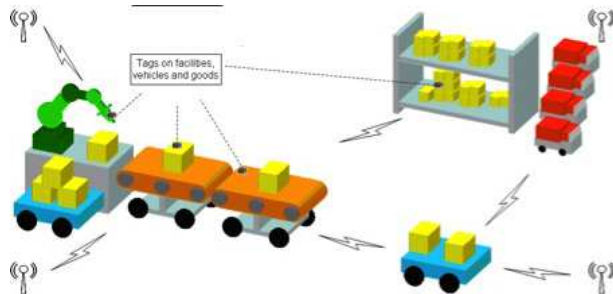


Figure 2: Food quality monitoring example application.

2.2 Variables to be sensed and measurement techniques

In the context of this proposal, we have to cope with the basic sensing constraints related to the precision and bandwidth trade off that is the energy budget of sensing. In general, in the field of Radio frequency identification (RFID) devices, the sensing inputs or measurands are restricted to slow varying quantities for two reasons. First, the ultra-wide band (UWB) communication process used in the project is restricted to about one sample transmission every millisecond, reducing the signal bandwidth to 1Hz (sampling frequency). Second, the applications devised here are related to environmental and biological variables that are characterized by quite slow varying inputs. Thus, in energy of sensing calculation we will assume as typical variables to be sensed: temperature, humidity and chemical quantity that are subject to Fick's diffusing laws. Diffusing mechanisms in the environment and in the human body are typically very slow setting the time-constant of the physical mechanisms to be sensed of the order of seconds, thus defining the maximum signal bandwidth below 1Hz. Another application could be devised for force measurements using strain gauges. Even in this application the expected time constants should not exceed the 1Hz bandwidth.

For our purpose, since the sensing interface should be as low in power consumption as possible, we will restrict the class of possible sensors to mostly capacitive and secondly to resistive sensors. Capacitive sensors are widely used for sensing humidity and chemical substances by various detection techniques and are intrinsically low-power due to the zero static currents. On the other hand, resistive sensors do need current to be sensed but it can be reduced using short duty-cycles readout techniques. Capacitive and resistive sensors could be embedded in the same substrate of the RFID and could be implemented by using organic electronic and materials. On the other end, temperature sensors could be easily implemented in the electronic substrate of the silicon chip using “band-gap” references.

In order to readout different kind of sensors we need two main blocks:

1. a sensor interface
2. an A/D converter to digitalize the signal

To calculate a typical sensing energy/power we will refer first to the state of the art in analog-to-digital converters (ADCs) capabilities. Two main figure of merits (FOMs) are used for evaluating the ADCs. The most used one is the Walden-FOM defined as

$$F_{A1} = \frac{P}{2^{ENOB} F_S} \quad (1)$$

where P is the power consumed, $ENOB$ is the number of equivalent bit of conversion and F_S the sampling frequency. Recently it has been proposed a new one called Thermal-FOM, which is more adherent to the trend in evolution of both architecture and technology, and is defined as

$$F_{B1} = \frac{P}{2^{(2ENOB)} F_S} \quad (2)$$

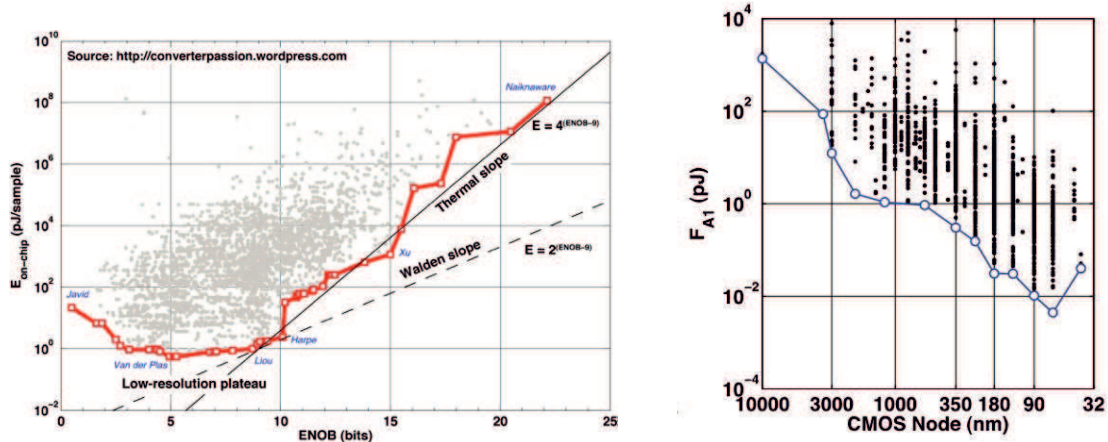


Figure 3: Figures of merit of the ADCs published in the last decades of the Walden FOM [2].

A general classification of ADCs presented in the literature in the last decades is shown in Fig. 3. Both FOMs are given in energy per samples units. The current best example in energy conversion is given by [1] with $F_{A1} = 2.2\text{fJ}/\text{sample}$ with 12b in submicron (65nm) that means 9pJ for conversion sample. Most of the ultra-low-energy ADCs are based on the search and rescue (SAR) architecture.

However, for our project we will refer to a less advanced technology in the 350nm technology node. As shown in Fig. 3, the energy per sample is between 1pJ to 1nJ using F_{A1} . Since our application will refer to 10b conversion depth, the typical energy required for a conversion is given by

$$\text{Minimum energy conversion per sample} = F_{A1} 2^{(ENOB)} \quad (3)$$

meaning that the energy required for converting 10b into a 350nm technology is ranging from 1nJ to $1\mu\text{J}$ so that for 1Hz of sampling frequency it requires a power varying from 1nW to $1\mu\text{W}$.

We must add the energy for the sensor interface to the above energy of conversion. This strongly depends on the kind of sensor. For example in the case of a capacitive sensor of value C_s we have to charge and discharge it at least once per sampling period with a required energy of

$$\text{Minimum energy for sensor interface per sample} = C_s V^2 \quad (4)$$

where V is the voltage swing. Thus, for a capacitive sensor of 1nF and 1V of swing, we have an estimated energy of at least 1nJ. In other words, we have to consider an energy of the sensor interface conversion which is about of the same order of the energy of conversion.

The approach we propose in this project will be based on the use of oscillators as sensing technique. The capacitance or resistance sensor is placed in a multivibrator (or ring oscillator) circuit whose time period is measured by an internal oscillator. This approach has several advantages:

- It merges the sensor interface and the digital conversion into a unique architecture.
- It shows a simple approach that could be easily implemented into organic electronic technology in view of the “green-RFID” specifications.

The last point is particularly important since the implementation of a SAR architecture, even if energetically efficient, could be very complex and expensive in terms of devices.

To estimate the energy consumption we can assume that for 10b we need at least 1024 cycles of frequency difference into a sampling period. Therefore, assuming a $\frac{\Delta C}{C_s}$ almost equal to $\frac{\Delta f_0}{f_0}$ and fixing it to be lower than 30% we estimate a resonance central frequency to about 3kHz. Then, assuming an internal 350nm CMOS technology capacitance node of 100fF, the minimum power consumption of the internal oscillator is:

$$\text{Minimum power for oscillator} = C_i V^2 F \quad (5)$$

where C_i is the internal node capacitance and F is the frequency of the oscillator. For the above values we get a minimum energy of 0.3 nW to be summed to the sensor consumption as seen above. In the case of ring oscillators the power should be multiplied for the number of stages.

Care should be accounted to the energy of the back-scattering switch since it will be implemented in discrete components and is switched thousands of times more than sampling time. Assuming a switch capacitance of about 10pF the energy per switch is given by

$$\text{Minimum energy per back-scattering switch} = C_s V^2 \quad (6)$$

which is in the order of 10pJ. Assuming that for every sample the switch is closed 1024 times for each bit, the number of switches is in the order of one million every sample giving a minimum power of 100 μW at 1Hz sampling.

In conclusion: the power for sensing and digital encoding is by far lower than the energy required for physical driving the back-scattering switch of the antenna which is in the order of hundreds of μW . This is the reason why the reducing of the switch capacitor capacitance is very important and its integration into the same substrate instead of using discrete components could be very important in terms of power consumption.

2.3 UWB backscattering communication techniques

2.3.1 Introduction

RFID technology for use in real-time object identification is facing a rapid adoption in several fields such as logistic, automotive, surveillance, automation systems, etc. [3, 4]. A RFID system consists of readers and tags applied to objects. The reader interrogates the tags via a wireless link to obtain the data stored on them. Tags equipped with a complete radio frequency (RF) transmitter are denoted as *active*. The cheapest RFID tags with the largest commercial potential are *passive* or *semi-passive*, where the energy necessary for tag-reader communication is harvested from the reader's signal or the surrounding environment. In current ultra high frequency (UHF) (semi-)passive RFID technology the reader sends an unmodulated continuos wave (CW) field that the tags modulate and scatter back to the reader. The backscatter modulation is realized by properly changing the tag's antenna load according to the data, so that no active RF transmission happens [5].

It is expected that the global revenues coming from the RFID technology will amount to tens of billion dollars in the near future. This includes many new markets that are being created, such as the market for real-time locating systems (RTLS), which will itself be more than 6 Billion in 2017 [6, 7]. Therefore, future advanced RFID systems are expected to provide both reliable identification and high-definition localization of tags [8]. Accurate real-time localization at sub-meter level, high security, large number of tags management, in addition to extremely low power consumption, small size and low cost, will be new important requirements. Unfortunately, most of these requirements cannot be completely fulfilled by the current first and second generation RFID or wireless sensor network (WSN) technologies such as those based on ZigBee standard [9]. In fact, RFID systems using standard CW-oriented communication in the UHF band have an insufficient range resolution to achieve accurate localization, are affected by multipath signal cancellation (due to the extreme narrow bandwidth signal), are very sensitive to narrow-band interference and multi-user interference, and have an intrinsic low security [3]. Although some of these limitations, such as security and signal cancellation due to multipath, are going to be reduced or overcome in future versions of UHF RFID systems, a technology change is required to fully satisfy new applications requirements, especially those related to high-definition localization at sub-meter level.

A promising wireless technique for future identification and localization systems is the UWB technology characterized, in its impulse radio UWB (IR-UWB) implementation, by the transmission of sub-nanosecond duration pulses. The employment of wideband signals enables the resolution of multipath, and extraordinary localization precision based on time-of-arrival (TOA) estimation signals. In addition, UWB allows for low power consumption at the transmitter side, extremely accurate ranging and positioning capability at sub-meter level, robustness to multipath, low detection probability, efficient multiple

channel access and interference mitigation thus leading to potentially large number of devices operating and co-existing in small areas [10].

Thanks to their low power consumption, IR-UWB transmitters can be successfully adopted both for active and passive tags. UWB has been proposed to realize low consumption and low complexity active RF tags for precision asset location systems. Recently some commercial proprietary RTLSs have been introduced based on tags emitting UWB pulses with extremely low duty cycle to ensure high battery duration, and the IEEE 802.15.4f working group has been formed to define a dedicated standard to cover the RTLS segment.

As anticipated, passive tags solutions are of particular interest thank to their potential lower cost and power consumption. To this purpose, the idea of passive tags based on UWB backscatter signaling was introduced in [8], where tag architectures as well as backscatter signaling schemes robust to the presence of clutter (i.e., reflections coming from surrounding objects) are presented. Nevertheless, UWB RFID analysis based on backscatter modulation is at the beginning and different issues have still to be investigated [11].

2.3.2 The UWB technology

2.3.2.1 UWB, definitions and regulatory issues

The UWB technology has been around since 1960, when it was mainly used for radar and military applications, whereas nowadays it is a very promising technology for advances in wireless communications, networking, radar, imaging, positioning systems, WSNs and RFID as well [9, 12–15].

The most widely accepted definition of a UWB signal is a signal with instantaneous spectral occupancy in excess of 500 MHz or a fractional bandwidth of more than 20% [16]. The fractional bandwidth is defined as B/f_c , where B denotes the -10 dB bandwidth, and f_c is the center frequency. A way to generate such signals is by driving an antenna with very short electrical pulses with duration in the order of one nanosecond or less.

In 2002, the US federal communications commission (FCC) issued the First Report and Order (R&O), which permitted unlicensed UWB operation and commercial deployment of UWB devices. There are three classes of devices defined in the R&O document: (i) imaging systems (e.g., ground penetrating radar systems, wall imaging systems, through-wall imaging systems, surveillance systems, and medical systems), (ii) vehicular radar systems, and (iii) communications and measurement systems. The FCC allocated a block of unlicensed radio spectrum from 3.1 to 10.6 GHz at the maximal effective isotropic radiated power (EIRP) spectral density of -41.3 dBm/MHz for the above applications, where each category was allocated a specific spectral mask as described in [16] and UWB radios overlaying coexistent RF systems can operate. In Fig. 4 an example of FCC spectral mask for indoor commercial systems is reported. With similar regulatory processes, currently under way in many countries worldwide, government agencies responded to this FCC ruling. Regarding Europe, it is important to mention that on February 21, 2007, the Commission of the European Communities released a decision on allowing the use of the radio spectrum for equipments using UWB technology in a harmonized manner in the community [17]. The decision concerns the use of the radio spectrum on a non-interference and non-protected basis by equipments using UWB technology, with the definition of maximum allowed EIRP densities both in the absence and in the presence of appropriate interference mitigation techniques. In Fig. 4 the maximum EIRP density in the absence of appropriate mitigation techniques is reported. In particular, the upper frequency band 6 - 8.5 GHz has been identified in Europe for long-term UWB operation with a maximum mean EIRP spectral density of -41.3 dBm/MHz and a maximum peak EIRP of 0 dBm measured in a 50MHz bandwidth without the requirement for additional mitigation [18]. Within the lower band 3.1 - 4.8 GHz, low duty-cycle (LDC) or interference Detect and Avoid (DAA) UWB devices are permitted to operate with the same limits for the EIRP. In addition, dedicated standards have been amended for specific UWB applications such as RTLS [19,20]. Table 2.3.2.1 reports an overview of the current worldwide UWB emission masks.

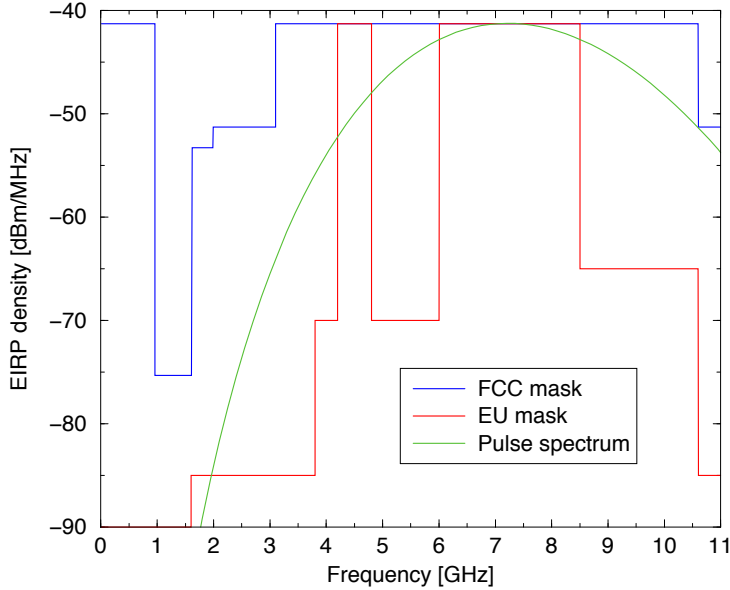


Figure 4: FCC and EU spectral masks, respectively, for indoor commercial systems in the absence of appropriate mitigation techniques. An example of 6th derivative of the Gaussian pulse spectrum with $\tau_p = 0.192\text{ ns}$, compliant with FCC mask, is also reported.

2.3.2.2 Impulse radio UWB

UWB transmission systems can be realized through conventional modulation schemes by stretching the bandwidth to be larger than 500 MHz, for example, by adopting orthogonal frequency division multiplexing (OFDM) signaling. This approach has been followed by the WiMedia alliance standard for multimedia applications requiring high data rate transmissions [21]. One promising UWB technique, especially for RFID and WSN applications, is named IR-UWB. The IR-UWB technique relies on ultra-short (nanosecond scale) pulses that can be free of sine-wave carriers and do not require intermediate frequency processing because they can operate at baseband, thus drastically reducing the hardware complexity and power consumption. The IR-UWB technique has been selected as the physical layer (PHY) layer of the IEEE 802.15.4a Task Group for wireless personal area network (WPAN) Low Rate Alternative PHY layer [13, 22], and for the standard proposal IEEE 802.15.4f related to RTLS [23] as will be detailed in Sec. 2.3.3.3.

As said, in IR-UWB the information is encoded using pulses. Typically the adopted pulse $p(t)$ is derived by the Gaussian pulse $p_0(t) = \exp(-2\pi(t^2/\tau_p^2))$ and its derivatives due to its smallest possible time-bandwidth product which maximizes range-rate resolution and are readily available from antenna pattern. Alternatively, the IEEE 802.15.4a standard suggests the following band-pass pulse with center frequency f_0 and root raised cosine/radio resource control (RRC) envelope [22]

$$p(t) = \frac{4v\sqrt{2}}{\pi\sqrt{\tau_p}} \frac{\cos((1+v)\pi t/\tau_p) + \frac{\sin((1-v)\pi t/\tau_p)}{4vt/\tau_p}}{1 - (4vt/\tau_p)^2} \cos(2\pi f_0 t) \quad (7)$$

where parameter τ_p and roll-off factor v determine the bandwidth $W = (1+v)/\tau_p$.¹

In Fig. 4 the 6th derivative of the Gaussian pulse with $\tau_p = 0.192\text{ ns}$ is shown in the frequency domain. It can be noted that this pulse is compliant with the FCC specifications. In general, due to the short pulse duration (typically less than 1 ns), the bandwidth of the transmitted signal can be on the order of one or more GHz.

¹Two different values of τ_p are recommended [22]: $\tau_p = 1\text{ ns}$ and $\tau_p = 3.2\text{ ns}$ with $v = 0.6$, corresponding to two different bandwidths, $W = 1.6\text{ GHz}$ and $W = 500\text{ MHz}$, respectively.

Table 1: Worldwide UWB emission masks

Band	EIRP	Mitigation technique
China		
4.2 - 4.8 GHz	-41.3 dBm/MHz	DAA
6.3 - 8.9 GHz	-41.3 dBm/MHz	No mitigation
Europe		
3.1- 4.8 GHz	-41.3 dBm/MHz	LDC or DAA
2.7 - 3.4 GHz	-70 dBm/MHz	No mitigation
3.4 - 3.8 GHz	-80 dBm/MHz	No mitigation
3.4 - 6 GHz	-70 dBm/MHz	No mitigation
6 - 8.5 GHz	-41.3 dBm/MHz	No mitigation
8.5 - 9 GHz	-41.3 dBm/MHz	DAA
Japan		
3.4 - 4.8 GHz	-41.3 dBm/MHz	DAA
4.8 - 7.25 GHz	-70 dBm/MHz	No mitigation
7.25 - 10.25 GHz	-41.3 dBm/MHz	No mitigation
Korea		
3.1 - 4.8 GHz	-41.3 dBm/MHz	LDC or DAA
7.25 - 10.25 GHz	-41.3 dBm/MHz	No mitigation
USA		
3.1 - 10.6 GHz	-41.3 dBm/MHz	No mitigation

To allow for multi-user communication in a typical IR-UWB communication system, each symbol (bit) is associated to multiple pulses.

In time-hopping (TH) schemes, symbols of duration T_s are divided in time intervals T_f called frames (see Fig. 5a). The frames are further decomposed into smaller time slots T_{slot} . The UWB pulse $p(t)$, with duration $T_p < T_{\text{slot}}$, is transmitted in each frame in a slot position specified by a user-specific pseudo-random TH code $\{c_k\}$ having period N_s , where N_s is the number of pulses per symbol [12]. In delay spread (DS) schemes (see Fig. 5b), each pulse is modulated according to a pseudo-random binary code $\{c_k\}$ having period N_s and transmitted at regular intervals of T_c seconds usually named, in this case, chips. The frame/chip time T_f/T_c is usually chosen to be greater than the maximum multipath delay to avoid inter-symbol interference. The information can be associated to pulse polarity leading to pulse amplitude modulation (PAM) signaling or to pulse position thus obtaining a pulse position modulation (PPM) signaling scheme.

Implementing an impulse-based radio allows for a simple circuit structure with low power dissipation since there is no need to up-convert a carrier signal [24]. The transmitter feeds these impulses to a very large bandwidth non-resonating antenna, or sometimes the antenna itself shapes the pulses to the required frequency of operation. In Fig. 6 an example of simple UWB pulse generator schematic proposed in [24] is reported which consists of a delay line, a NOR gate and a pulse shaping circuit.

The basic UWB receiver is a correlation receiver [12] where the received signal is correlated with a local replica (template) of the transmitted pulse $p(t)$ or, equivalently, is filtered by a filter matched to $p(t)$ (matched filter (MF)). In a single-user additive white Gaussian noise (AWGN) scenario, the bit error probability (BEP) of a UWB link employing binary antipodal PAM is simply

$$P_b = \frac{1}{2} \operatorname{erfc} \sqrt{\frac{E_r N_s}{N_0}} \quad (8)$$

where E_r is the energy of the received pulse, N_0 is the thermal noise one-side power spectral density and $\operatorname{erfc}(\cdot)$ is the complementary error function. The received energy per symbol is $E_s = N_s E_r$.

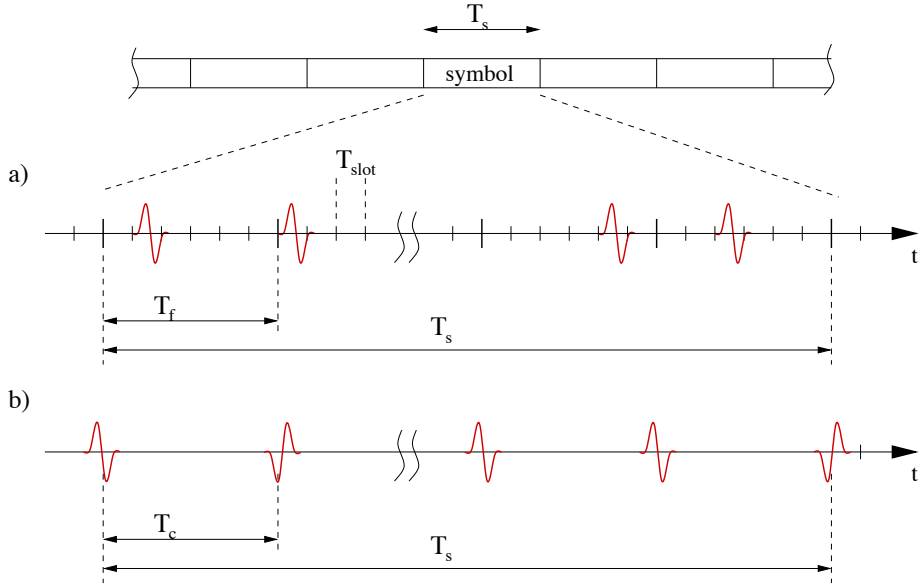


Figure 5: (a) UWB time-hopping frame structure; (b) UWB direct-sequence frame structure.

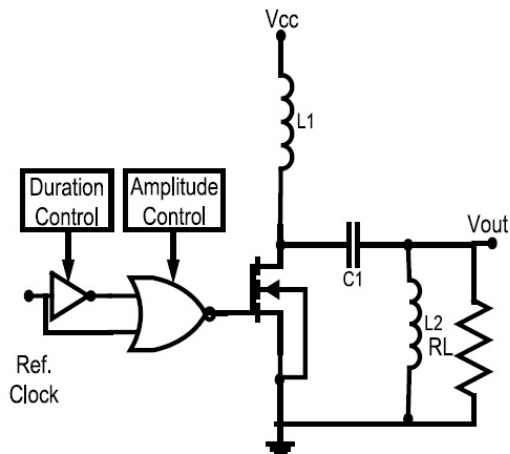


Figure 6: Example of UWB transmitter schematic [24].

Typical indoor environments often exhibit the presence of dense multipath with delay spread much larger than the resolution capability of the signal being employed [25, 26]. The transmission of ultra-short pulses can potentially resolve extremely large number of paths experienced by the received signal, especially in indoor environments, thus eliminating significant multipath fading [25]. This may considerably reduce fading margins in link budgets and may allow low transmission power operation. In addition, rich multipath diversity can be collected through the adoption of Rake receivers which combine the signals coming over resolvable propagation paths in a way that maximizes the signal-to-noise ratio (SNR) [27].

It can be shown that the bit error probability of a Rake receiver is

$$P_b = \frac{1}{2} \operatorname{erfc} \sqrt{\frac{E_s \eta_{cap}}{N_0}} \quad (9)$$

where η_{cap} is called the *energy capture efficiency* and accounts for the ability of the Rake receiver to collect the energy coming from different propagation paths. For more information on the fundamentals of UWB, we refer to [12, 15, 27, 28] and references therein.

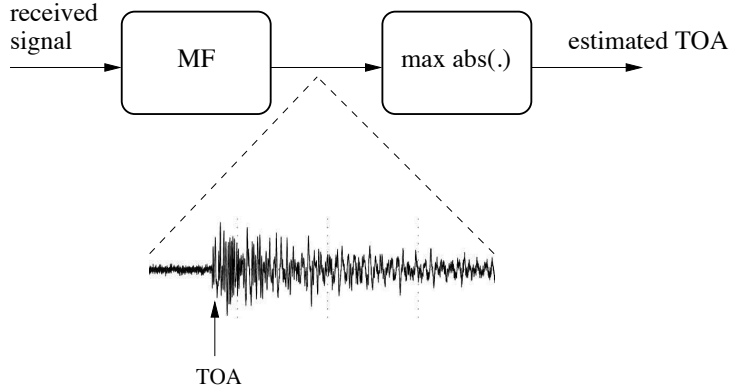


Figure 7: Classical MF based TOA estimator.

2.3.2.3 Ranging capability of UWB signals

Distance estimation (ranging) between tags and multiple readers represents the first step to localize the tag using, for example, multi-lateration algorithms [7]. Considering that the electro-magnetic (e.m.) waves travel at the speed of light $c = 3 \cdot 10^8$ m/s, the distance estimate can be obtained from the measurement of the time-of-flight (TOF) τ_f of the signal and by observing that $\tau_f = d/c$, where d is the actual distance between the tag and the reader. This requires an accurate estimation of the TOA of the received signal.

To understand which fundamental system parameters dominate ranging accuracy, we present an overview of the performance limits of TOA estimation in AWGN channels. We consider a scenario in which a unitary energy pulse $p(t)$ is transmitted (with duration T_p) through a AWGN channel.² In the absence of other error sources, the received signal can be written as

$$r(t) = \sqrt{E_r} p(t - \tau) + n(t) \quad (10)$$

where E_r is the received energy and $n(t)$ is AWGN with zero mean and two-sided power spectral density $N_0/2$. The goal is to estimate the TOA τ , and hence the distance d , by observing the received signal $r(t)$. This task can be challenging due to the presence of thermal noise and multipath components. Under this simple model, TOA estimation is a classical non-linear parameter estimation problem, with a solution based on a MF receiver [29]. As shown in Fig. 7, the received signal is first processed by a filter matched to the pulse $p(t)$ (or equivalently by a correlator with template $p(t)$). The TOA estimate is given by the time instant corresponding to the maximum absolute peak at the output of the MF over the observation interval. This scheme yields a maximum likelihood (ML) estimate, which is known to be asymptotically efficient, that is, the performance of the estimator achieves the Cramér-Rao bound (CRB) for large SNRs.³

The MSE of any unbiased estimate \hat{d} of d , derived from TOA estimation, satisfies the following inequality [29]

$$\text{Var}(\hat{d}) = \mathbb{E}\{\varepsilon^2\} \geq \frac{c^2}{8\pi^2 B_{\text{eff}}^2 \text{SNR}} \quad (11)$$

where $\varepsilon = \hat{d} - d$ is the ranging estimation error. The right hand term in (11) represents the CRB. Here $\text{SNR} \triangleq E_r/N_0$ and parameter B_{eff}^2 represents the second moment of the Fourier transform $P(f)$ of $p(t)$,⁴ that is

$$B_{\text{eff}}^2 \triangleq \frac{\int_{-\infty}^{\infty} f^2 |P(f)|^2 df}{\int_{-\infty}^{\infty} |P(f)|^2 df}. \quad (12)$$

²In general $p(t)$ can be a part of a multiple access signaling such as DS or TH as explained in Sec. 2.3.2.2. For bandlimited signals, we consider T_p as the interval duration containing most of the signal energy.

³The CRB gives the theoretical limit on the mean squared error (MSE) of any unbiased estimator and hence it represents a useful benchmark to assess the performance of any practical estimator.

⁴Parameter B_{eff} is often called *effective bandwidth*.

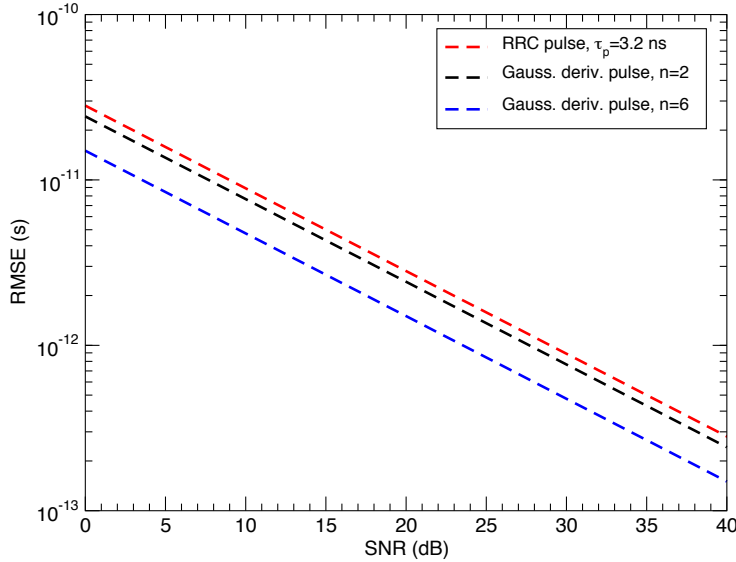


Figure 8: CRB on the TOA estimation RMSE as a function of SNR in an AWGN channel. The RRC pulse, the 2nd-order Gaussian, and the 6th-order Gaussian monocycle pulses with, respectively, $\tau_p = 3.2$ ns, $\tau_p = 1$ ns and $\tau_p = 0.192$ ns are considered.

Notice that the lower bound in (11) decreases with both SNR and the constant B_{eff} , which depends on the shape of the pulse. This reveals that signals with high power and/or wide transmission bandwidth are beneficial for ranging.

It is known that the ML estimation error tends asymptotically to the Gaussian distribution. Denoting d the true distance, the measured range \hat{d} can be expressed as

$$\hat{d} = d + \varepsilon \quad (13)$$

where the ranging estimation error ε can be modeled, as first approximation, as a Gaussian random variable (RV) with zero-mean and variance σ^2 , where σ^2 is bounded by (11).

Fig. 8 shows the root mean square error (RMSE) for CRB using the RRC, 2nd and 6th order Gaussian monocycle pulses. Note that higher derivative Gaussian monocycles or lower τ_p reduce the bound. It can be observed that centimeter level accuracy (e.g., RMSE on TOA less than 1 ns) is potentially feasible using UWB signals. Other improved but more complex bounds can be found in [29].

In more realistic environments, numerous practical factors might affect ranging accuracy. Sources of error from wireless signal propagation include multipath, direct path excess delay and blockage incurred by propagation, respectively, of a partially obstructed or completely obstructed direct path component that travels through obstacles such as walls in buildings. For more information about ranging using UWB signal please refer to [29, 30] and references therein.

2.3.3 UWB RFID and localization with active tags

2.3.3.1 Low duty cycle UWB tags

As already mentioned, a IR-UWB transmitter can be very simple and it is characterized by an extremely low duty cycle transmitted signal. Therefore, such a transmitter has low complexity and low consumption (less than 10 mW depending on the pulse repetition rate) [32, 33]. On the contrary, a UWB receiver, even simple, is typically characterized by higher values of consumed power that could be in the order of 100 mW [32]. Therefore devices based on the IEEE802.15.4a standard for WSNs, which allows for bi-directional communication, do not fit typical RFID applications requirements. For this reason most of proposed UWB RFID devices, designed for RTLSs, have only transmitting active tags operating with low duty cycle in order to extend battery operation up to a few years [34–37].

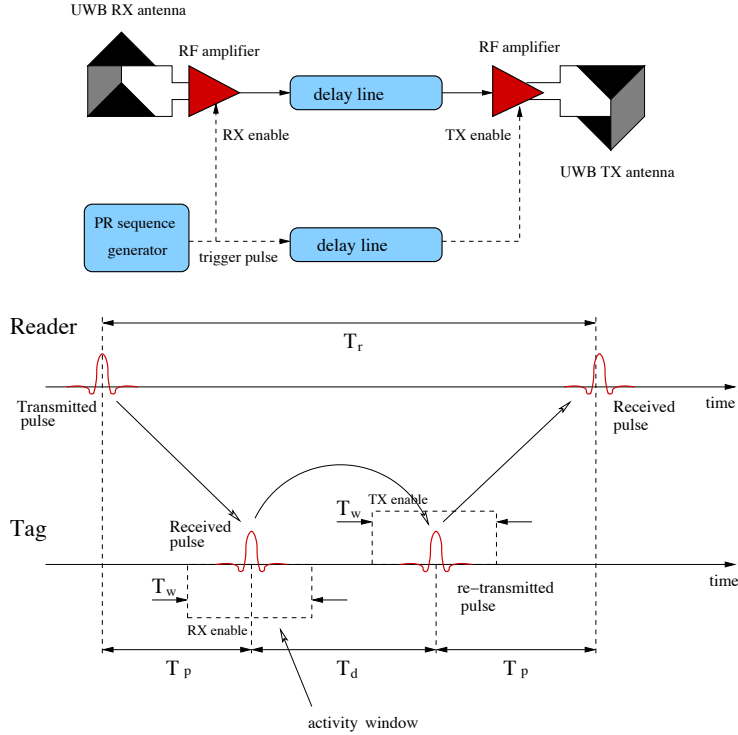


Figure 9: Pseudo-random Active UWB reflector scheme and example of timing structure in case of single pulse transmission [31].

An alternative solution is proposed in [31] where the concept of *pseudo-random active reflector* is introduced. As shown in Fig. 9, it consists of a simple device that repeats a slightly delayed version of the received UWB signal only in certain time intervals according to a suitable Pseudo-random (PR) TH sequence. In particular, the signal received by the antenna is amplified with gain G and delayed by a fixed quantity T_d of a few nanoseconds. The delayed version of the signal is used to drive the transmitter section composed of a power amplifier and a UWB antenna. The trigger pulse at the output of the PR generator enables the receiver amplifier for a certain time window T_w (activity window). A delayed version, by the quantity T_d , of the same trigger pulse is used to enable the transmitter. The transmission and receiving windows are not time overlapped so that no transmitter-receiver coupling occurs and the same antenna can be used for both the transmitter and receiver. The reader emits pulse trains with the same PR TH sequence used by the reflector it wants to communicate with. Each reflector has a unique PR sequence and reflects, with a delay T_d , the received UWB signal for a short time interval according to the TH sequence (see Fig. 9). When synchronized, all transmitted pulses are reflected only by the tag adopting the same PR sequence of the reader thus making the reader able to collect coherently the energy from that particular tag. As stated in [31], the advantages of this solution are in the hardware simplicity since only the analog section is present, in the low power consumption of the tag, and in the low timing constraint regarding the relative transmitter and reflector clock rates.

2.3.3.2 Localization capability

The first application of UWB technology in the RFID and RTLS fields was for precision asset location systems operating in indoor environments [34–37]. In these systems only UWB transmitting tags are employed, then tag position estimation cannot rely on absolute distance estimate between tag and readers and localization schemes based on time difference-of-arrival (TDOA) are usually adopted. In TDOA-based localization systems burst UWB signals are broadcast periodically by the tag and are received by several readers placed in known positions (see Fig. 10a). The readers share their estimated TOA and compute the TDOA provided that they have a common reference clock. Considering that time measurement accuracy

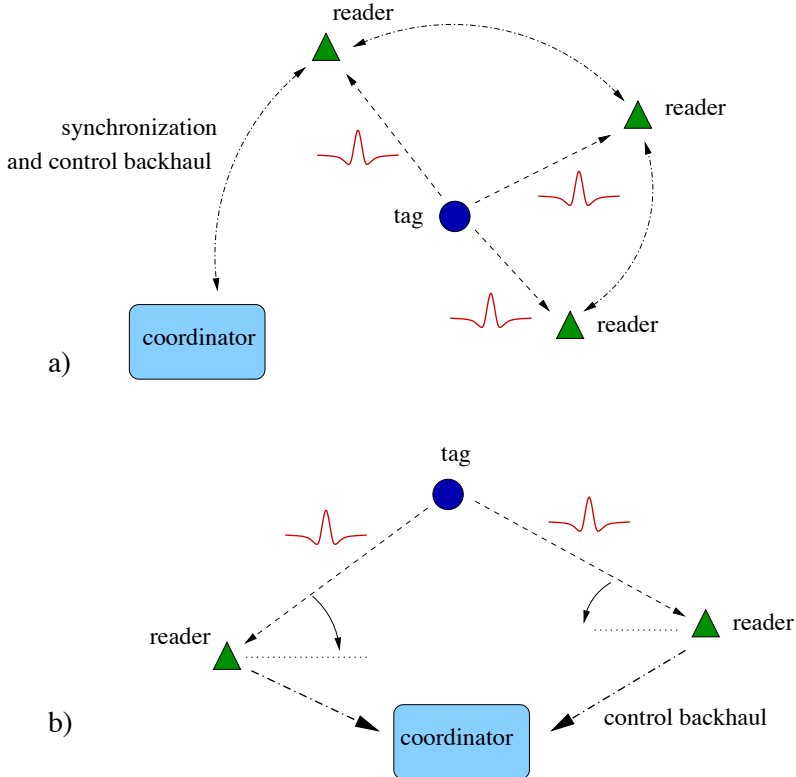


Figure 10: Active tag localization using TDOA (a) and AOA estimation techniques (b).

should be in the order of 1 ns or less, readers must be kept tightly synchronized through a wired network connection. To calculate the position of the tag, at least three readers with known position and two TDOA measurements are required. Each TDOA measurement can be geometrically interpreted as a hyperbola formed by a set of points with constant range-differences (time-differences) from two readers [7].

Time Domain Plus RTLS is an example of commercial proprietary system designed for locating personnel or mobile assets adopting TDOA technique [35]. The active tag is a compact IR-UWB battery powered transmitter that is designed for long battery duration, up to 4 years (at 2 Hz update rate) or up to 1.5 years (at 4 Hz update rate). The system can locate and track thousands of tags with sub-meter location accuracy using an adequate number of tightly synchronized readers which perform the function of receiving tag signals, demodulating the tag data, measuring the TOA for each tag and computing the TDOA for location estimation.

Another possibility to localize the tag is to measure the angle-of-arrival (AOA) of the signal thus obtaining the information about tag direction to neighboring readers (see Fig. 10b). The AOA of an incoming radio signal can be estimated by using multiple antennas with known separation (antenna array) and by measuring the TOA of the signal at each antenna. Given the differences in arrival times and the array geometry, it is possible to estimate the direction of propagation of a radio-frequency wave incident on the antenna array. AOA does not require the precise time synchronization needed for TOA and TDOA techniques. Two angle measurements are required to determine node position (*triangulation*) [7]. In non-line-of-sight (NLOS) environments, the measured AOA might not correspond to the direct path component of the received signal and large angle estimation errors can occur. Due to the presence of multiple antenna elements, AOA techniques are in general more expensive in terms of cost and device dimensions than TDOA-based techniques.

The Ubisense platform is an example of commercial precision localization system where active tags are localized using TDOA or AOA techniques [36]. When AOA localization is performed no tight synchronization among readers is required thus drastically reducing network requirements, but the positioning accuracy is less than that obtainable using TDOA measurements.

Zebra Enterprise Solutions commercializes its RTLS, called Sapphire DART [37]. The location system is TOA/TDOA-based, the tag emits in the 6.5GHz band and the blink rate is similar to that of Ubisense at a few Hz.

2.3.3.3 The IEEE802.15.4f Standard Proposal

The IEEE 802.15.4f Active RFID System Task Group is chartered to define new wireless PHY layers and enhancements to the 802.15.4-2006 standard medium access control (MAC) layer [23]. This amendment defines a PHY layer, and only those MAC modifications required to support it, for active RTLS. It allows for efficient communications with active tags and sensor applications in an autonomous manner in a promiscuous network, using very low energy consumption (low-duty-cycle), and low transmitter power. The PHY layer parameters are flexible and configurable to provide optimized use in a variety of active tag operations including simplex and duplex transmission (reader-to-tags and tag-to-readers), multicast (reader to a select group of tags), unicast (reader to a single tag), tag-to-tag communication, and multi-hop capability.

At the time of writing, the group achieved a common proposal on the PHY layer which is based on 3 different physical sub-layers, respectively, UWB, UHF at 433 MHz, and 2.4 GHz. The UWB PHY is based on the on-off keying (OOK) modulation with 1-2 MHz pulse repetition frequency enabling high-accuracy TOA-based ranging.

The UHF interface is in the frequency range 433.05 MHz - 434.79 MHz and 1.74MHz bandwidth. The modulation is Minimum-shift Keying (MSK) with data rates of 250 Kb/s or 31.25 Kb/s. Received signal strength indicator is used as low-accuracy location determination mechanism.

The 2.4 GHz air interface is built on IEEE 802.15.4 standard PHY layer. It could be used standalone for low-precision RTLS or to provide assistance to UWB PHY layer. The operating bands have been chosen in order to do not affect Wi-Fi and Zigbee nearby devices. Again the MSK modulation is used with a bit rate of 250kbps found as a compromise between range, bandwidth, and power consumption.

The PHY layer specification supports a large tag population (hundreds of thousands) and basic functionalities such as read and write with authentication and accurate localization. The communication reliability of the system is expected to be high for applications such as active tag inventory counting or auditing, high-value asset location tracking, and personnel tracking. Typical requirements are: operation in dense, metallic environments with sub-meter localization accuracy, real-time presence and location updates in seconds, small tag sizes for easy placing on typical high-value assets. The active IEEE 802.15.4f PHY layer is capable of working in the presence of interference from other devices operating within the band of operation.

2.3.4 UWB RFID and localization with (semi-)passive tags

When tag cost, size, and power consumption requirements become particularly stringent, passive or semi-passive tag solutions have to be taken into consideration. As already mentioned, communication with passive tags usually relies on backscatter modulation even though the tag's control logic and memory circuits have still to be energized in order to have the tag working properly. Typically, passive RFID tags obtain the necessary power to operate from the RF signal sent by the reader. As a consequence, in conventional UHF RFID systems the corresponding operating range is restricted to be no more than 7-8 meters with a transmission power level of 2 – 4 W [5]. Unfortunately, due to regulatory constraints, the transmission power allowed for UWB devices is lower than 0dBm. This means that no sufficient power can be derived from the received UWB signal to power up a remote tag at significative distance. A possible solution is represented by hybrid tag architectures, as will be illustrated in Sec. 2.3.5.

Besides the adoption of semi-passive tags with battery-powered control logic, a promising possibility to retrieve the necessary energy is to use energy scavenging techniques which, in many cases, provide sufficient power (about $1 - 10 \mu\text{W}$) for the control logic [38]. An interesting alternative is represented by chipless tags characterized by the absence of any control logic circuit as will be illustrated in Sec. 2.3.6.

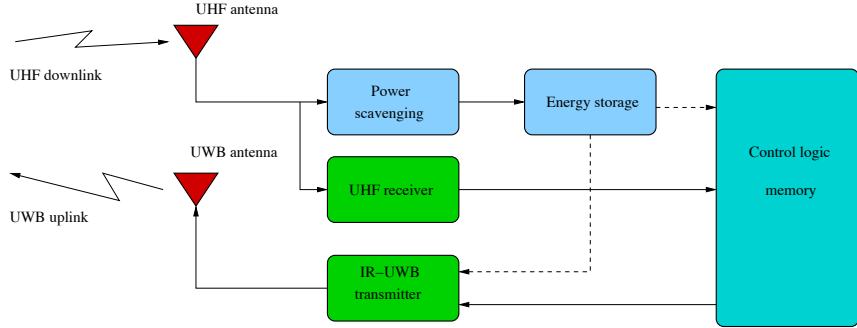


Figure 11: Hybrid UWB tag architecture proposed in [24].

2.3.5 Hybrid tags based on UHF and UWB modulations

Hybrid tags solutions are proposed in [24, 39–42]. The main idea is to have an asymmetric link where in the downlink (reader-tag) a conventional transmission protocol at UHF is adopted to power-up the tag and accumulate enough energy to allow an IR-UWB transmitter send data for a short time interval at high data rate in the uplink (tag-reader).

The block diagram of the module proposed in [24] can be seen in Fig. 11. It consists of a UHF receiving antenna, a power scavenging unit, an energy storage unit (basically a big surface mounted capacitor), an UHF receiver, a low power IR-UWB transmitter, an UWB transmit antenna and the control logic. Similarly to conventional passive tags, the incoming RF signal transmitted by the reader at UHF is used to provide power supply and receive the data. In particular, the reader radiates the RF signal with no data for at least 7ms which is the time for full charge of the storage capacitor. After enough energy has been collected, the tag goes to the receiving mode to receive commands from the reader at low data rate (40Kbps). The uplink transmission is performed using the IR-UWB transmitter. Thanks to the high transmission data rate (1 Mbps with $N_s = 10$ pulses per bit) and the low transmitter consumption ($64\mu\text{W}$), the energy stored in the capacitor is sufficient to allow the transmission of packets containing more than 128 bits. Circuit implementation and simulations have shown that up to 10.7 meters operating range with 4W EIRP emission is feasible from the energy budget point of view. Unfortunately, no results are reported by the Authors related to the uplink data transmission performance and the associated operating range.

Remote powering of a passive UWB tag by UHF has recently been achieved for high data rate exchanges ($> 50\text{Mbits/s}$ at a few tens of centimeters) from a cell phone to a tag embedding a large memory [41].

2.3.6 Chipless tags

The evermore demanding cost reduction of RFID technologies, aiming to substitute presently worldwide diffused bar code labels with RFID tags, has yield the conviction that the price challenge cannot be won without a radical technological change in e.m. tags. This has brought to the development of chipless or fully passive RFID technologies which are currently emerging as some of the options for the future of RFID tags. Even if promising cost reduction of more than one magnitude order (from current US\$0.50 to US\$0.01), chipless technologies are still in an almost embryonic stage and it is not clear from the present state of the art literature whether solutions to all the currently open problems will be found. In particular both the problem of large data encoding and multiple access, that are strictly related as we will later briefly explain, must still be solved since experimentally evidenced studies assure only small data encoding (in the order of a few bits per tag) without or with too little multiple access capabilities. Parallel to cost reduction, chipless tags are very interesting from an energetic efficiency point of view since neither the micro-controller nor backscatter modulator are present, then no energy source is required. This, that on one hand is a potentially shocking novelty, is on the other hand a source of limitations as the achievable

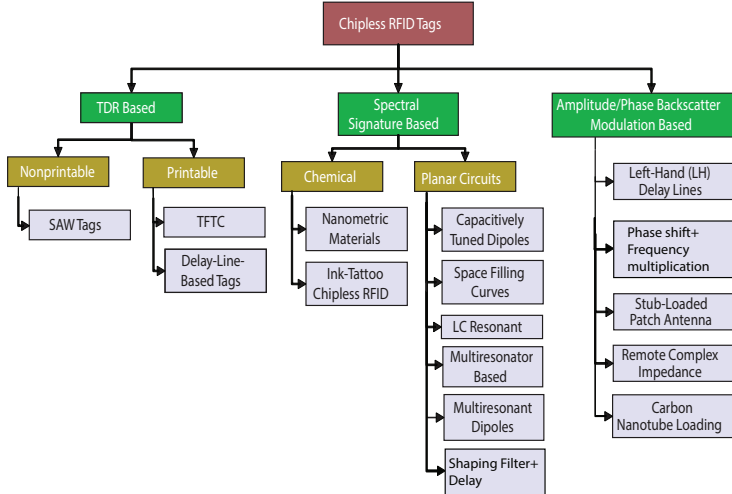


Figure 12: Chipless tags classification as proposed in [43]. Time-domain reflectometry (TDR); surface acoustic wave (SAW); Thin Film Transistor Circuit (TFTC).

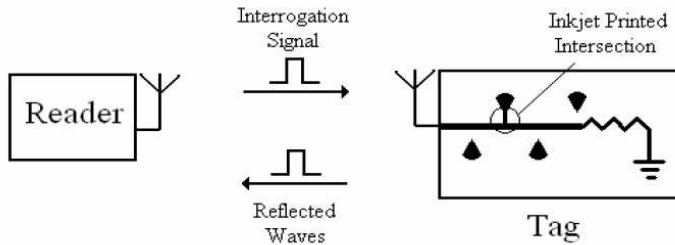


Figure 13: Example of UWB chipless tag proposed in [44].

reading distances fall at bar codes levels (few cm). Having in mind these background ideas we now proceed to a survey exposition of progresses in chipless technologies which integrates and expands the clever classification made in [43].

As reported in Fig. 12, three main categories of chipless tags may be identified, based on the different underlying technology: Time-domain reflectometry (TDR) based tags, spectral signature based tags, and amplitude/phase backscatter modulation based tags.

TDR based chipless tags cause several time-resolvable echoes of the received UWB signal to reflect back along the tag particular structure, in order to make different IDentifications (IDs) distinguishable. This class of chipless tags can be further divided in two more categories: Printable and Nonprintable tags. Surface acoustic wave (SAW) tags are nonprintable since the devices causing reflections consist of piezoelectric materials. SAW tags are the only commercial chipless tags, nevertheless they are not competitive with bar codes since their cost is sensibly higher. Among printable tags, Thin Film Transistor Circuit (TFTC) tags promise higher capabilities (the ones obtainable with traditional electronics operating at low frequencies) in terms of functionality with respect to other chipless tags, at the price of little power absorption: In fact these tags employ organic printed transistors so they are chipless in the sense that they are not provided with an usual chip, but still are capable of some traditional switching operations. Delay-line based tags are the e.m. counterpart of SAW tags. Reflections are caused by e.m. discontinuities along a microstrip delay line: Spatial separation is translated into temporal separation of the reflected echoes. An example of delay line based tags may be found in Fig. 13 where the proposed tag is composed of a transmission line with mismatched impedances encoding the tag ID. The main limit of this technology is the very restricted number of resolvable bits (discontinuities) that can be integrated in a quite long microstrip line (tens of cm as reported in [44]).

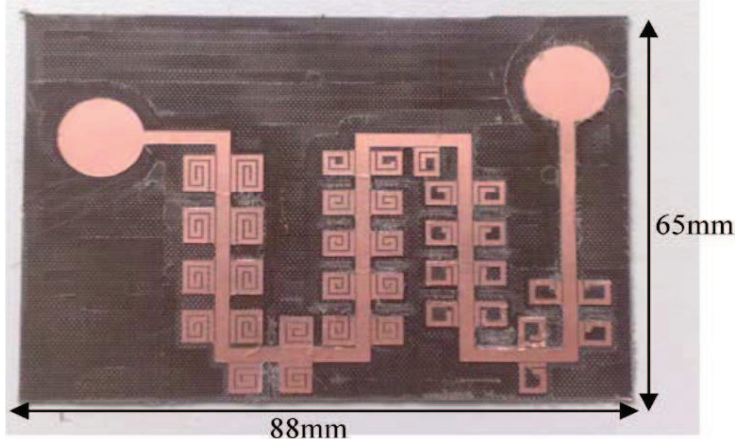


Figure 14: Multiresonator based 35-bit chipless tag, presented in [46].

Spectral signature based tags can also be divided in two more categories depending on the materials they are composed of. Chemical chipless tags, nanomaterials based as well as ink-tattoo based, take advantage of materials properties to generate resonances in the reflected signal spectrum. Planar circuit based tags all employ the traditional electronics materials with the purpose to encode information bits in particular reflected signal spectrum shapes. Capacitively tuned dipoles and space-filling curves are used to create dips corresponding to resonance frequencies of the on-tag placed elements. Both these kinds of chipless tags pose concerns regarding the achievable tag dimensions. LC resonant chipless tags are one bit tags, this obviously limiting their employment, that exploit the coupling of an on-tag mounted LC resonant circuit with the reader antenna: Whenever the reader frequency corresponds to the one causing the LC circuit to resonate, oscillation is generated and a dip in voltage at the reader end is produced. Multiresonator based (an example in Fig. 14) and multiresonant dipoles based chipless tags take on the same founding principle in a slightly different manner: Only a certain portion of the received spectrum is retransmitted back to the reader. This is done by means of a couple of cross-polarized antennas with a number of resonant structure in between: In multiresonator based tags the resonant structures are resonators, while, in multiresonant dipoles based tags, the resonant structures are the several elements of the retransmitting antenna. This latter kind of tags enhances space efficiency with respect to the former one. A shaping filter (based on coplanar waveguide theory) may be used instead of multiple resonating structures: This is reported in [45] where a delay line was also introduced to time separate the structural mode and the antenna mode backscattering components of the reflected tag signal.

For what concerns amplitude/phase backscatter modulation based tags, the underlying principle is to distinguish different tag IDs backing on a different tag antenna load modulation, as done in semipassive RFID tags. Left-hand delay line based tags adopt multiple reflecting structures to vary the reflected signal phase differently at each reflecting section. A similar principle is employed in the structure proposed in [47]: Here a passive tag end frequency multiplication is used to remove clutter at the reader end while information is encoded in a phase shift of one of the two tag retransmitted signals. The phase shift is operated by organic electronics and the information is then recovered at the reader side by means of confrontation. Remote complex impedance based and stub loaded patch antenna based chipless tags rely on phase modulation caused by the tag antenna terminating structure: The case of stub loaded tags is likely to be more favourable since this kind of tags also employs cross-polarization diversity together with phase modulation. This is done by means of involving phase difference between the E-plane and H-plane signals at the reader end, rather than utilizing a circularly polarized reader antenna. Carbon nanotube loaded chipless tags are similar to semipassive tags with the substantial difference of the amplitude modulation being caused by the sensed physical quantity (typically ammonia) which provokes an impedance change of the carbon nanotube. This adds sensing capability to this particular kind of chipless tags.

Whereas all the categories in the reviewed first two macroclasses of chipless tags intrinsically rely

on UWB technology, the amplitude/phase backscatter modulation based chipless tags can also operate in a narrowband context, even if UWB technology enhances all the previously explained features that narrowband technologies are weak at or simply lack.

As last but not least consideration, we pose attention on the number of encoded bits/multiple access capabilities trade off. Due to the absence of a chip, it is impossible to implement a collision avoidance protocol which is not directly implemented within the information data encoding strategy. To make the concept clearer, we refer to TDR based tags, considering, in particular, the case of delay line based tags. The modulation occurs by means of different delay, hence different transmission line length: What if two tags are not at the same distance from the reader? What if the received antenna modes are not correctly associated to the respective structural mode and consequently the delay deduction is wrong? These problems may have particular solutions in case just two tags need to be detected simultaneously by means of ensuring certain constraints in data encoding to be respected, this limiting the already not abundant information encoding capabilities of tags. Other solutions, not restricted to the class of TDR based tags, may also be possible, and are under current investigation, though always at the price of a reduced data encoding capability. This motivates the initial concerns we expressed about the near future commercial possibility of chipless technology. Nonetheless our efforts will aim at solving these scientifically challenging problems.

2.3.7 Semi-passive tags based on backscatter modulation

As anticipated, passive tags solutions are of particular interest thank to their potential lower cost and power consumption. To this purpose, the idea of passive tags based on UWB backscatter signaling was introduced in [8], where tag architectures as well as backscatter signaling schemes robust to the presence of clutter (i.e., reflections coming from surrounding objects) are presented. Nevertheless, UWB RFID analysis based on backscatter modulation is at the beginning and different issues have still to be investigated [11].

Recently, some applications of the UWB technology in tags based on backscatter modulation have been proposed [8, 11]. Due to its extremely low complexity backscatter communication appears very promising, especially in the perspective of the adoption of efficient energy scavenging techniques for tag's control logic alimentation. For this reason in the following we deserve more details to this solution.

In Fig. 15 the architectures analyzed in [11] for tag and reader are reported. The reader is composed of a transmitter and a receiver section.

During the interrogation cycle, the reader transmits a sequence of UWB pulses modulated by a periodic binary spreading sequence $\{d_n\}$ of period N_c with $d_n \in \{-1, 1\}$, specific to that particular reader (reader's code). In general, N_{pc} pulses are associated to each code symbol (chip). To accommodate the signals backscattered by tags corresponding to an entire packet of N_r bits, the UWB interrogation contains $N_t = N_r N_s$ pulses, where $N_s = N_c N_{pc}$ is the number of pulses associated to each bit. Pulses are separated by T_p seconds. Then the UWB transmitted signal takes the form

$$s_{\text{reader}}(t) = \sum_{k=0}^{N_r-1} s(t - kN_c T_c) \quad (14)$$

characterized by a transmission power P_t , where $T_c = N_{pc} T_p$ is the chip time, $s(t)$ is the composite sequence

$$s(t) = \sum_{n=0}^{N_c-1} d_n g(t - nT_c), \quad (15)$$

and

$$g(t) = \sum_{i=0}^{N_{pc}-1} p(t - iT_p) \quad (16)$$

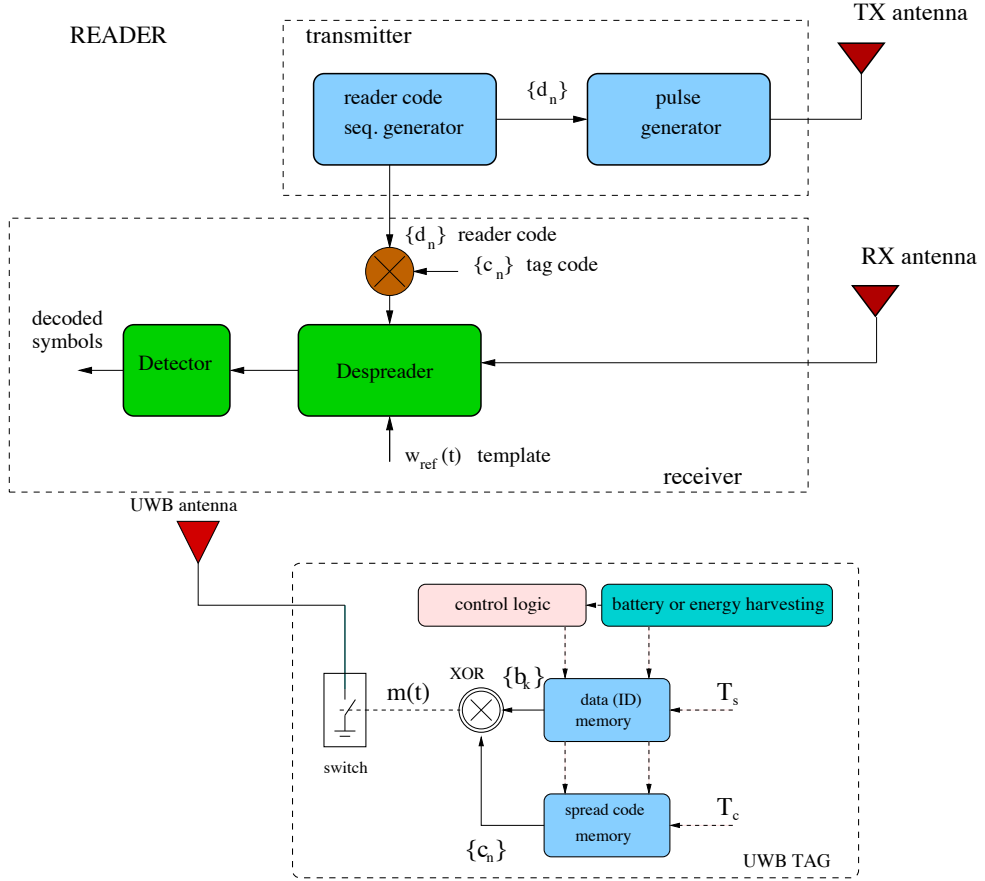


Figure 15: The considered scheme of the tag and the reader composed of a transmitter and a receiver section.

is the waveform associated to each chip d_n composed of N_{pc} elementary UWB pulses $p(t)$. The pulse repetition period T_p is chosen so that all signals backscattered by the environment are received by the reader before the transmission of the successive pulse. In indoor scenario $T_p = 50 - 100\text{ ns}$ is usually sufficient to this purpose.

Each pulse in (38) is backscattered by the tag's antenna as well as by all the surrounding scatterers present in the environment which form the clutter component.

The main task of the receiver section of the reader is to detect the useful backscattered signal (i.e., that coming from the tag's antenna mode scattering which depends on antenna load changes) from those backscattered by the antenna structural mode and other scatterers (clutter) which are, in general, dominant. To make the uplink communication robust to the presence of clutter, interference, and to allow multiple access, a proper backscatter modulation strategy is necessary at tag side.

In Fig. 15, an example of tag architecture employing a binary backscatter modulator composed of an UWB switch is shown. The switch is controlled by a micro-controller which purpose is to change the switch status X (short or open circuit) at each chip time T_c according to the data to be transmitted and a zero mean (balanced) periodic tag's code $\{c_n\}$, with $c_n \in \{-1, +1\}$, of period N_c . Specifically, each tag information bit $b_k \in \{-1, +1\}$ is associated to N_s pulses, thus the symbol time results $T_s = T_c N_c = T_p N_s$ as illustrated in Fig. 16. In this way the polarity of the reflected signal changes according to the tag's code during a symbol time, whereas the information symbol affects the polarity of all pulses composing the sequence each symbol time. Therefore, the backscatter modulator signal, commanding the tag's switch,

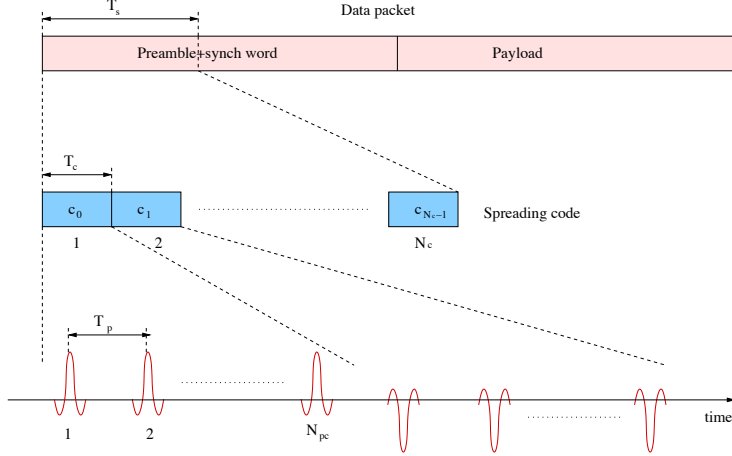


Figure 16: Example of backscattered signal structure. Only useful component reported.

can be expressed as

$$m(t) = \sum_{k=0}^{N_r-1} b_k \sum_{n=0}^{N_c-1} c_n \Pi\left(\frac{1}{T_c}(t - nT_s - iT_c - \Delta)\right) \quad (17)$$

having defined $\Pi(t) \triangleq 1$ for $t \in [0, 1]$ and zero otherwise. Note that in general reader and tag have their own independent clock sources and hence they have to be treated as asynchronous. Then the tag's code $\{c_n\}$ is not in general time aligned to the reader's code $\{d_n\}$. The parameter Δ in (17) denotes the clock offset of the tag with respect to the reader's clock.

Once the tag and reader codes are aligned and the TOA is estimated, the reader can adjust its internal clock so that it becomes synchronous to that of the intended tag. A more general analysis considering asynchronous multiple tags can be found in [11]. For the sake of illustration, in the following we refer to a single tag scenario and consider perfect synchronization between reader and tag, i.e., $\Delta = 0$. In addition, the tag response due to the antenna mode is examined whereas the antenna structural mode will be treated as part of the clutter, since it does not depend on data symbols. As a consequence, any clutter removal technique adopted will be effective on the antenna structural mode component as well.

Considering perfect backscattered pulse symmetry, i.e., $w(t; 0, d, \Theta) = -w(t; 1, d, \Theta) \triangleq w(t)$, the received signal at the reader can be expressed as [11]

$$\begin{aligned} r(t) &= \sum_{k=0}^{N_r-1} \sum_{n=0}^{N_c-1} d_n \sum_{i=0}^{N_{pc}-1} w(t - iT_p - nT_c - kT_s) \cdot m(t) \\ &\quad + \sum_{k=0}^{N_r-1} \sum_{n=0}^{N_c-1} d_n \sum_{i=0}^{N_{pc}-1} w^{(c)}(t - iT_p - nT_c - kT_s) + n(t), \\ &= \sum_{k=0}^{N_r-1} b_k \sum_{n=0}^{N_c-1} d_n c_n \sum_{i=0}^{N_{pc}-1} w(t - iT_p - nT_c - kT_s) \\ &\quad + \sum_{k=0}^{N_r-1} \sum_{n=0}^{N_c-1} d_n \sum_{i=0}^{N_{pc}-1} w^{(c)}(t - iT_p - nT_c - kT_s) + n(t), \end{aligned} \quad (18)$$

where $n(t)$ is the AWGN with two-sided power spectra density $N_0/2$, and the signal $w(t)$ represents the backscattered version of the pulse $p(t)$ when short-circuit load is applied to the antenna, which is in general distorted due to antennas and channel frequency selectivity. The signal $w^{(c)}(t)$ represents the backscattered version of the pulse $p(t)$ due to the clutter component which also accounts for pulse distortion and tag antenna structural mode.

Looking at (18), it can be noted that only the antenna mode scattered component results to be modulated by the combination of the tag's and reader's codes $\{c_n\}$ and $\{d_n\}$, whereas all clutter signals components (included the antenna structural mode scattering) are received modulated only by the reader's code $\{d_n\}$. This property can be usefully exploited to remove the clutter component through a proper receiver and code design.

An example of possible receiver scheme is that reported in Fig. 15 where a correlator-based demodulator is adopted with template

$$s_{\text{ref}}(t) = \sum_{n=0}^{N_c-1} d_n c_n \sum_{i=0}^{N_{\text{pc}}-1} w_{\text{ref}}(t - iT_p - nT_c). \quad (19)$$

The optimum receiver can be obtained by ideally choosing as pulses composing the local template in the correlator the waveform $w_{\text{ref}}(t) = w(t)$ (perfect matched receiver). Unfortunately in practical situations $w_{\text{ref}}(t) \neq w(t)$; we indicate with ρ the normalized cross-correlation between the actual received pulse $w(t)$ and the template $w_{\text{ref}}(t)$, which accounts for the mismatch due to pulse distortion (note that $\rho = 1$ in case of perfect matched receiver). In substance this scheme performs a de-spreading operation using the combined code $\{c_n \cdot d_n\}$, which identifies both the reader and the desired tag.⁵

Every T_s seconds, the output of the correlator is sampled thus obtaining the decision variable for the k th bit b_k :

$$y_k = b_k E_r \rho N_s + \gamma^{(\text{c})}(kT_s) \sum_{i=0}^{N_c-1} c_i + z_k \quad (20)$$

where z_k is the thermal noise sample with variance $\sigma_z^2 = \frac{N_0}{2} N_s$ and E_r represents the average received energy per pulse. E_r is given by

$$E_r = \int_{-\infty}^{\infty} |W(f; 0, d, \Theta)|^2 df. \quad (21)$$

As can be deduced from (20), to completely remove the clutter component it is sufficient that the tag's code $\{c_n\}$ has zero mean, i.e., $\sum_{n=0}^{N_c-1} c_n = 0$. In such a case (20) can be further simplified leading to

$$y_k = b_k E_r N_s \rho + z_k. \quad (22)$$

In general, from (22), it is easy to show that the BEP is given simply by

$$P_b = \frac{1}{2} \operatorname{erfc} \left(\sqrt{\frac{E_r N_s \rho^2}{N_0}} \right). \quad (23)$$

For further convenience, we define G_{ref} the round-trip channel power gain at the reference distance d_{ref} and at the maximum direction of radiation Θ_{\max} in AWGN scenario. In addition, we assume a typical exponential path loss law where the power path loss exponent β usually ranges between ≈ 1.8 and ≈ 4 . The BEP can be rewritten as

$$P_b = \frac{1}{2} \operatorname{erfc} \left(\sqrt{\frac{P_t G_{\text{ref}} \rho^2 \left(\frac{d_{\text{ref}}}{d} \right)^{2\beta}}{N_0 R_b}} \right) \quad (24)$$

where $R_b = 1/(N_s T_p)$ is the data rate (bit rate). It is interesting to note that the exponent 2β is present in (24) instead of β to account for the two-way link.

⁵Multiple readers can access the same tag by using different reader codes provided that they are designed with good cross-correlation properties.

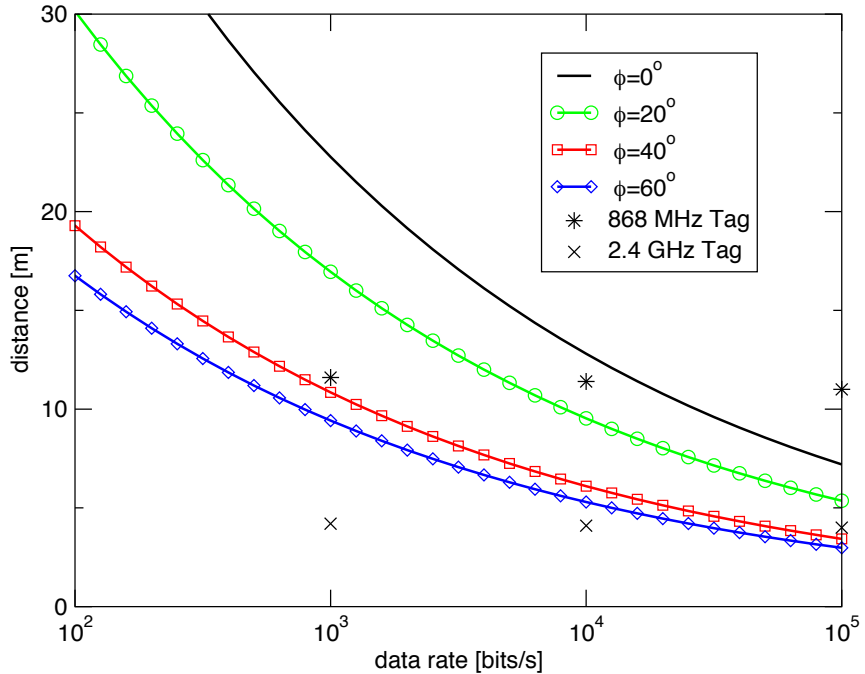


Figure 17: Tag–reader operating range in meters as a function of the data rate for $P_b = 10^{-3}$ and different tag orientations in the anechoic chamber scenario [11]. BAV antenna for the tag is considered. Cross and star dots refer to the corresponding performance of UHF tags operating at 868 MHz and 2.4 GHz, respectively.

2.4 Localization techniques

The localization and tracking process typically consists of two phases: (i) a measurement phase, during which tags make intra- and inter-node measurements using different sensors; (ii) a location-update phase, during which tags positions are inferred using an algorithm that incorporates both prior knowledge of their positions and new measurements. For instance, a tag can update its position estimate based on inertial measurements using an inertial measurement unit (IMU) and distance measurements with respect to some fixed readers using a remote measurement unit (RMU). In particular, distance measurements are most likely available for UWB backscattering modulation based localization.

The localization accuracy strongly depends on the quality of the measurements, which are affected by impairments such as network topology, multipath propagation, environmental conditions, interference, noise, and clock drift. In addition to the underlying technologies used in the measurement phase, the localization performance is also dependent on the specific processing or data fusion algorithm used in the location-update phase. Hence, a deep understanding of information evolution in different phases of the localization process is necessary for the design and analysis of localization systems.

Consider a network with a set \mathcal{R} of N_R fixed nodes (readers) and a set \mathcal{T} of N_T tags, where each tag is equipped with multiple sensors that can provide intra- and inter-node measurements (e.g., using IMU and RMU, respectively) for the purpose of localization and tracking. Using these intra- and inter-node measurements, represented by $\mathbf{z} = [\mathbf{z}_{\mathcal{T},\mathcal{T}} \mathbf{z}_{\mathcal{R},\mathcal{T}}]$, the tags aim to infer their positions $\mathbf{x}_{\mathcal{T}} = [\mathbf{x}_1 \mathbf{x}_2 \cdots \mathbf{x}_{N_T}]$. The accuracy of location estimates is inherently limited due to random phenomena affecting \mathbf{z} , and fundamental limits of such accuracy have been derived using the information inequality [48].

The measurement process has a crucial impact on the overall system tag localization accuracy. In the scenarios of GRETA the requirement on localization accuracy is stringent and the link budget of backscattered pulse is poor. The TOA-based ranging techniques will be adopted to exploit the properties of UWB signals. In this context, the scheme representing the signal processing for localization and tracking of a tag j by a set of reader \mathcal{R} is showed in Fig. 18. In particular, we consider the set $\mathbf{r}_{\mathcal{R}}(t)$

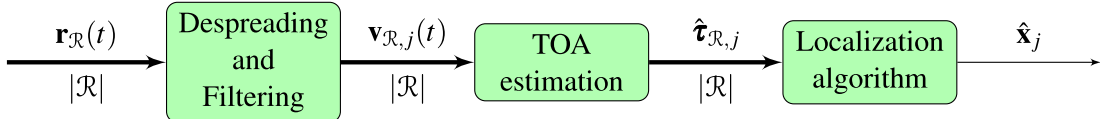


Figure 18: Signal processing for localization and tracking

of signals $r_i(t)$ received by the reader $i \in \mathcal{R}$ due to the transmission of a sequence of pulses by the same reader $i \in \mathcal{R}$. Each signal $r_i(t)$ is received at reader i after backscattering with modulation from all the tags and without modulation from all the objects in the environment. To infer the position of the tag j , each signal $r_i(t)$ is processed to mitigate clutter, interference, and noise effects (e.g., reader and tag code despreading, clutter removal techniques, noise filtering). The resulting set of signals $v_{R,j}(t)$ depends on the specific tag j and from each signal $v_{i,j}(t)$ the estimated TOA $\hat{\tau}_{i,j}$ is determined via ranging techniques (e.g., energy detection, matched filter, etc.). The set of estimated TOA $\hat{\tau}_{R,j}$ serves as input of the localization algorithm to infer the tag position. The tag position is updated with a localization update rate $R_L = \frac{1}{T_L}$ (i.e., the number of position estimates computed per second) by exploiting the new TOA estimates available at each $t_i = iT_L$.

The requirements of location-aware networks are driven by applications. A local performance metric is the RMSE of position estimates. In particular, the position estimation error is given by the Euclidean distance between the estimated position $\hat{\mathbf{x}}$ and the true position \mathbf{x}_j as $e(\mathbf{x})_j = \|\hat{\mathbf{x}}_j - \mathbf{x}_j\|$. A global performance metric evaluated over the entire localization area and time is the Localization Error Outage (LEO) defined by $P_{\text{out}} = \mathbb{P}\{e(\mathbf{x}) > e_{\text{th}}\}$, where e_{th} is the target (i.e., the maximum allowable) position estimation error, and the probability is evaluated over the ensemble of all possible spatial positions and time instants. Other requirements include localization update rate and coverage area of the localization system. In particular, localization update rate is important for tracking (tracking of pedestrians and vehicles typically requires different localization update rates), which drives algorithm complexity and node cost.

2.5 Multi-reader and multi-tag scenarios

Goods management and inventory control are the most relevant applications for RFID. In these applications, a large number of low-cost passive tags and a plurality of readers are often concentrated in the same environment (e.g., stores, supermarkets). This situation is referred as a multi-reader and multi-tag scenario. The main advantages of a multi-reader and multi-tag scenario are:

1. Identification in a larger area;
2. Fast identification;
3. Tag/reader localization.

However, there are interdependent challenges to consider:

- A reader should be able to interrogate many tags simultaneously.
- A tag might be required to respond to more readers at the same time.

Due to the shared communication channel, in the absence of specific channel access procedures multiple interrogations and responses interfere with each other and may determine losses. It is therefore necessary to implement tag anti-collision algorithms, so that their responses can be detected individually. Moreover, synchronization techniques should be implemented at the readers to coordinate the interrogations.

For RFID systems operating with UHF transceivers, many anti-collision protocols have been proposed and standardized (e.g., EPC Gen2 [49], ISO 18000-6 [50]). Readers and tags communicate through query messages and signaling in the UHF band.

For NG-RFID systems that use UWB signals the aforementioned techniques are not always viable solutions. In this context, the tag uses backscattering techniques to transfer information to the reader. The low complexity of the UWB RFID system and, in particular, tag complexity does not allow the

system to perform queries. The tag can transmit only default information, such as ID and some sensor measurement, upon reception of the UWB signal, but it is not able to interpret the information sent by the RFID reader. To overcome this limitation, it is often assumed that each tag is also equipped with an UHF receiver, which is used to energize and to synchronize the tags. In our setup, we consider initially i) the case where this is not possible due to the need of a simple tag implementation, and ii) the case where an UHF receiver is integrated. Moreover, a different code spreading at each tag could be implemented to avoid collisions [11]. However, this procedure requires the reader to be able to decode multiple spreading sequences that are required to be known a priori. Again, this might not be allowed in our setup whenever we assume that a limited number of spreading codes for the tags are available and there is a certain probability of having tags belonging to the same family (i.e., same spreading code) in the same range of interrogation.

Considering these restrictive specifications, a thorough analysis of the possible scenarios is required.

2.5.0.1 Identification

The reader interrogates the tags in its communication range by sending an UWB signal with a specific spreading code. A tag replies with its ID by modulating the backscattered signal from its antenna. The system needs more complex capabilities, depending on the scenario.

- 1 reader / 1 tag scenario: the reader should be able to discriminate the backscattered signal from the clutter.
- 1 reader / N tags scenario: the reader should also implement techniques to discriminate the backscattered signals from tags using the same spreading code.
- M readers / N tag scenario: a reader should also discriminate its signal and the backscattered signals from other concurrent interrogations. Differently from tags, readers can implement protocols to coordinate their interrogations (time division and/or code division multiple access).

The types of collisions can be divided into three cases:

1. Tag-tag collision: thanks to the short duration of the UWB impulses backscattered by the tags, the reader is able to distinguish responses of tags located at different distances (different ToAs). However, the signals backscattered by tags (approximately) at the same distance may overlap and prevent a correct identification. A limitation to the number of tags that can be identified in a single interrogation round depends also on the capacity of the reader to process simultaneous identifications.
2. Reader-tag collision: this happens when a reader is in the region of interference of another reader, namely the area in which the signal of a reader has sufficient intensity to cause interference to the response of tags in the vicinity of the second reader. Different spreading codes for the readers can be used to prevent or attenuate this inconvenience.
3. Reader-reader collision: this occurs when two readers with overlapping interrogation area are active at the same time. Different spreading codes and time-division multiple access among readers can be used to prevent this situation.

To characterize the probability of collision, critical parameters are the number of spreading codes (for the readers and the tags), and the spacial distribution of readers and tags.

2.5.0.2 Localization

By measuring the ToA of the backscattered signal, a reader is able to determine the distance and the relative position of the tag (ranging). To perform localization of tags and/or readers, it is required the interplay of at least one reader and/or more tags. In the case of nomadic readers, the first problem is to solve the uncertainty of their position. The possibilities are:

1. Distance estimation with respect to an anchor tag with known coordinates.
2. Communication among adjacent readers using appropriate localization algorithms.

To obtain good accuracy for the localization in the case of nomadic readers, also the network of readers is expected to operate with UWB technology. The number of readers needed for localization depends on the area of deployment (2D and/or 3D), and from a tradeoff between the desired resolution and the maximum speed of the tag. By using cooperative algorithms, the number of required readers can be reduced.

3 ARCHITECTURE AND TECHNOLOGIES

The purpose of this section is the identification of the application requirements, including the viable technologies.

3.1 System tag architecture

RFID tags are classified in active, semi-passive and passive tags. Active tags have an internal power source meanwhile semi-passive and passive tags must be energized and activated by waves from an outside source, generally supplied by the reader. The fundamental difference between passive and semi-passive is the capability to store energy for a short period. Another difference between active and passive/semi-passive tags is the RF transmitting section: active tags have a complete transmitter able to generate and modulate the signal; passive and semi-passive tags are generally based on backscattering modulation exploiting the signal generated by the reader. For these reasons and their low complexity, passive and semi-passive tags and backscatter communications are very promising, especially in the perspective of the adoption of efficient energy scavenging techniques to supply the control logic.

The passive/semi-passive tags architecture [8,51], chosen for this project and shown in fig. 19, consists of these fundamental blocks:

- antennas;
- power management unit;
- control unit;
- backscatter modulator;
- sensors;
- substrate.

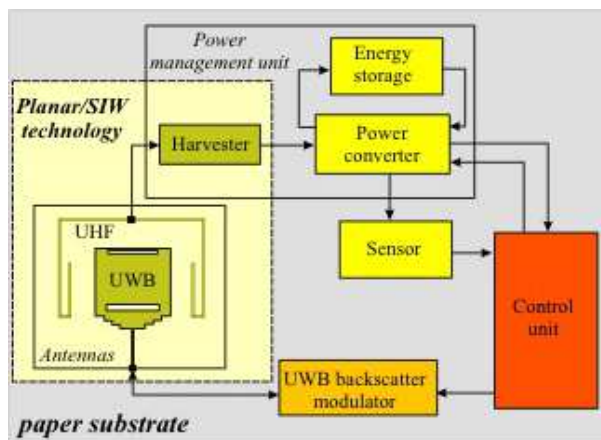


Figure 19: NG-RFID tag architecture.

The antennas, one operating in the UWB and the other one at UHF, allow the reader-tag communication and the energy harvesting for the tag power supply, respectively. The RF power used to supply the tag can be provided by the reader or by RF energy shower, dependently on the operating context.

The UHF antenna provides the RF energy to the power management unit. This unit is able to convert the RF energy in DC power, to store the energy, and to supply the other active blocks of the tag (control unit, backscatter modulator and sensors).

The control unit performs the acquisition and processing of the data provided by the reader and the sensors. This unit controls all the other units, in particular the backscatter modulator in order to transmit the processed information to the reader.

The backscatter modulator performs the signal modulation backscattering the E.M. waves generated by the reader and received by the tag. Generally, for UWB application this component is a switch reducing drastically the complexity of the transmitting section of the tag with respect to standard transmitters.

The RFID tag can be equipped with various sensors to monitor environment variables. The type of the sensors depends on the application. The sensors provide the information to the control unit.

The substrate proposed for the implementation of the tag is the paper according to the eco-compatibility requirements.

The various blocks must be able to operate in the UWB frequency band in according with the communication standard. Other important aspects of these blocks are the efficiency, the circuital complexity and the materials used in order to reduce the energy consumption, to increase the autonomy and to realize a eco-compatible tag.

3.2 Energy harvesting architecture

The purpose of this section is to convert, store and manage the impinging RF energy made available by rectennas which provide rectified signals. For this reason power converters will be essentially based on DC/DC architectures. In this perspective the main goals will be:

1. Minimization of intrinsic power, in order to allow operation even in the harshest conditions
2. Minimization of silicon area, by defining solutions which minimize component count and the volume of the silicon chip with respect to tag size
3. Extraction of the maximum possible power, by providing an optimal bias to rectennas.

In this context, several methods have proven to provide suitable platforms for converting available power. As an example ultra-low power microcontrollers have been successfully used to control power conversion while achieving a positive power budget even with very low levels of available power [52,53] (see the architecture in Fig. 20). This type of solutions also allows to share the microcontroller, which normally would operate in sleep modes, for running the user applications.

However, in this project, this type of solution is likely to be taken into account in case of sufficient impinging power. In fact, solutions on discrete components are expected to consume at least few μW during power conversion. It is also worth to mention that solutions based on a high number of electronic components may prevent from reaching the target of a “green” system. However, they may represent a suitable platform for testing purposes, in order to assess the performance of specific energy harvesting or power management policies.

For this reason, a viable solution that will be investigated is the use of micro- and nano-electronic technologies. The use of integrated processes, such as Complementary Metal Oxide Semiconductor (CMOS), may bring significant advantages with respect to discrete electronics: a first advantage resides in the extreme minimization of circuit area (about 1 mm^2), thus contributing to achieve the objective of “green” tags. In this perspective, both the sensing interface and digital application circuits (e.g. for driving backscatter communications) may be integrated without affecting silicon area; secondly, the use of miniaturized circuit structures allows to significantly decrease their intrinsic power consumption. Recently, ultra-low values of intrinsic power of tens-hundreds of nW have been demonstrated for harvesting power from multiple independent sources [54]. Several techniques will be considered, e.g. sub-threshold design, active duty-cycle modulation, reduction of bias currents, use of asynchronous logic for control, and so on. This will allow to operate even with very low levels of available input power from energy sources, as low as $1 \mu\text{W}$ or less. Microelectronic design should guarantee an optimal bias to rectennas in order to achieve the highest possible RF-to-DC energy conversion efficiencies. However, this should be dealt by defining suitable trade-offs between the harvested power and power spent by control circuits. Policies based on fractional open circuit voltage MPPT algorithms have shown to represent a satisfactory trade-off. As a reference, the current state of the art proposes integrated solutions for power conversion of tens/hundreds of μW by spending tens/hundreds of nW, with electrical efficiencies around 75-85%.

Besides all this, even if sufficient input power levels were available, the voltages output from rectennas might be very low, in the order of tens/hundred mV, well below the threshold voltages of active devices. For this purpose, the use of specific bootstrap structures, such as step-up oscillators, or sub-threshold circuits will be investigated. In this case an integrated design of rectennas and electronic circuits is expected

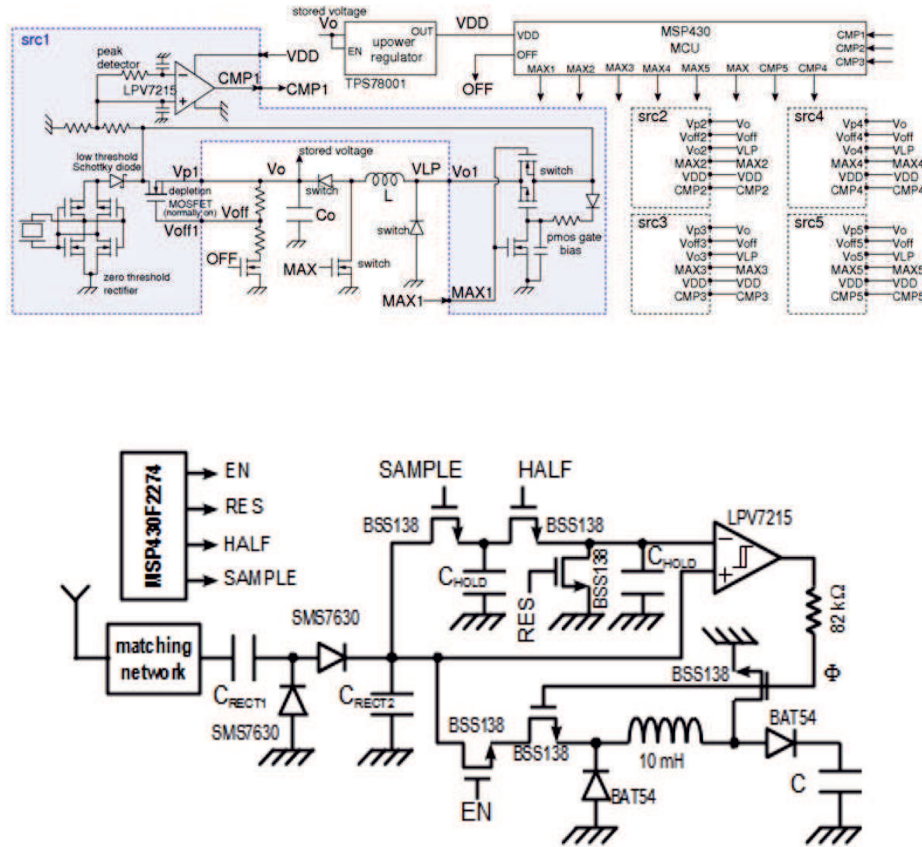


Figure 20: Micro-power implementations of power conversion circuits from environmental sources [52, 53].

to bring significant optimizations [55].

The energy harvesting architecture will be based on the structure presented in Fig. 21.

Another important aspect to deal with in energy harvesting is energy storage. This is usually accomplished by using capacitors or batteries. As a matter of fact, only limited values of on-chip capacitances can be implemented in a CMOS chip, typically lower than 1 nF. This limitation lets us foresee several scenarios for system architecture, depending on the values of impinging power and of application requirements.

1. *Short-term energy storage.* The tag does not contain external energy storage devices and is normally inactive (off). When subject to impinging RF power, the tag wakes-up and, thanks to its very low power consumption, is able to sustain an ultra-low power sensing/communication application. This solution minimizes the volume required by electronic components. However, because of the very low values of integrated capacitances, the application is not likely to be sustained energetically when incident RF radiation is no more available, i.e. the tag is available only upon interrogation and no data logging features are available.
2. *Medium term energy storage.* The tag includes an external capacitor as energy storage device. The use of an external capacitor allows to store higher amounts of energy for prolonged sustainability of user applications. This may be accomplished without any significant area increase, e.g. with tiny Surface Mounting Device (SMD) capacitors. The application circuits, with respect to the previous case, can have higher peak power requirements. In this context, energy can be provided periodically, e.g. by means of RF energy showers, so that the energy harvesting module converts

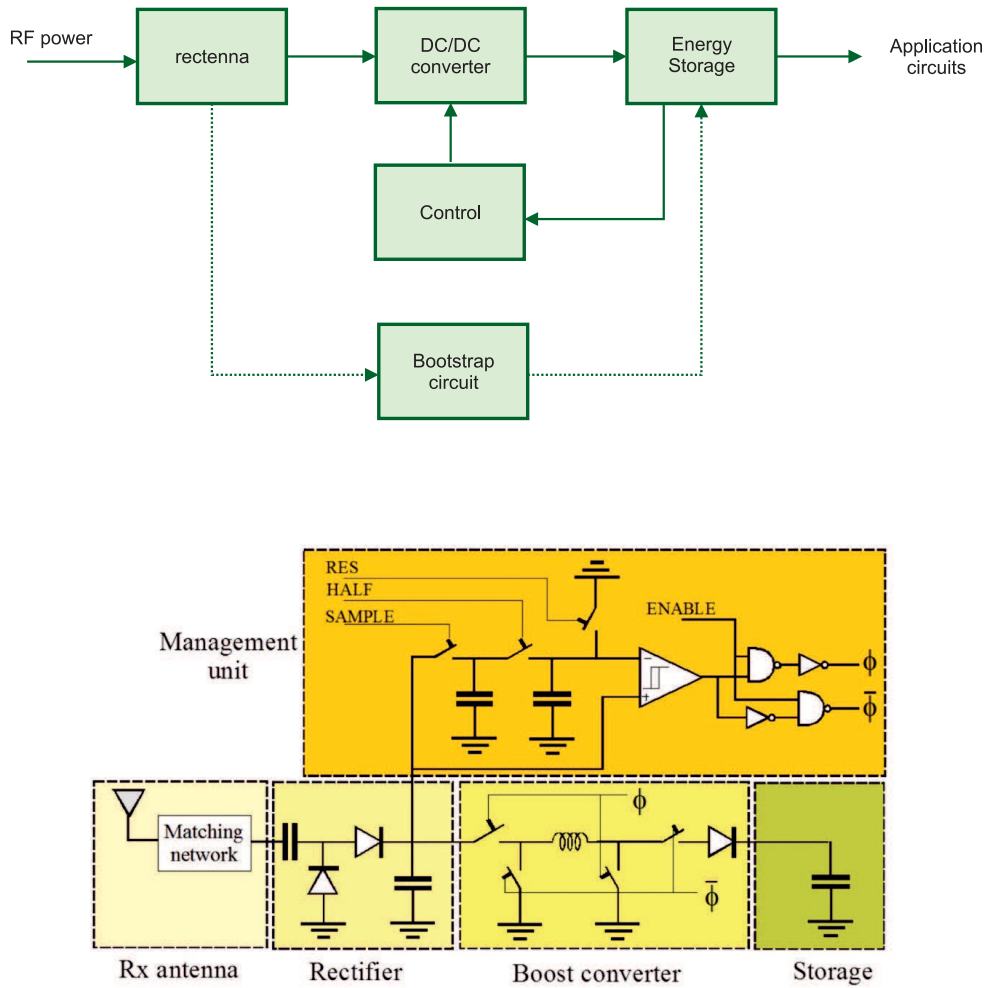


Figure 21: Block diagrams of the energy harvesting sub-system and of a possible basic implementation.

and stores it. The medium-term availability of energy allows applications such as data-logging. Bootstrap circuits have to be included, since the tag may reach a fully discharged mode without reference voltages.

3. *Long-term energy storage.* The tag includes a (rechargeable) battery as energy storage device. This type of solution allows to design active tags, with miniaturized electronics. Tiny SMD rechargeable batteries able to sustain active RF transmissions are available [56] and may be easily embedded in limited space. Reference voltages are available from batteries, so that bootstrap circuits are generically not required.

3.3 Sensor architecture

In a sensor architecture, a primary role is played by its electrical interface. Transduced quantities have to be detected and converted into digital form with satisfactory accuracy, repeatability, and precision. In GRETA, one of the most challenging issues is the definition of an acceptable trade-off with energy consumed during operation.

Since several types of sensors are available commercially, or can easily be embedded in a CMOS substrate, the proposed sensing electrical interface will be designed for being compatible with generic

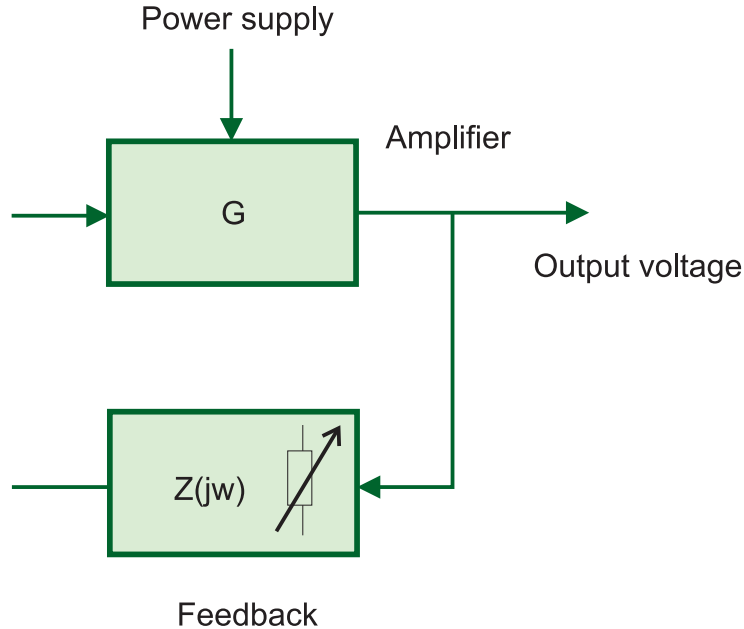


Figure 22: Generic structure of sensing architecture.

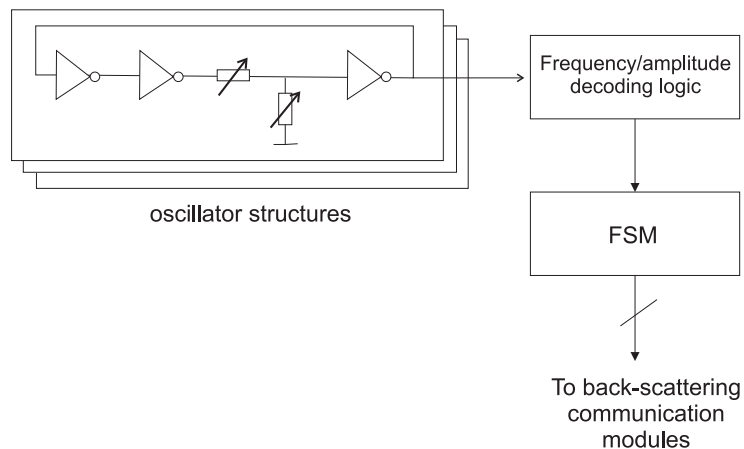


Figure 23: Proposal of a low-power sensing architecture.

impedance sensors. Suitable architectures will be investigated, for ensuring reliable operation in the strict power budgets:

1. SAR ADCs, which have shown to operate with very low power [57, 58]
2. Architectures based on micro- and nano-power oscillators. Variations in impedance associated to transduction are expected to produce changes in frequency or amplitude of the generated waveforms. One of the simplest oscillating structures is the ring oscillator. Mechanisms for transducing variations in frequency based on digital logic hold the promise of nano-power operation. This type of architecture should also deal with issues related to mismatch of devices, stability over temperature.
3. Use of conventional high-accuracy interfaces with limitations in the duty cycle of operation.

3.4 Low power microcontroller

A series of ultra-low power microcontroller have been available on the market for some years. Such devices typically offer 8 bit or 16 bit architectures with current consumption in the order of 200 uA/MHz

in their active mode, as well as the ability of operating in deep sleep modes characterized by nano-power consumption. As an example, the TI MSP430 family [59] showed to achieve good performance and very low power requirements, and was used as control engine in several energy harvesting systems [52, 53]. New generations, such as the Wolverine devices from TI holds the promise of even further power reduction [60]. Among the notable technological innovations, it is worth to mention the integration of ferroelectric RAMs for implementing both code and data memories, which ensure state-of-the-art power consumptions. Several competitors also offer products with comparable performance, among which Microchip PIC XLP micro-controllers with nanoWatt technology [61]. In micro-power applications, extreme power reduction are achieved by alternating active modes to deep sleep modes with a very low duty cycle. Basically, the micro-controller should execute the minimum number of instructions in the minimum possible time, e.g. with high frequency bursts, in order to get back as soon as possible in a sleep mode:

$$I_{avg} = \frac{T_{on}I_{active} + T_{off}I_{sleep}}{T_{on} + T_{off}} \quad (25)$$

As long as $T_{off} \gg T_{on}$ and $I_{sleep} \gg I_{active}$, the objective of extreme power reduction is achieved. For extremely low duty cycles of operation, the average drawn current approaches the value of the sleep current, which represents the baseline consumption.

The use of commercial products, although leading to notably low values of consumed power, cannot achieve the performance obtained by custom integrated solutions. As an example, the 8 bit Phoenix processor [62] achieved a 2.8 pJ energy consumption per cycle, corresponding to 297 nW at 106 kHz in active mode, while 30 pW stand-by mode was implemented. Another notable example of micro-power processor, with 32 bit architecture and DSP capabilities is the Icyflex core achieving 120 μ W/MHz at 1.0V, just below the threshold voltage of transistors.

In this context, the use of custom integrated solutions may offer flexibility while guaranteeing strict power budgets. In this project the most important function of the micro-controller is to control switch modulation during back-scattering communications. A proposal that will be investigated in GRETA is the use of custom digital control logic, to be coupled both with sensing interface and with the energy harvesting integrated circuits. As an example, a series of finite state machines controlling basic digital structure (e.g. tens or hundreds of transistors) will be taken into account and assessed for this purpose. The main advantage of this approach is to achieve further reduction of intrinsic power, in order to operate with very low impinging RF power, or for longer periods when powered by the energy storage device. A custom logic should significantly reduce the number of switching nodes with respect to a wired micro-controller. In addition, basic features of configuration can be easily included, in order to allow some degrees of flexibility during operation.

3.5 UWB backscatter modulator

Passive RFID tags are fundamentally different from conventional radio transceiver because they have no conventional RF receiver components (mixers, amplifiers, ...). The tag serves only as a passive transponder that returns a portion of its received power with modulation. The modulation is performed by means of a backscatter approach changing the antenna reflection properties according to information data: when an E.M. wave encounters an antenna, it is partially reflected depending on antenna configuration. Theoretical and analytical formulation of the backscatter communications and of the link budget can be found in [63, 64].

The backscatter modulator allows to change the load impedance connected to the antenna, and, therefore, to backscatter the signal. There are several ways to accomplish this. One is using a switch at the terminals of the antenna: if it is open there is no mis-match between the antenna and the load; meanwhile, if it is closed, the terminals of the antenna are short-circuited resulting in a reflection-coefficient change. To implement the switch, several nonlinear semiconductor devices (Schottky diodes, varactor diodes, PIN diodes, FETs and MOSFETs) can be used. In order to activate the switch, a pulse generator devices having sub-nanosecond transition is required [65]. The modulator architecture and its complexity vary with

the operating frequency and the adopted modulation type: for example it can change the input capacitance rather than the input resistance, leading to a phase modulation like the Phase Shift Keying (PSK) rather than Amplitude Shift Keying (ASK). For UWB tags three type of modulation are generally used: On-Off Keying (OOK), Pulse Position Modulation (PPM), and Pulse Amplitude Modulation (PAM); but also other types like the Binary Phase Shift Keying (BPSK) and the Time Hopped Pulse Position Modulation (TH-PPM) can be used. Several architectures and design criteria are described in [8, 51, 67–75].

Two architectures are proposed for the UWB backscatterer modulator: the first one based on diodes, fig. 24a, and the second one based on MOSFETs, fig. 24b. In these cases, the backscatter modulator reduces to a simple switch. The devices must be chosen in order to operate in the overall UWB frequency range (3.1 – 10.6 GHz). The modulator based on diodes generates a short circuit between the antenna terminals applying a bias voltage to the diodes. The high-impedance line avoids to short the RF signal, to obtain a balanced configuration, and it can be implemented with an inductor. The configuration based on MOSFETs generates a short circuit between the antenna terminals applying a bias voltage between the gates and the sources of the two transistors. Also in this case a balanced configuration is obtained avoiding the use of an high-impedance line between the antenna terminals. The symmetry of the two architectures allows to obtain RF virtual grounds at the bias terminals.

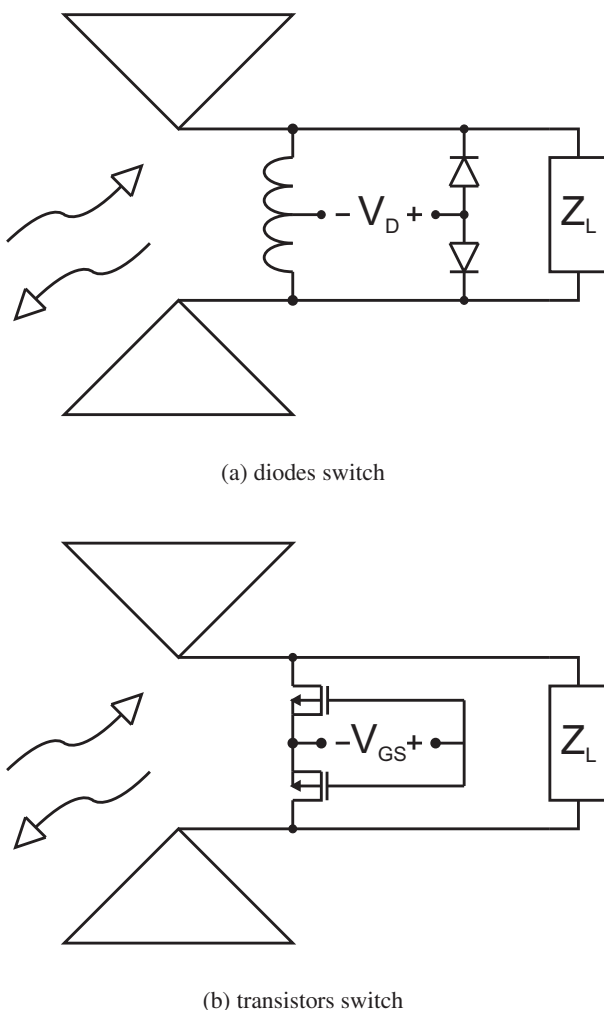


Figure 24: Modulator architecture based on diodes (a) and on transistors (b).

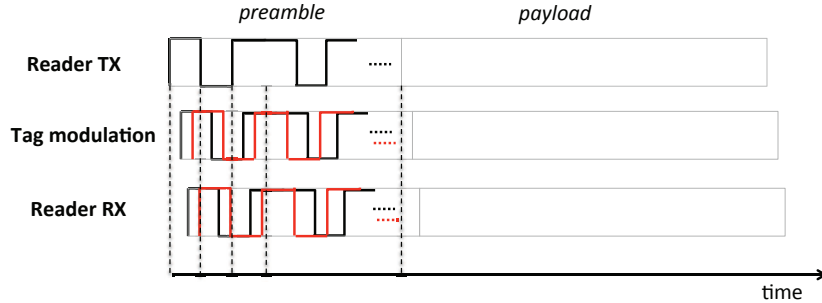


Figure 25: System time evolution for data synchronization architectures.

3.6 Data synchronization architectures

Time synchronization is critical in backscattered UWB data due to the peculiar system architecture. A system time representation is reported in Fig. 25. Typical synchronization algorithms for UWB localization are derived in the context of conventional UWB system, which involves one-way channel propagation and the signal modulations are done at the transmitter. Consequently, classical techniques cannot be directly applied to UWB backscattering RFID system.

We distinguish two important aspects of the synchronization.

- Clock synchronization: the internal clock of the tag might differ from the reader's clock. By keeping a simple tag's implementation, a free running oscillator could be implemented in the tag. However, clock drifts and code offsets become critical problems for the complexity of the reader. Powerful acquisition techniques and the TOA estimator robust to clutter, e.g. as those proposed in Xu and Law [76], can be adopted at a reader's side to compensate for clock offset. The complexity of the synchronization algorithms is reduced when tags are equipped with UHF receivers. By the exchange of UHF signaling, the reader can force alignment of the tag's clock. This is performed with standard mechanisms as for EPC Gen2 [49] devices.
- Code synchronization: the tag's spreading code is not in general time aligned to the reader's code. Hence the received signal model of UWB backscattering system is significantly different from that of conventional UWB system. The code synchronization is achieved in two steps. First, the reader should synchronize with the tag's code. Once the reader and tag are aligned, the reader needs to recover its own code for the TOA estimation.

An investigation of the synchronization problem in terms of procedures, algorithms and architecture in both scenarios is a major near term research topic.

3.7 System integration

This section is intended to provide an overview of the technological approach adopted for complete system integration, based on the use of the innovative substrate integrated waveguide (SIW) technology in conjunction with eco-friendly materials and manufacturing techniques.

Planar technologies represent the ideal choice for the implementation of microwave and mm-wave integrated complex circuitry. Traditional solutions are based on microstrip line and coplanar waveguide (CPW) technology, which are suitable to be realized on thin dielectric substrates. If the frequency is low (e.g., few GHz), these planar structures ensure inexpensive manufacturing, good electromagnetic performance, and low radiation losses. Nonetheless, when the frequency increases (e.g., above 30 GHz), losses become unacceptable. In all cases, however, planar transmission lines are subject to cross talk between adjacent lines, and the circuits require a packaging for practical applications. All these issues are solved by adopting a shielded waveguide, such as the metallic rectangular waveguide. Hollow rectangular waveguides guarantee low losses, complete shielding, and no radiation loss. On the other hand, the major

drawbacks of metallic waveguides are the bulky structure, high cost, and the difficulty to integrate active devices.

A novel solution is represented by the Substrate Integrated Waveguide (SIW), which combines the advantages of planar structures and of metallic rectangular waveguides [77–82]. SIW structures are similar to traditional rectangular waveguides, and are implemented in dielectric substrates by using two rows of metalized holes that connect the two ground planes of the substrate (Fig. 26). In this way, waveguide-like structures (that are non-planar) can be fabricated by using the standard process of planar circuits (chemical etching, LTCC, …). SIW structures exhibit most of the properties of traditional metallic waveguides (e.g., propagation constant, losses, field pattern) and share the same advantages (high quality factor, high power handling capability). Compared to planar transmission lines (microstrip or coplanar waveguide), SIW structures exhibit lower losses [81, 83]. Moreover, SIW-to-microstrip transitions can be easily realized, and this opens new perspective, both for implementing SIW and microstrip components on the same substrate and for the possibility of integrating microelectronic chips and microwave components on the same board.

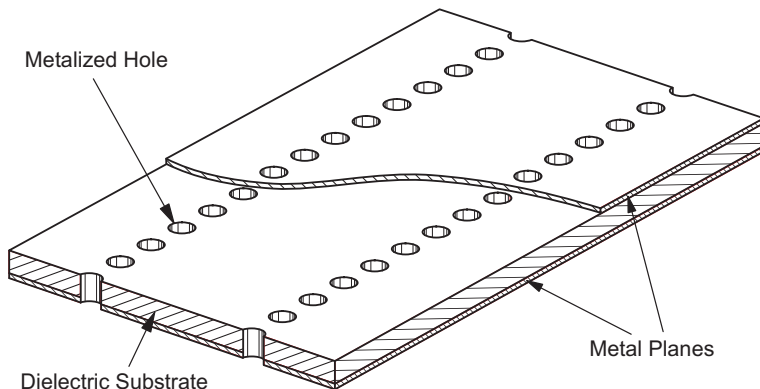


Figure 26: Geometry of a substrate integrated waveguide (SIW) structure.

A very important consideration in SIW design is related to the mechanisms of loss. Three mechanisms of loss are involved in the propagation of electromagnetic waves in SIW structures: conductor losses, dielectric losses and radiation losses [81, 83, 84]. Conductor loss is related to the power dissipated by Joule effect on the metal surfaces, and it depends on the finite conductivity of top and bottom metal layers as well as of metal posts. Conductor loss is affected by the substrate thickness, and it can be reduced by increasing the substrate thickness. The dielectric loss is related to power dissipation in the dielectric substrate, and it depends on the dielectric loss tangent of the substrate material. This kind of loss depends only by substrate characteristics and not on the geometry of the SIW structure. Standard substrates exhibit a value of loss tangent in the order of 10^{-3} . In several cases, dielectric loss is the major source of loss in SIW structures. The third mechanism of loss is related to radiation leakage. It is caused by the gaps between pairs of metal posts and could be minimized with proper design rules. Typically, the longitudinal spacing of the metal posts should not exceed 2.5 times the post diameter [81].

The main advantage of SIW technology is the possibility to monolithically integrate all components in a single substrate, with no need for interconnects or transitions between elements fabricated with different technologies, thus dramatically reducing losses and parasitics. This design approach leads to the "System on Substrate" (SoS) concept [85, 86]: it represents the ideal platform to develop low-cost, high performance, easy-to-fabricate mm-wave circuits, which integrate passive components, active elements, and antennas (Fig. 27). SIW technology has been used in the implementation of several components,

including filters, couplers, oscillators, antennas [81]. Compact and broadband interconnects, particularly suited to the development of UWB systems, have been proposed and experimentally verified [87, 88].

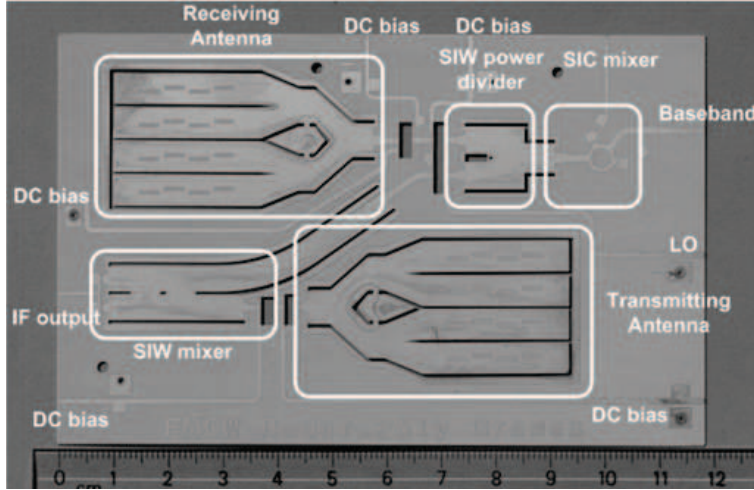


Figure 27: Example of "System on Substrate" (SoS) concept: 24-GHz Frequency-Modulation Continuous-Wave radar front-end [86].

Another important aspect is related to the manufacturing of the microwave components. The manufacturing of planar microwave circuits (including both microstrip and SIW circuits) is typically based on the chemical metal etching on plastic or ceramic substrates. In this way, it is possible to reproduce arbitrary shapes on a face of dielectric substrates: chemical etching is widely spread for several applications, it is cheaper and a lot of substrates could be manufacturing all together. Nevertheless, this approach results in significant environment impact because chemical toxic solution and heavy metal (i.e. copper) are involved. Moreover, standard substrates are not eco-compatible and at the end of their operational life have to be dumped. For these reasons, since a long time there is an open discussion about possible alternative fabrication techniques, aiming at reducing the environmental impact of electronic circuits fabrication.

Among the proposed alternative solutions, the use of paper looks like an optimal candidate [89–104]: in fact, paper is a widely available and extremely cheap material, and it is completely environmental friendly, both during its production and at the time of its dumping. Paper employed in order to manufacturing microwave circuits has a hydrophobic coating and is commercially available. The single sheet of paper is 0.230 mm thick and multi-layer design is possible by heat bonding. Electromagnetic features of paper have been measured in a frequency range up to few GHz, showing a dielectric permittivity $\epsilon_r = 2.85$ and a loss angle $\tan \delta = 0.053$ [105, 106]. Manufacturing of paper-based circuits is straightforward, cheap and eco-friendly, as no toxic chemical solutions are required. In particular, special ink with silver nano-particles is used in order to realize conductive shapes, transmission lines and ground layers. The ink is simply printed and after a proper curing process it achieves high conductivity. Not only planar shapes could be realized on paper substrates, but also metalized via holes can be manufacturing on the same substrate. In detail, the single hole is drilled by a standard drilling machine and the metallization is achieved by using conductive paste.

This fabrication process appears very suitable for the realization of SIW components, as it allows for arbitrary geometry and multi-layer configuration, thus fully exploiting the design flexibility of SIW technology. Preliminary examples of SIW interconnects, components, and antennas on paper substrates have been recently proposed [105–107].

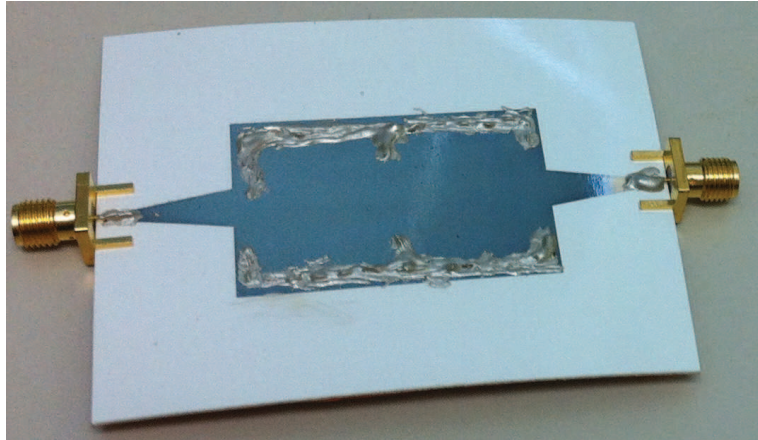


Figure 28: Preliminary example of SIW component on paper: inkjet-printed paper-based SIW filter [105, 106].

3.8 Antenna system

3.8.1 UWB antenna

Planar antennas in SIW technology can be obtained in different ways: the most common structures are the SIW slot array antenna, the SIW leaky-wave antenna, and the SIW cavity-backed slot antenna [82].

SIW slot array antennas look very similar to classical slotted-waveguide antennas, where a number of longitudinal resonant slots are etched in the broad wall of the waveguide (Fig. 29). The longitudinal spacing of the slots is usually half guided-wavelength and the slots are alternatively positioned, slightly offset from the vertical symmetry plane: this topology permits to feed the radiating slots with the proper amplitude and phase for broadside radiation at the desired operation frequency [108]. SIW slot arrays can be designed by adopting the method developed by Elliott [109], taking care to include the effects of internal high-order mode coupling: in fact, this coupling mechanism cannot be ignored in SIW structures, since the substrate thickness is usually much smaller than the SIW width. Circular polarization is obtained by alternate rotation of slots by $+45^\circ / -45^\circ$.

Leaky-wave SIW antennas are straight SIW structures, with increased longitudinal spacing in one row of side-wall metal cylinders and located near the edge of the dielectric substrate (Fig. 30) [110]. These antennas exploit the radiation leakage due to the sufficiently large gaps between the side-wall metal cylinders. The radiation leakage increases if the gaps are large, and this permits to reduce the overall length of the leaky-wave antenna at the cost of large beam-width. Nonetheless, large gaps may lead to band-gap effects, which prevent the propagation of the electromagnetic field inside the SIW and reduce the operation bandwidth of the antenna. In leaky-wave SIW antennas, the direction of maximum radiation depends on the propagation constant of the waveguide mode, and the radiation pattern can be computed from the value of the electromagnetic field at the edge of the SIW structure. One of the major issues in the design of leaky-wave SIW antennas is related to the field reflection at the interface between dielectric and air: a maximum value of allowed dielectric permittivity can be calculated, which prevents total internal reflection at the dielectric/air interface [110].

Several topologies of cavity-backed SIW antennas have been also developed [111–113]. The structure proposed in [111] is very simple: it consists of a SIW cavity, fed by a coplanar waveguide etched on one side of the substrate, with a rectangular slot located on the opposite side (Fig. 31). A more compact solution was proposed in [112], where the rectangular slot is replaced by a meander line. A Ku-band SIW

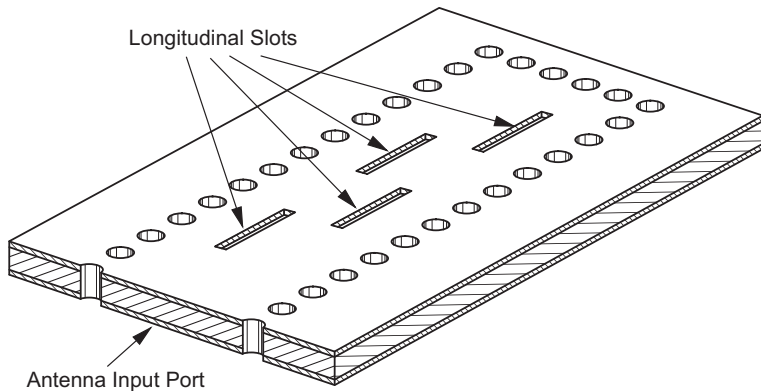


Figure 29: SIW slot array antenna.

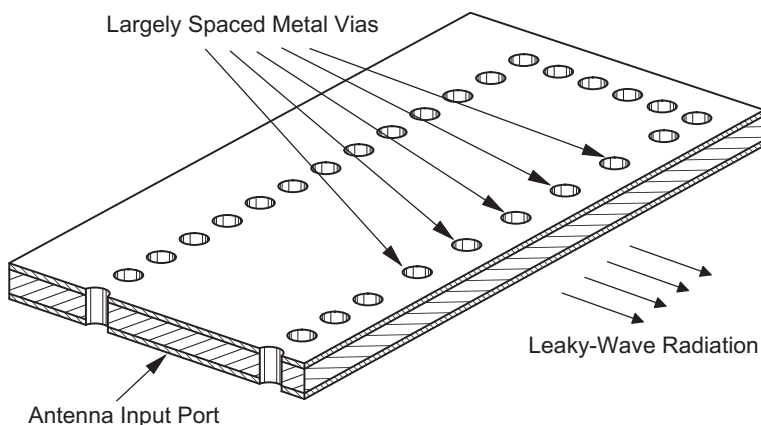


Figure 30: SIW leaky-wave antenna.

cavity-backed antenna array was developed in [113]: this antenna consists of a 2x2 array of metal patches, backed by SIW cavities. The structure was implemented by adopting a double layer PCB fabrication process, with the metal patches fed by a microstrip feeding line in the top layer, and SIW cavities in the bottom layer. This solution guarantees a relatively high aperture efficiency of 70% over a reasonably wide bandwidth (9%), and a front-to-back ratio of 20 dB.

Active SIW cavity-backed antennas were also developed, by integrating a transistor oscillator in a cavity-backed antenna. The first implementation [114] was based on the simple structure proposed in [111], where the gate of the transistor is connected to the input coplanar waveguide of the antenna. In this configuration, the role of the SIW cavity is twofold: it is used as a feedback by the transistor, with a beneficial effect on the phase noise of the oscillator, and simultaneously it permits to improve the slot antenna performance, by suppressing the excitation of surface waves. A more compact version of active SIW cavity backed antenna was proposed in [115], where the entire circuitry is located on top of the SIW cavity, thus permitting the implementation of two dimensional arrays.

Besides the major SIW antenna categories described above, other antenna configurations have been

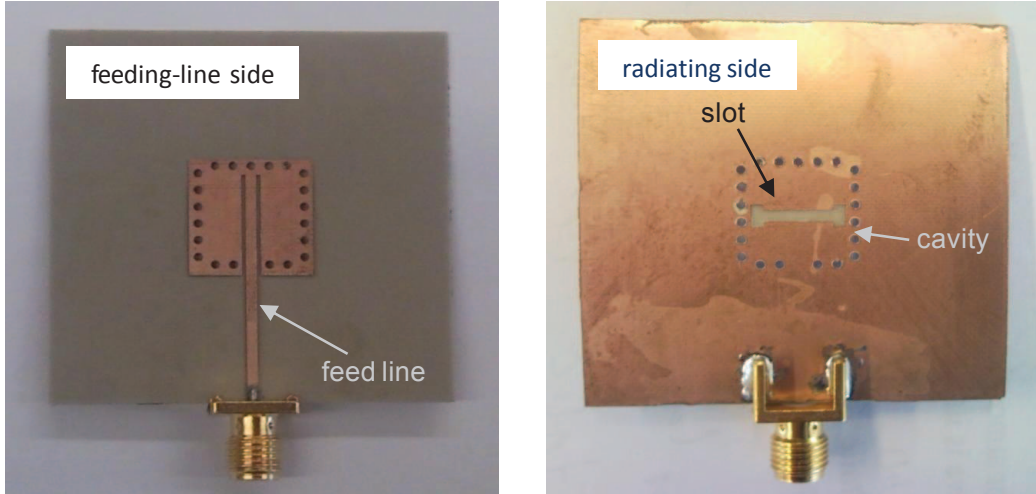


Figure 31: SIW cavity backed antenna.

proposed for implementation in SIW technology.

An H-plane sectoral horn antenna in SIW technology was proposed in [116]. The flares of the horn are realized by using metal vias, and a dielectric loading, integrated in the same substrate, allows high gain and narrow beam-widths in both the E- and H-plane.

The concept of the Yagi-Uda antenna has been exploited to develop SIW antennas. The first version [117] consists of a truncated SIW structure, with an additional row of metal cylinders axially aligned in front of the aperture to act as the directors of a Yagi-Uda antenna. A prototype operating at 60 GHz was demonstrated, with a gain of 12 dB. Another version was proposed in [118] and consists of a stacked multilayer array, resulting in a very small footprint of the entire geometry.

The dual V-type linearly tapered slot antenna [119] represents a modified version of the Vivaldi antenna. Due to its multimode SIW feeding network, this structure is able to generate both the sum and difference beams, and for this reason it is particularly suitable for monopulse antenna applications.

The major limitation of classical SIW antennas is related to bandwidth, which is limited to 10-15% in most cases. For this reason, special care is needed in the choice of the antenna topology for the UWB system to be designed, in order to meet the specifications in terms of operation bandwidth.

3.8.2 Harvester antenna

The purpose of this section is to provide a highly efficient rectifying antennas (rectenna) able to collect energy from the environment and to provide sufficient DC power to supply the entire GRETA system. Energy harvesting from ambient RF sources has demonstrated to be a potential solution to this problem [120, 121]. However DC powers collected by such a kind of subsystem are typically of the order of few μ Ws [122], even without considering channel dispersion and antennas misalignment effects. We thus foresee the presence of dedicated RF sources (“RF showers”) able to provide on demand the needed amount of energy to be collected by the harvesting section of the tag. One of the typical requisites of rectennas is the circular polarization property of the receiving antenna in order to be able to capture any kind of receiving field. In the considered scenario, the known position of the “RF showers” could allow to reduce the degrees of freedom of the radio link, since the polarization of the incoming RF signal could be properly determined. Therefore we devote great attention to efficiency and to dimensioning of the

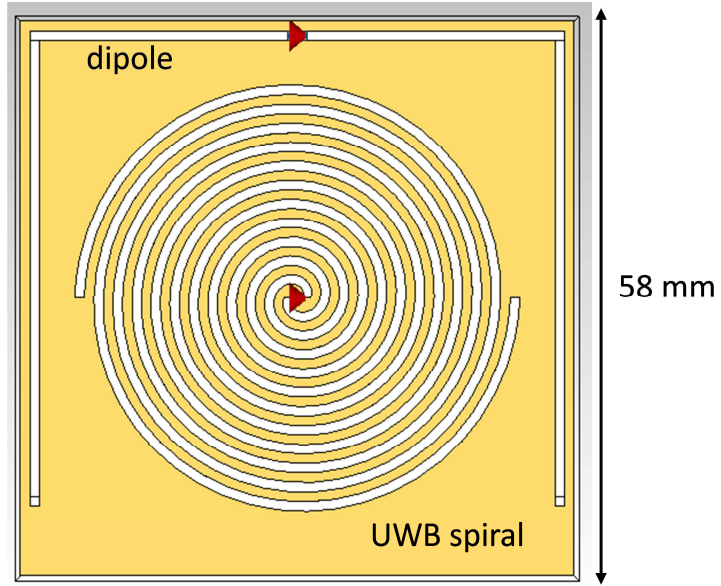


Figure 32: Solution with one UWB antenna and one dipole harvester antenna on paper substrate.

harvester antenna. However, in order to permit a random distribution of the tags, solutions able to recover energy from both vertically and horizontally polarized signals will be developed, too.

In this scenario, two different architectures of the harvester antenna will be investigated.

3.8.2.1 First harvester antenna solution

A first possible solution is to separate the harvester antenna from the UWB communication antenna. In this case traditional UHF antennas can be used: a meandered planar dipole [123] is considered first, due to its high efficiency (limited only by paper substrate losses), low-directivity property and ease of realization in the space around the UWB antenna. A possible implementation is shown in Fig. 32, where a U-shaped dipole is placed near an UWB antenna (an Archimedean spiral antenna, in this case). The meandered topology of the dipole, slightly affects its polarization properties with respect to a straight dipole; however the main component of the radiated field is horizontally polarized (referring to the situation depicted in Fig. 32). The behaviour of the present rectenna will force to properly place the tags with respect to the “RF showers” in order to maximize the power transfer link (i.e. the antennas are placed in the maximum link direction).

Alternatively, the harvester antenna subsystem (and consequently the rectifying section, too) can be extended by placing two cross-polarized dipoles around the UWB antenna. A possible solution is reported in Fig. 33, where different meanderization is retrieved, due to lack of space.

Preliminary study of the simple U-shaped topology of Fig. 32, for a dipole antenna operating at 868 MHz has been carried out on a paper substrate with the following characteristics: $\epsilon_r = 2.85$, $\tan(\delta) = 0.053$, thickness = 0.69mm (corresponding to 3 layers of paper), conductive ink conductivity = $1.5 \cdot 10^7$ S/m. Of course the presence of the UWB antenna must be considered in the electromagnetic design, due to the strong interference with the near-field dipole (i.e. antenna impedance). For this purpose the antenna system consisting of dipole and the UWB spiral is computed as a two-port antenna instead of two one-port antennas. Fig. 34 shows the simulated results in terms of scattering parameters of the two-port network. Very good predicted results can be observed which are: i) the wide-band behaviour of the spiral (S_{11}), ii) the resonance of the dipole (S_{22}), and, above all, the ports de-coupling requirement (S_{21}).

Efficiencies of the order of 85% with omnidirectional radiation pattern in the plane orthogonal to the horizontal arm of the dipole can be easily obtained, as shown in Fig. 35, where the electric field dipole radiation surface is plotted.

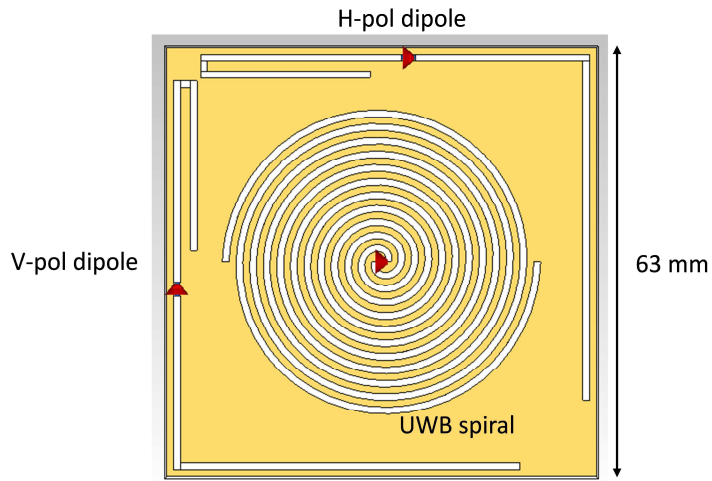


Figure 33: Solution with one UWB antenna and two cross-polarized dipole harvester antennas on paper substrate.

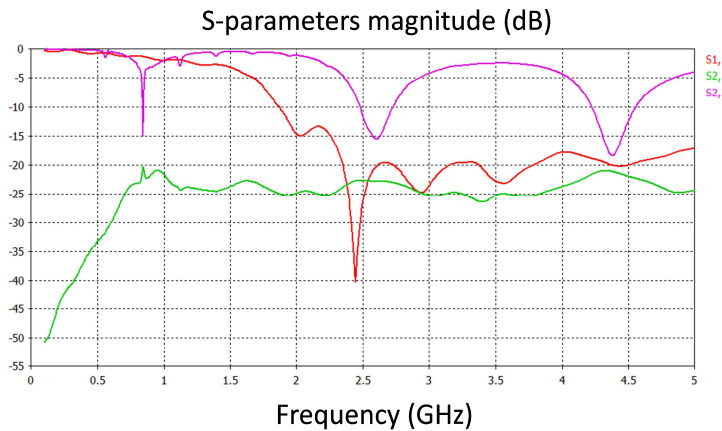


Figure 34: Scattering parameters behaviour of the antenna system of Fig. 32.

3.8.2.2 Second harvester antenna solution

A more challenging solution is to exploit a unique UWB antenna for both communicating and harvesting. The “RF showers” operating frequency, in this case, has to be carefully selected in the available operating bandwidth. A possible solution for harvesting purposes could be the use of frequencies near the lower edge of the UWB band (e.g. WiFi frequency = 2.45 GHz) in order to keep the UWB band completely free for communication. In this case in cooperation with UNIPV the proper UWB antenna topology. However a preliminary study of this solution must be carried out: we have thus considered as a possible solution an Archimedean Spiral antenna [124] of the same kind reported in Fig. 1. In order to cover the desired band (roughly from 2.4 up to 5 GHz) a 53 – mm² piece of paper is needed (see Fig. 36).

The simulation of such subsystem predicts efficiencies ranging from 75% up to 85%, from 2.4 up to 5 GHz, respectively, and a bidirectional behaviour in the whole frequency band, as demonstrated by the radiation surfaces at 3 and 5 GHz of Fig. 37. In this case also circular polarization is automatically guaranteed. Other UWB antenna topologies will be also considered, such as logarithmic spiral antenna or simple UWB monopoles [125].

One delicate issue of the harvester (and also UWB) antenna(s) is the absence of a background shield. This fact has a twofold drawback: i) on the one hand, the omni-directional (in the dipole-like solution) or bi-directional (in the spiral-like solution) radiation pattern degrades the power link budget, since in

E-field @ 868 MHz (linear scale)

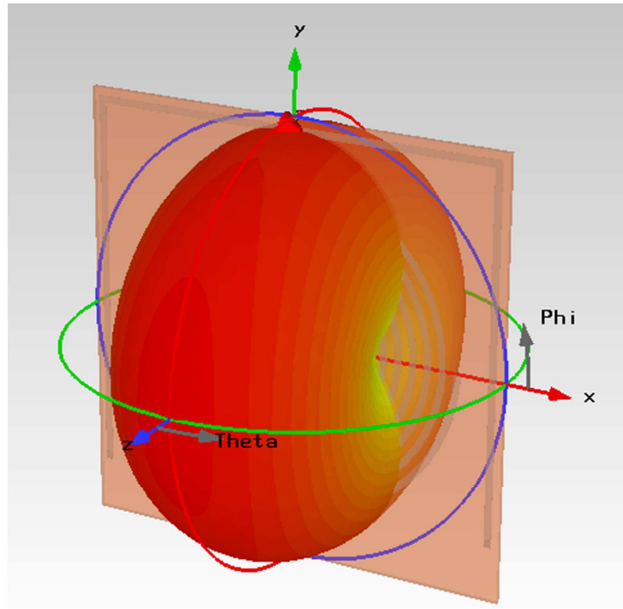


Figure 35: Radiation pattern of the dipole antenna of Fig. 32.

the presence of “RF showers” the Direction of Arrival (DoA) of the signal is usually known, and a low-directivity behaviour can be a limiting factor; ii) on the other hand, the absence of a ground-plane implies a strong dependency of the antenna radiating properties on the background material on which the tag is placed. Denser materials behind the paper substrate (e.g. liquids, or human bodies) could drastically change or damage at all both the near- and the far-field behaviour of the antenna.

This is the reason why these antennas should have a background shield. The well-known theory of the shielded dipole [126] or of cavity-backed antennas [127] prevent from having low-profile antennas, since a ground plane at a minimum distance of $\lambda/4$ should be used. In order to maintain both a thin tag structure and the presence of a background shield, we want to investigate the use of Electromagnetic Band Gap (EBG) structures as background layers of the proposed antennas [128]. These solutions allow to provide, for instance, a further separator with perfect magnetic conductor-like behaviour: this way, the thickness of the whole tag is simply doubled (about 1 mm-thick), while the directivity of the antennas (both dipoles and spiral) is augmented (with a corresponding advantage in the power link budget) and the no-dependency on the background material is achieved.

Several topologies of EBG planes have been presented in literature [128, 129]. The most suitable to our green solution are those not involving lumped components [130]. An example of this kind is shown in Fig. 38, for a straight dipole antenna, where the dipole paper substrate is made transparent for visualization reasons.

3.9 Localization and tracking algorithm

Localization and tracking are processes of estimating position and trajectory of a target object, respectively, based on observations (measurements). The target position is not directly observable, therefore we refer to range-based, angle-based, or hybrid estimation depending on the nature of the measurements (distance, direction, or both, respectively) that have to be jointly processed to infer the target position. In particular, range-based localization is the most suitable for ultra-wide band (UWB) systems based on backscattering modulation. In this case, the TOA of the received signal is estimated as described in previous sections.

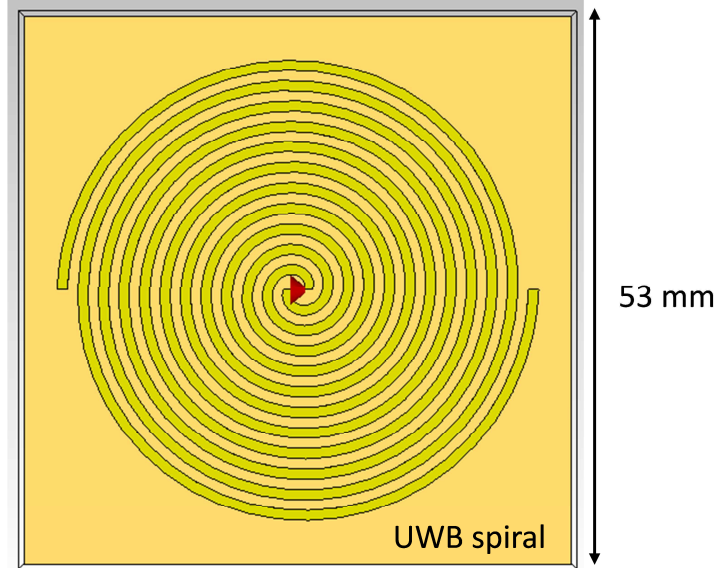


Figure 36: Standalone UWB spiral antenna.

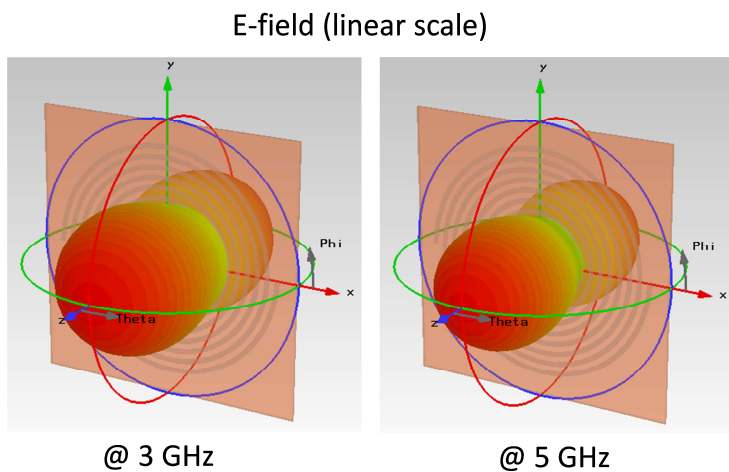


Figure 37: Radiation performance of the UWB spiral antenna of Fig. 36.

The preciseness of position and trajectory estimation depends on the accuracy of measurements and on the prior information available. Therefore, the choice of the suitable estimator requires a proper modeling of the variables to be estimated (target position and its dynamics) and the statistical characterization of the disturbances affecting the measurement process (operating environment and measurement system).

In general, localization deals with static targets and the estimation of their position, which are time-invariant vectors, while tracking deals with dynamic targets and the estimation of their trajectory, which are time-variant vectors evolving according to stochastic equations. Therefore, in the estimation theory, localization and tracking are related to the parameter estimation and the state estimation problems, respectively. In the following, we present the state of the art for the parameter and state estimators used in localization and tracking contexts.

3.9.1 Localization via parameter estimators

The localization process involves the estimation of the parameter \mathbf{x} , which is the static position of the target, based on a set of measurements $\mathbf{z}_{(1:k)}$ collected at each sensor from time 1 to k depending on the

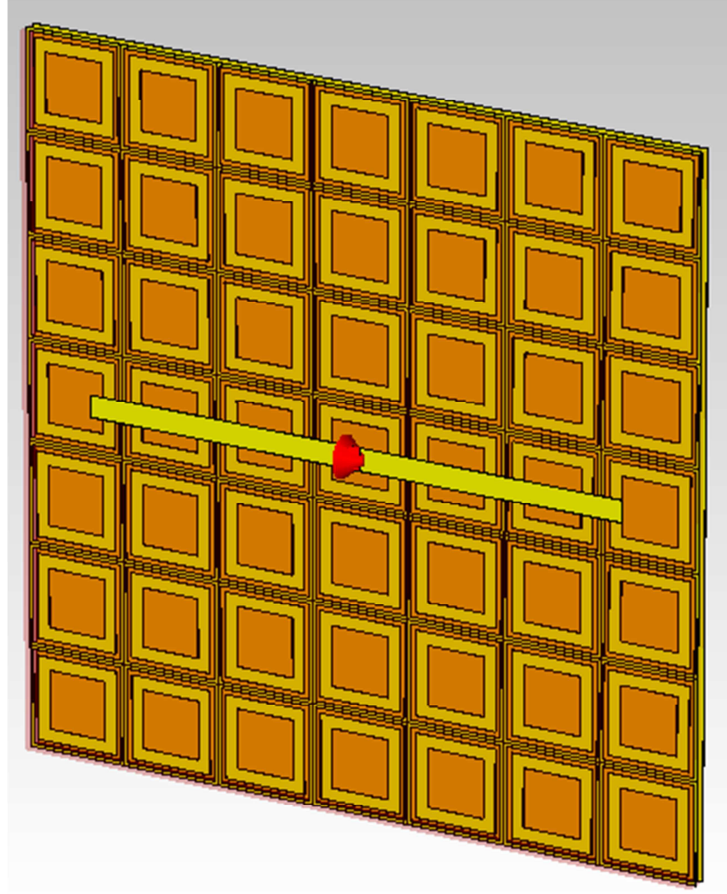


Figure 38: Dipole with EBG back plane.

system configuration. The problem of estimating a parameter \mathbf{x} given the set of measurements $\mathbf{z}_{(1:k)} = \{z_j\}_{j=1}^k$ in the presence of disturbances $\mathbf{w}_{(1:k)}$ requires the definition of a function $f(\mathbf{z}_{(1:k)})$, which is called estimator, and whose value is the parameter estimate $\hat{\mathbf{x}}_k = f(\mathbf{z}_{(1:k)})$ [131].

There are two different approaches to model the estimation problem. In the first approach, called non-Bayesian approach, the parameter \mathbf{x} is assumed to be deterministic (i.e., its true and unknown value is \mathbf{x}_0). In the second approach, called Bayesian approach, \mathbf{x} is a random variable with prior probability density function (pdf) $p_{\mathbf{X}}(\mathbf{x})$ and the parameter to be estimated is a realization of such random variable, which is invariant during the measurement process.

3.9.1.1 Maximum a posteriori and minimum mean squared error

The Bayesian approach relies on the determination of the posterior pdf (positional belief), which is obtained from the prior pdf by using the Bayes' rule $p_{\mathbf{X}|\mathbf{Z}}(\mathbf{x}|\mathbf{z}) = p_{\mathbf{Z}|\mathbf{X}}(\mathbf{z}|\mathbf{x})p_{\mathbf{X}}(\mathbf{x})/p_{\mathbf{Z}}(\mathbf{z}) = C p_{\mathbf{Z}|\mathbf{X}}(\mathbf{z}|\mathbf{x})p_{\mathbf{X}}(\mathbf{x})$, where C is the normalization constant. The estimate $\hat{\mathbf{x}}$ can be obtained from the positional belief with different methods. The most widely used methods are the maximum a posteriori (MAP) and the minimum mean squared error (MMSE), in which the mean or mode of the positional belief is considered, respectively [132].

3.9.1.2 Maximum likelihood and least squares

The estimators corresponding to the MAP and MMSE in the non-Bayesian approach are the maximum likelihood estimator (MLE) and the least squares estimator (LSE), respectively.

The MLE maximizes the likelihood function $p_{\mathbf{Z}|\mathbf{X}}(\mathbf{z}|\mathbf{x})$, which is a measure of the evidence from measurements. The corresponding estimate is given by

$$\hat{\mathbf{x}}_{\text{ML}} = \arg \max_{\mathbf{x}} \{ p_{\mathbf{Z}|\mathbf{X}}(\mathbf{z}|\mathbf{x}) \}. \quad (26)$$

The LSE minimizes the cost function represented by the squared measurement error $|z_j - h(j, \mathbf{x})|^2$, where $h(\cdot)$ is the measurement function, which relates the observation data to the parameter (e.g., the distance as a function of the target position to be estimated, given the sensor positions). The corresponding estimate is

$$\hat{\mathbf{x}}_{\text{LS}} = \arg \min_{\mathbf{x}} \left\{ \sum_j |z_j - h(j, \mathbf{x})|^2 \right\}. \quad (27)$$

We refer to linear or nonlinear LSE depending on whether the function $h(\cdot)$ is linear or nonlinear in \mathbf{x} , respectively. If the measurement errors are Gaussian and independent, then the LSE and the MLE provide the same estimate $\hat{\mathbf{x}}_{\text{LS}} = \hat{\mathbf{x}}_{\text{ML}}$.

3.9.2 Tracking via bayesian filters

The tracking process involves the estimation of position and velocity of the dynamic target, which are related to the first two moments of a state vector associated to a dynamic system. A dynamic system can be fully described by two equations: the evolution equation, which relates the current state vector to the prior state vector, and the stochastic measurement equation, which relates the observation data to the current state vector as

$$\mathbf{x}_n = f_n(\mathbf{x}_{n-1}, \mathbf{v}_{n-1}) \quad (28)$$

$$\mathbf{z}_n = h_n(\mathbf{x}_n, \mathbf{w}_n) \quad (29)$$

where \mathbf{x}_n is the state vector at time t_n , \mathbf{v}_n is the process noise vector, \mathbf{z}_n is the measurements collected by sensors at time t_n , and \mathbf{w}_n is the sensor noise. In general, these two equations are nonlinear. The state estimator, called filter, represent the algorithm for the recursively estimation of the state $\hat{\mathbf{x}}_n$ from the measurements $\mathbf{z}_{(1:n)}$.

The Bayesian filters rely on the quantification of the posterior pdf (positional belief) and require the pdf of the current state conditional on the previous state, and the pdf of the observation state conditional on the current state as

$$p(\mathbf{x}_n | \mathbf{z}_1, \dots, \mathbf{z}_n) = \frac{p(\mathbf{z}_n | \mathbf{x}_n) p(\mathbf{x}_n | \mathbf{z}_1, \dots, \mathbf{z}_{n-1})}{p(\mathbf{z}_n | \mathbf{z}_{n-1})} = C p(\mathbf{z}_n | \mathbf{x}_n) p(\mathbf{x}_n | \mathbf{z}_1, \dots, \mathbf{z}_{n-1}), \quad (30)$$

where C is the normalization constant. Different implementations of the posterior pdf lead to different state estimators. The most widely used are the extended Kalman filter (EKF) and the particle filter (PF) [133, 134]. Recently, new recursive nonlinear filters have been studied (e.g., grid-based methods [134], Monte Carlo methods, Gauss quadrature methods [135] and the related unscented filter [136]), which are based on numerical integration techniques. However, the aforementioned solutions lead to intolerable complexity with respect to the GRETA project scenario, therefore they will not be discussed in this section.

3.9.2.1 Extended Kalman filter

The Kalman filter recursively estimates the state of a linear system at a given time from the estimated previous states and the new measurements. First, a predicted value of state and covariance matrix of the estimation error is determined based on the estimated previous state. Then, they are updated using the

new measurements available at the current time. This filter can be also seen as a sequential MMSE in additive noise. When the additive noise is Gaussian-distributed the KF is the optimal solution.

The EKF is a particular case of the KF with nonlinear dynamics, which are linearized around the estimated previous state. The linearization requires the computation of the Jacobian matrix of the state vector. As an alternative, approximations based on Gauss-Hermite quadrature, the unscented filter, and Monte Carlo integration have been studied [134–136]. However, they are sub-optimal solutions with accuracy depending on the noise distribution and the linear approximation. In general, when the noise is non-Gaussian and the approximations is too rough, the EKF is not a suitable solution.

3.9.2.2 Particle filter

The recursive PF is a valuable approximate solution for nonlinear and non-Gaussian problems [133, 134]. PFs approximate the optimal solution numerically based on a physical model, rather than applying an optimal filter to an approximate model as in EKFs. In particular, the positional belief is approximated by a set of randomly chosen and weighted samples (particles). If the number of particles is sufficiently large, the PF ensures convergence to the true pdf.

Therefore, PFs can be seen as recursive implementations of Monte Carlo based statistical signal processing. Several versions of particle filters are present in literature and they can be classified into two categories: the first category require resampling to prevent divergence by re-using the particles; the second category does not require resampling because do not re-use particles.

In the scope of the project GRETA, we will focus on the PFs that require resampling combined with particle re-use at each iteration, which lead to the SIS-PF. A particular case will be also investigated, called box PFs, which is suitable for distributed filtering and reduces computational complexity [137].

3.10 Network management protocols

The presence of multiple active radio nodes densely deployed in the same area is challenging from a communication point of view, and channel access mechanisms are needed to rule transmissions, thus limiting collisions and data losses. In the reference scenario considered in this project, we can identify two levels of data exchange: Tag-Reader and Reader-to-Reader. These two communication levels of the network architecture have different requirements and energy constraints, which are related to the protocols used to manage the system.

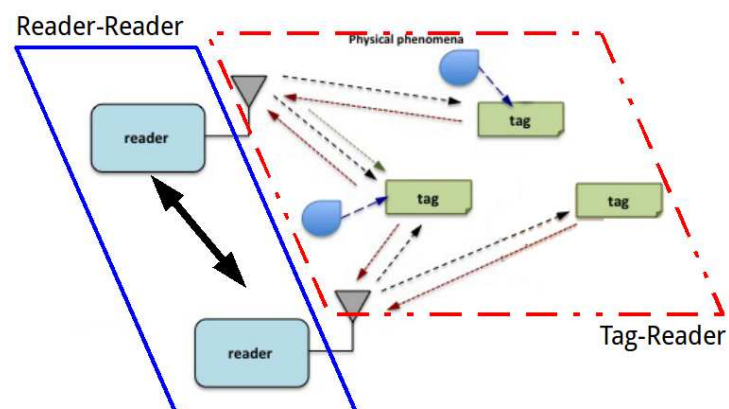


Figure 39:

3.10.1 Tag-reader

Independently from their passive, active or semi-passive nature, RFID tag are usually characterized by an unique identifier and are able to send information to the reader. At this network level, channel access is crucial to reduce tag collisions, when multiple tags transmit to a reader at the same time. Avoiding collisions results in less energy used for transmissions, saving the limited power budget of tag and increasing network lifetime [138]. Besides collisions, interferences and multipath are two additional issues in UWB sensor networks that should be taken into account [139–141]. Although energy efficiency and collisions affect all kinds of tags, their main issues are related to the backscatter nodes. Backscatter-based devices exploit reader's originated signal to send the reply by capturing the energy of its radio-frequency signal: hence a node can communicate at almost zero power. The simplest case is a binary value indicating the presence of tag within reader communication radius, but more complex values might be transmitted by properly modulating the signal [64]. However, a major problem is that backscatter communication is not reliable: backscatter nodes cannot sense each other, and hence tend to suffer from colliding transmissions and generate clutter, which is not suppressed by traditional UWB systems [76]. Another problem with backscattering is its inefficiency at adapting the bit rate to channel conditions. Here, coding and decoding algorithms based on compressive sensing improve the efficiency of the data collection process by representing values as sparse signals [142, 143].

3.10.2 Reader-to-reader

Communication among readers is less critical from a power consumption perspective: RFID readers can be fixed, mobile or handheld, but their energy budget is usually not an issue. The reader detects the presence of RFID tags and collect their information: each node could then process data locally, in a distributed manner, or it might pass the acquired value to a central system, which will perform permanent storage and, optionally, further processing. Given a number of interconnected readers, some of them mobile, a possible solution might be a dynamic election of the best path for data exchange, and an assignment of channel resources basing on the knowledge of the network conditions and the quality of service required [144, 145]. Neighboring readers could collide while interrogating a tag simultaneously, thus having duplicated information at a global level. Hence, cooperation among nodes is fundamental to get rid of redundant readings and increase the overall throughput [146]. In non-critical application, readers produce RFID reading event and exchange values each other or deliver them to the central system without taking into account temporal issues. A best effort protocol, computationally efficient, could be the right choice for this type of applications. On the other hand, there are applications, e.g. real-time target tracking, that have strict notification latencies for RFID data and the main challenge is to guarantee deadlines while delivering messages [147]. In this case, specific protocols are needed to ensure that all readers will be able to satisfy the delivery requirements and deadlines imposed by the application [148].

4 PRELIMINARY LINK AND POWER BUDGET

4.1 Link budget

In this section we will provide a preliminary link budget analysis under simplified assumptions. A more accurate analysis will be provided in the next deliverable.

This analysis is developed considering a central frequency of $f_c = 4$ GHz and its aim is to show the level of path-loss at the receiver side in two different situations: monostatic and bistatic configuration. Furthermore the path-loss computation is compared with different SNR requirements at receiver side.

The RRC pulse with central frequency at 4 GHz, satisfying the EU-UWB regulation in the 3.1 - 4.8 GHz band as been taken as transmitted waveform (Fig. 40 and Fig. 41).

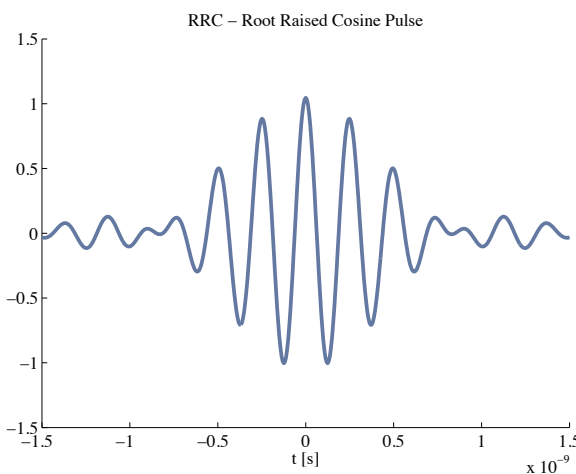


Figure 40: Transmitted pulse.

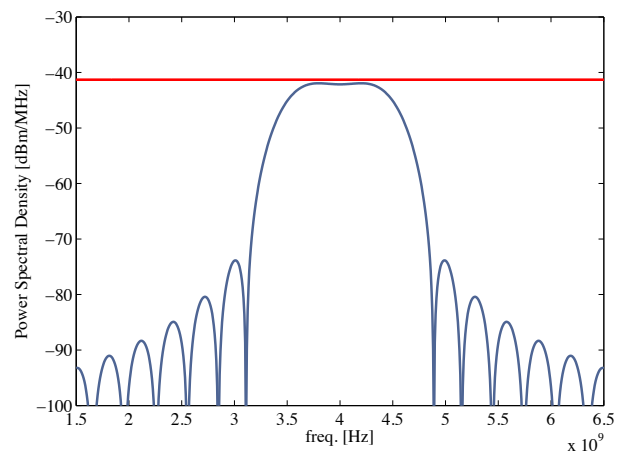


Figure 41: Transmitted pulse's power spectral density.

The complete list of simulation parameters of both monostatic and bistatic configurations are reported in tables:

Bistatic Configuration			
Parameter Symbol	Parameter Meaning	Value	Unit of Measure
T_f	Frame Time (pulse repetition period)	128	ns
N_s	Number of emitted pulses per symbol	8192	
P_{tx}	Transmitted Power	-18	dBm
G_{rx}	Transmitting Antenna Maximum Gain	3	dBi
G_{tx}	Receiving Antenna Maximum Gain	6	dBi
G_{tag}	Tag Antenna Maximum Gain	1	dBi
$EIRP$	Equivalent Isotropically Radiated Power	-12	dBm
T_w	Pulse Time Duration	1	ns
Γ	Roll-off factor	0.6	
f_c	Central frequency	4	GHz
β	Path-loss exponent	2	
W	Bandwidth	1.6	GHz
F	Receiver Noise Figure	4	dB
L_{supp}	Tag Losses	4	dB

Monostatic Configuration			
Parameter Symbol	Parameter Meaning	Value	Unit of Measure
T_f	Frame Time (pulse repetition period)	128	ns
N_s	Number of emitted pulses per symbol	8192	
P_{tx}	Transmitted Power	-15	dBm
G_{tx}	Reader Antenna Maximum Gain	3	dBi
G_{tag}	Tag Antenna Maximum Gain	1	dBi
$EIRP$	Equivalent Isotropically Radiated Power	-12	dBm
T_w	Pulse Time Duration	1	ns
Γ	Roll-off factor	0.6	
f_c	Central frequency	4	GHz
β	Path-Loss Exponent	2	
W	Bandwidth	1.6	GHz
F	Receiver Noise Figure	4	dB
L_{supp}	Tag Losses	4	dB

The path-loss is conventionally defined as:

$$PL(d) = \frac{P_{tx}}{P_{rx}} \quad (31)$$

where P_{tx} and P_{rx} are the transmitting and receiving powers, respectively.

The path-loss in dB (focusing on its distance and antenna gain dependence) is given by:

$$PL(d) = PL_0(d_0) + 10\beta \log\left(\frac{d}{d_0}\right) - G_1 - G_2 + L_{supp} \quad (32)$$

where d is the distance, d_0 is the reference distance (in the following it will be 1 mt), G_i is the maximum gain of the i th antenna and L_{supp} accounts for supplementary losses.

$PL_0(d_0)$ is the path-loss (free-space) at the reference distance in dB:

$$PL_0(d_0) = 20 \log\left[\frac{4\pi d_0 f_c}{c}\right] \quad (33)$$

The Figure 42 displays the two configurations.

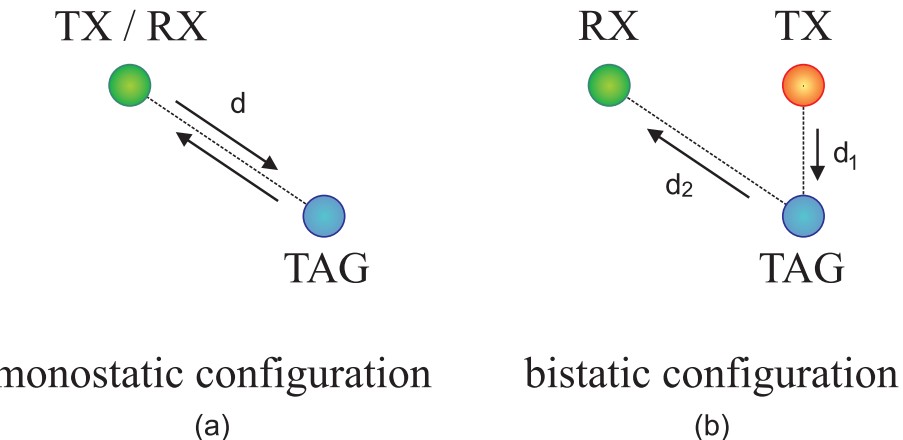


Figure 42: Monostatic and Bistatic Configuration.

The path-loss expressed in dB in Monostatic and Bistatic configurations is given by:

- Monostatic Configuration:

$$PL(d) = 2 PL_0(d_0) + 20\beta \log\left(\frac{d}{d_0}\right) - 2 G_{tx} - 2 G_{tag} + L_{supp} \quad (34)$$

- Bistatic Configuration:

$$PL(d_1, d_2) = 2 PL_0(d_0) + 10\beta \log \left(\frac{d_1}{d_0} \right) + 10\beta \log \left(\frac{d_2}{d_0} \right) - G_{tx} - 2 G_{tag} - G_{rx} + L_{supp} \quad (35)$$

where

d_1 is the distance between the transmitter and the tag and d_2 is the distance between the tag and the receiver.

d_1 and d_2 are typically different.

In both configurations L_{supp} is a supplementary loss in the tag due to the backscattering process (i.e. losses due to the internal architecture of the tag, UWB switch, etc.) and it is assumed to be 4 dB.

Moreover, we can calculate the maximum level of path-loss allowed at the receiver side once the minimum SNR is fixed considering N_s received pulses (spaced apart of T_f ns) and added coherently as:

$$SNR \triangleq \frac{P_{tx} \cdot T_f \cdot N_s}{N_0} = \frac{P_{tx} \cdot T_f \cdot N_s}{N_0 \cdot PL(d)} \quad (36)$$

As a consequence we find that:

$$SNR_{min} = \frac{P_{tx} \cdot T_f \cdot N_s}{N_0 \cdot PL_{max}(d)} \quad (37)$$

We show some numerical examples in which a room [10 mt x 10 mt x 5 mt] is considered with the receiver's position on [10 mt x 5mt x 2.5 mt] coordinates and the tag that can move on a grid of points equally spaced of 50 cm on the floor (height of 0 mt).

In the monostatic configuration the transmitter's node coincides with the receiver node (so it has the same coordinates) while in the bistatic configuration the transmitter node(s) is/are on the roof (height of 5 mt).

Firstly we have considered a unique transmitting unit placed on the roof's center ([5mt x 5mt x 5mt]) as shown in Figure 43.

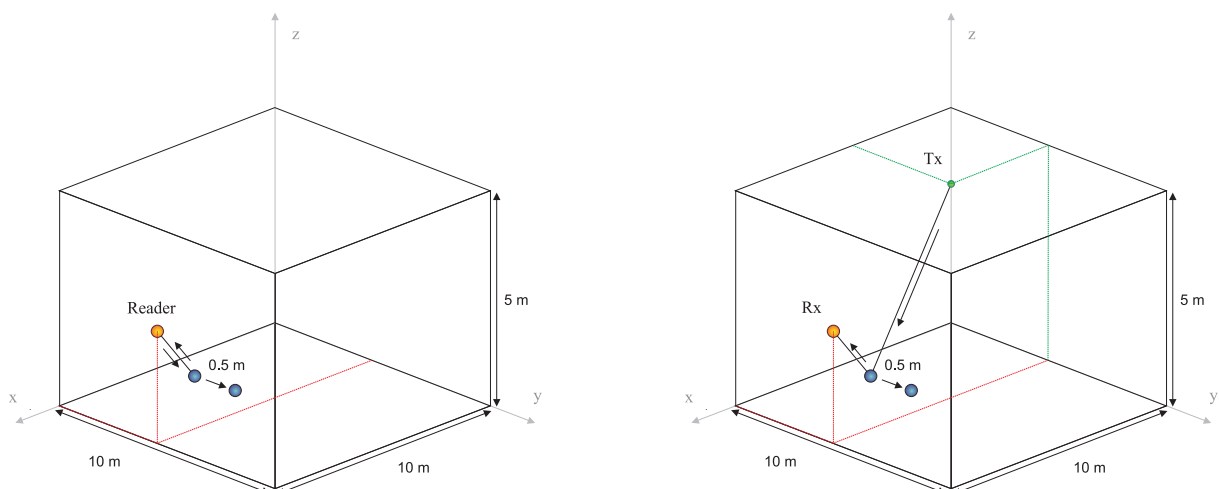


Figure 43: Scenario 1.

We resume the simulation results in the following tables for the Monostatic and Bistatic configurations:

Monostatic Configuration				
Parameter Symbol	Parameter Meaning	Value	Unit of Measure	
SNR	SNR requirements (minimum) at rx side	10, 14, 20		dB
PL _(max) ^(meas)	maximum measured PL	127		dB
PL _(min) ^(meas)	minimum measured PL	100		dB
PL _(mean) ^(meas)	mean measured PL	117		dB
PL _(max) (10 dB)	maximum allowed PL	115		dB
PL _(max) (14 dB)	maximum allowed PL	111		dB
PL _(max) (20 dB)	maximum allowed PL	105		dB
	coverage (SNR = 10 dB)	40 %		
	coverage (SNR = 14 dB)	22 %		
	coverage (SNR = 20 dB)	6.6 %		

Bistatic Configuration - Scenario 1				
Parameter Symbol	Parameter Meaning	Value	Unit of Measure	
SNR	SNR requirements (minimum) at rx side	10, 14, 20		dB
PL _(max) ^(meas)	maximum measured PL	122		dB
PL _(min) ^(meas)	minimum measured PL	107		dB
PL _(mean) ^(meas)	mean measured PL	114		dB
PL _(max) (10 dB)	maximum allowed PL	112		dB
PL _(max) (14 dB)	maximum allowed PL	108		dB
PL _(max) (20 dB)	maximum allowed PL	102		dB
	coverage (SNR = 10 dB)	33 %		
	coverage (SNR = 14 dB)	7 %		
	coverage (SNR = 20 dB)	0 %		

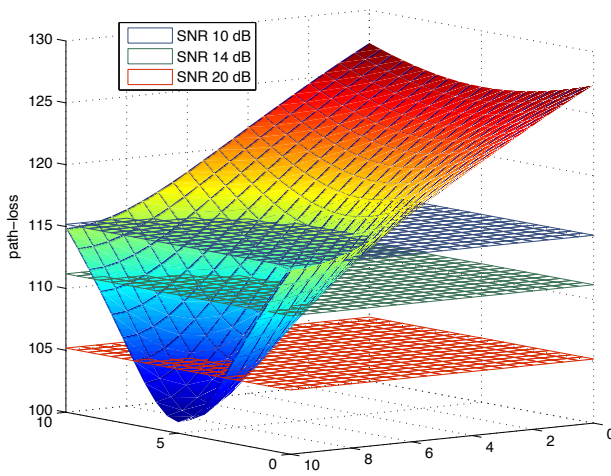


Figure 44: Monostatic Configuration - Path-Loss.

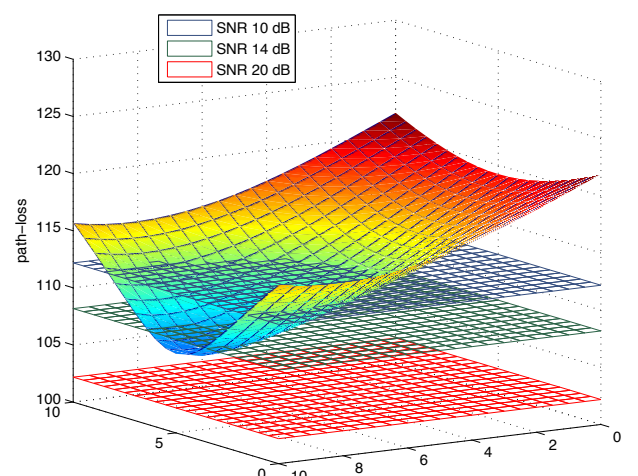


Figure 45: Scenario 1 - Path-Loss.

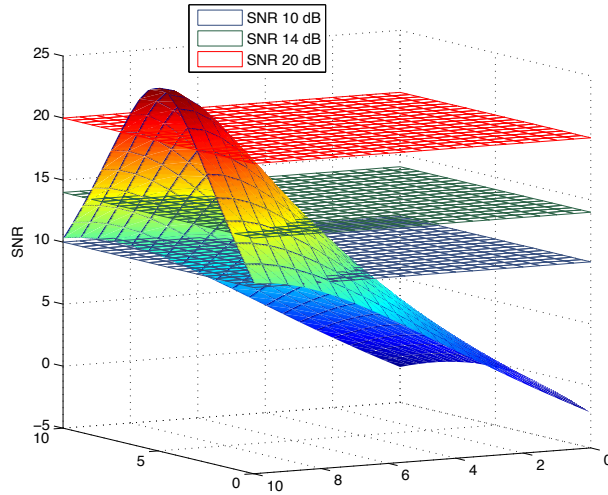


Figure 46: Monostatic Configuration - SNR.

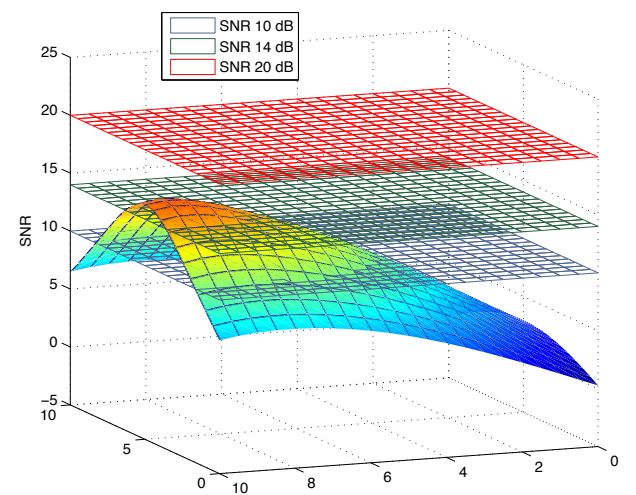


Figure 47: Scenario 1 - SNR.

As we can deduce by comparing the two situations reported, the level of the signal at the receiver side in term of attenuation is quite similar considering a nodes' disposition like in the first scenario or a monostatic configuration. The choice to put the transmitter in the middle of the roof maximizes the coverage area resulting in a levelling of the attenuation values while the adoption of a transmitter and a receiver in a unique node favors the closest points at the expense of those more distant.

The idea to privilege a bistatic configuration with the respect to a monostatic one aims at reducing the pathloss by exploiting the distance dependence: if the path between the transmitter and the tag decreases, for example by putting the transmitter near to a possible tag position, and if this path is not a-priori fixed as in a monostatic configuration, a reduction in the pathloss calculation is possible.

This is the reason why a single transmitter in the middle of the roof is not an appropriate disposition.

As a consequence, we can turn to the second scenario considered in which we have three transmitters nodes of [1.5 5 5], [5 5 5], [8.5 5 5] coordinates each controlling a certain region in the environment.

The scenario is ideally divided in three zones so that a tag in the i th region is visible only to the i th

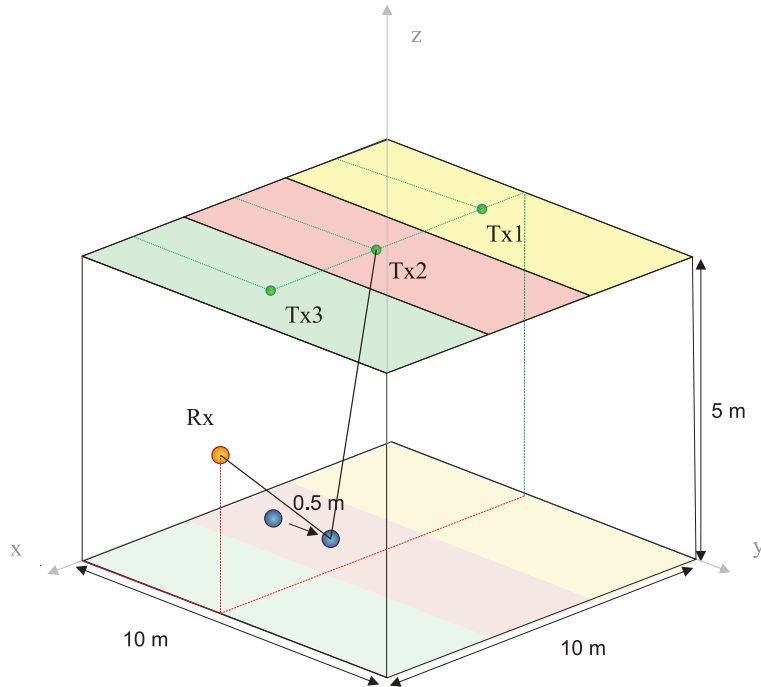


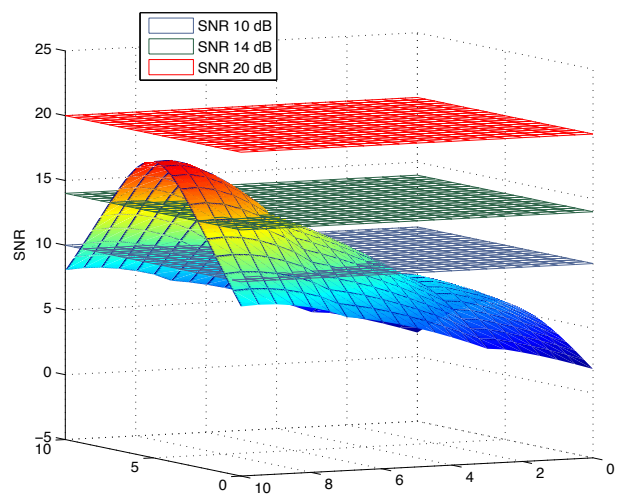
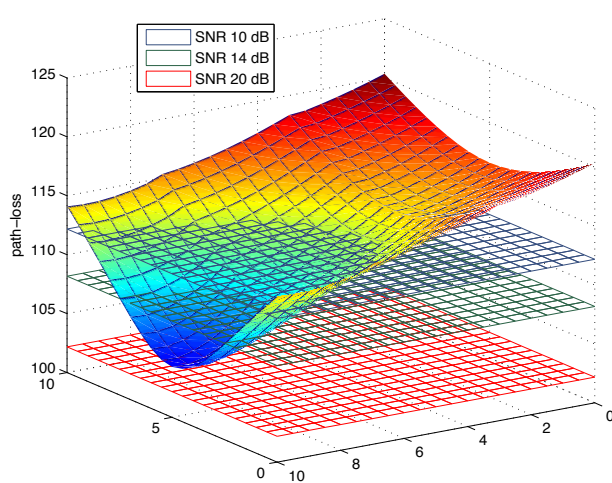
Figure 48: Scenario 2.

transmitter. In a real application, this on-off transmitter's visibility is not possible but we could exploit a smart radiation pattern for the antennas implicated.

In the following the results are reported:

Bistatic Configuration - Scenario 2				
Parameter Symbol	Parameter Meaning	Value	Unit of Measure	
SNR	SNR requirements (minimum) at rx side	10, 14, 20	dB	
PL _(max) ^(meas)	maximum measured PL	120	dB	
PL _(min) ^(meas)	minimum measured PL	104	dB	
PL _(mean) ^(meas)	mean measured PL	113	dB	
PL _(max) (10 dB)	maximum allowed PL	112	dB	
PL _(max) (14 dB)	maximum allowed PL	108	dB	
PL _(max) (20 dB)	maximum allowed PL	102	dB	
	coverage (SNR = 10 dB)	36 %		
	coverage (SNR = 14 dB)	12 %		
	coverage (SNR = 20 dB)	0 %		

As we can see from the tables, there is an improvement in term of path-gain and following the same principle as before we define a new scenario with nine transmitter nodes ([1.5 1.5 5], [1.5 5 5], [1.5 8.5 5], [5 1.5 5], [5 5 5], [5 8.5 5], [8.5 1.5 5], [8.5 5 5] and [8.5 8.5 5]). This is possible because the transmitters



have a low complicated architecture, they are just pulse generators, and this is why it is not an issue to dislocate a large number of them in the environment.

The last scenario is reported in Fig 51:

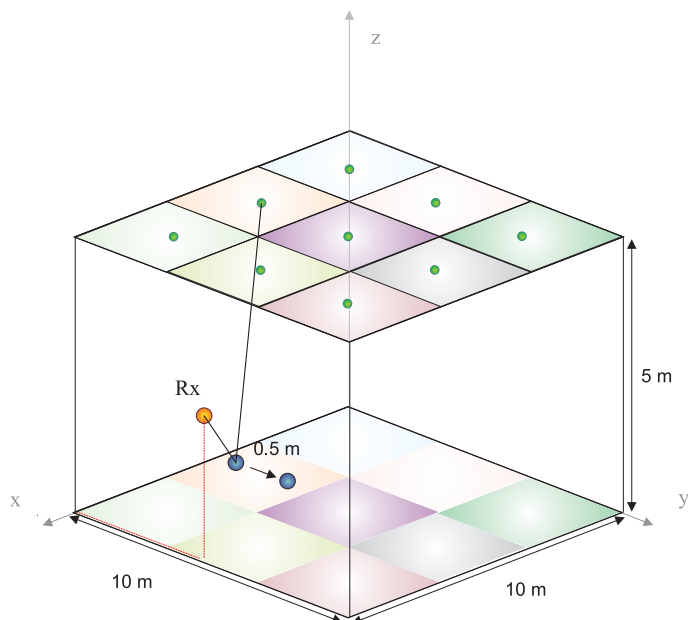


Figure 51: Scenario 3.

By adopting this configuration, the path-loss values are:

Bistatic Configuration - Scenario 3			
Parameter Symbol	Parameter Meaning	Value	Unit of Measure
SNR	SNR requirements (minimum) at rx side	10, 14, 20	dB
$PL_{(max)}^{(meas)}$	maximum measured PL	117	dB
$PL_{(min)}^{(meas)}$	minimum measured PL	104	dB
$PL_{(mean)}^{(meas)}$	mean measured PL	112	dB
$PL_{(max)}(10 \text{ dB})$	maximum allowed PL	112	dB
$PL_{(max)}(14 \text{ dB})$	maximum allowed PL	108	dB
$PL_{(max)}(20 \text{ dB})$	maximum allowed PL	102	dB
	coverage (SNR = 10 dB)	47 %	
	coverage (SNR = 14 dB)	14 %	
	coverage (SNR = 20 dB)	0 %	

The last case considered clearly shows how it is better to consider a bistatic configuration instead of a monostatic one when there is the possibility to deploy the transmitters closer to the tags possible positions or to increase the number of nodes in order to maximize the coverage.

In Fig. 52 we can see a comparison between the two situations considering the scenario with 9 transmitters:

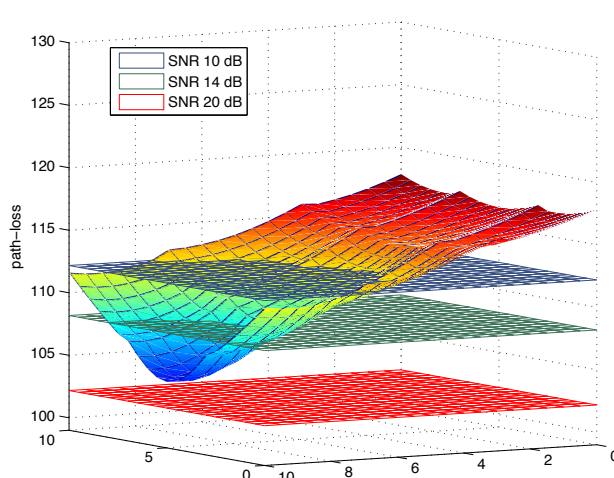


Figure 52: Scenario 3 - Path-loss.

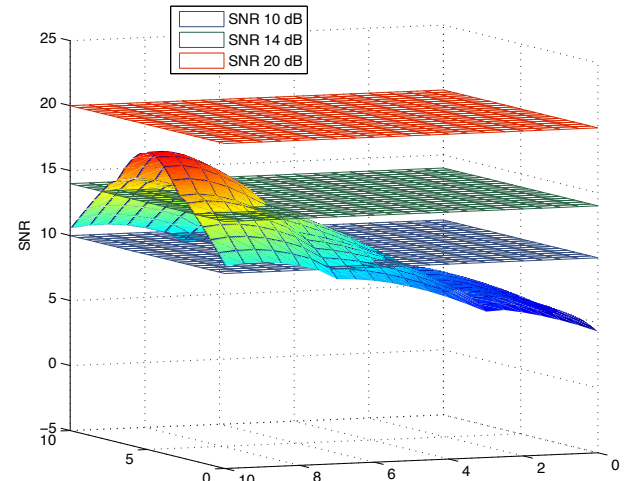


Figure 53: Scenario 3 - SNR.

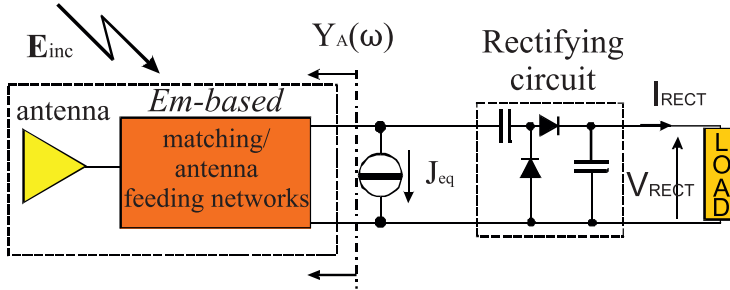


Figure 54: Rectenna equivalent circuit in RF stationary regime.

4.2 Power budget

4.2.1 RF-to-DC power budget

In order to estimate the available power budget at the rectenna output we need to define the rectifier topology. In this first realization we adopt the simplest standard topology, consisting of a single-stage full-wave peak-to-peak rectifier, as the best choice to minimize the extra losses introduced by a multi-stage rectifiers, which can degrade the rectenna performance for low-level incoming fields [149]. Furthermore we dedicate particular care to the selection of the proper diode technology, in order to minimize losses and allow rectification even for very low power levels. In this phase we make use of a multi-domain CAD platform, consisting of the concurrent use of a nonlinear circuit simulator based on Harmonic Balance (HB) technique and a full-wave electromagnetic tool. Due to the low-level of the incident power, it is of fundamental importance the accurate evaluation of the available power in the receiving harvester antenna location (P_{AV}). Referring to the equivalent rectenna representation in RF stationary regime of Fig. 54 [52], we are able to predict P_{AV} in the simple case of a single-frequency incident field, by means of:

$$P_{AV} = \frac{|J_{eq}(\omega)|^2}{8Re[Y_A(\omega)]} \quad (38)$$

where $Y_A(\omega)$ is the broadband e.m.-based admittance matrix of the antenna and feeding-network sub-assembly, while $J_{eq}(\omega)$ is the current source providing the Norton equivalent representation of the incident field, which can be rigorously evaluated by resorting to the EM theory application [150].

If the incident field is represented by a uniform plane wave, $J_{eq}(\omega)$ can be cast in the following way

$$J_{eq}(\omega) = j[1 + R_0 Y_A(\omega)] \frac{2\lambda r e^{j\beta r}}{\eta} \frac{\mathbf{E}_R(\theta, \phi) \bullet \mathbf{E}_i}{U} \quad (39)$$

where \mathbf{E}_i is the constant complex vector incident on the region occupied by the receiving antenna, $\mathbf{E}_R(\theta, \phi)$ is the far-field radiated by the harvester antenna computed in the direction of incidence (θ, ϕ) at an arbitrary distance r from the its phase center, when driven by a sinusoidal voltage source of frequency ω , electro-motive force U , and internal impedance R_0 , and η is the free-space wave impedance.

It has to be stressed that this is the only available approach able to accurately account for both rectenna-RF source and rectenna-channel interactions, since an approximate rectenna effective area definition is not involved and rectenna-incident field polarization mismatch is automatically taken into account. A realistic channel characterization can be included in the evaluation of $J_{eq}(\omega)$, and this will be mandatory for obtaining meaningful evaluations of the rectenna performance.

The network function to be maximized during the HB-based optimization process is the RF-to-Direct Current (DC) conversion efficiency

$$\eta_{RF-DC} = \frac{V_{RECT} I_{RECT}}{P_{AV}} \quad (40)$$

where $P_{DC} = V_{RECT} I_{RECT}$ is the DC power delivered to the optimum and fixed load port.

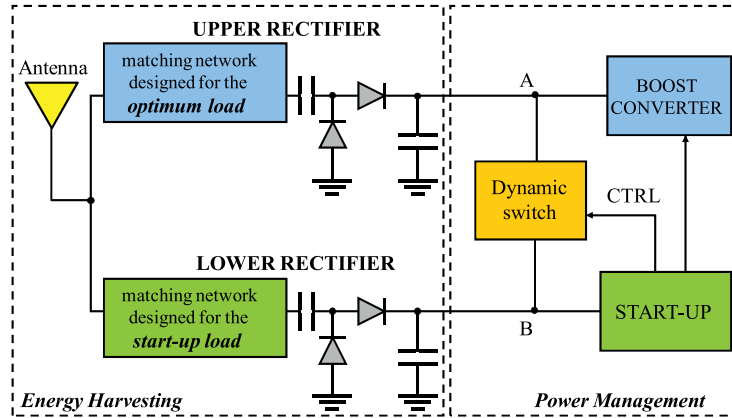


Figure 55: Block diagram of an energy autonomous system with a two-rectifier switched-topology.

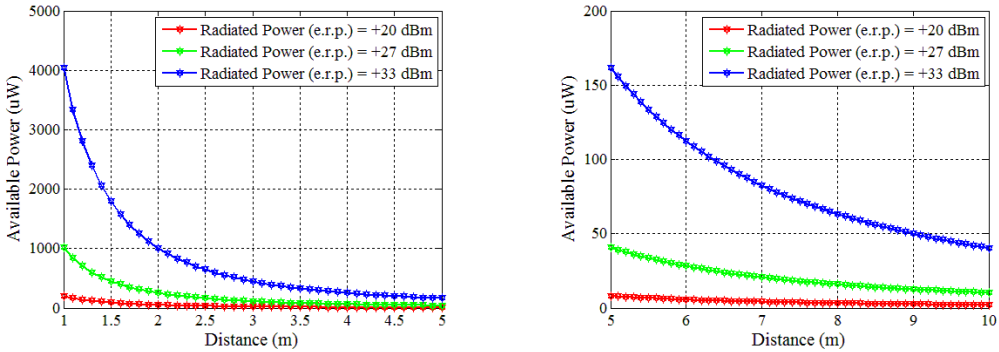


Figure 56: P_{AV} of the U-shaped dipole resonating at 868 MHz as harvester antenna as a function of the distance.

Since the device exploiting the rectenna output power operates with a very low duty cycle , (e.g., a sensor, normally in sleeping mode, activated only for read out purposes) it is not suitable for being directly connected to the the rectenna output port. On the contrary an energy buffer, consisting of the dynamic switch converter, is included as described in Section 3.2.

Hence it is necessary to quantify the rectified power P_{DC} and compare it to the total power consumption of the Power Management Unit (PMU) and of the sensor subsystems. We have thus carried out preliminary optimizations of the matching network between the harvester antenna and the rectifying section, for those feasible levels (-20 dBm up to 0 dBm) of P_{AV} , and for the two harvester-antenna topologies proposed in Section 3.8.2. In this way we provide the computation of such DC power levels in realistic conditions. This can be obtained by piece-wise designing a load-modulated matching network to guarantee the optimum load condition even in extremely low RF received power levels in order to ensure the best system efficiency for the PMU regime. We intend to design the two-rectifier switched-topology of Fig. 55, able to operate alternatively in the start-up and in the regime phases of the PMU. This design will be carried out by a CAD procedure based on the concurrent use of e.m. simulation, harmonic balance and time domain techniques. This way the actual nonlinear behavior of the rectenna in the time-domain design of the PMU can be rigorously accounted for.

For this purpose we have considered, among the UHF-RFID standard [151] three possible levels of transmitted power by the “RF showers” (20, 27 and 33 dBm, related to 15, 12 and 10 frequency channels, respectively).The obtained behavior are plotted in Fig. 56 in terms of the available power at the antenna port, and in Fig. 57 in terms of the DC power at the rectifier output port, with respect to the link distances.

These results show that, referring to link distances of the order of 5 m, the maximum radiated power

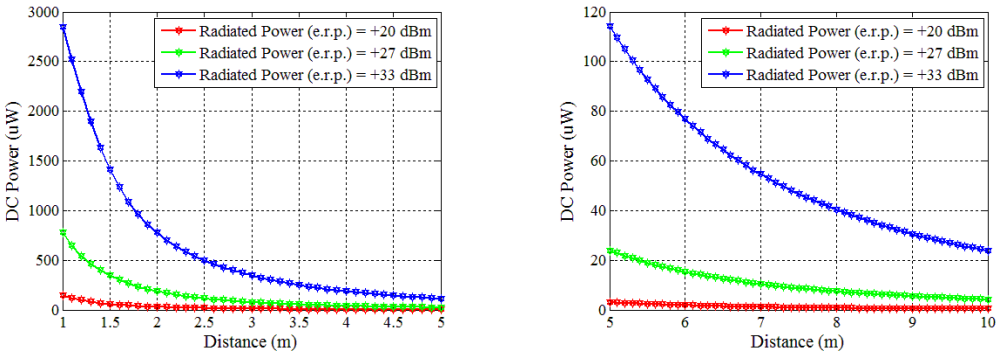


Figure 57: P_{DC} of the U-shaped dipole resonating at 868 MHz as harvester antenna as a function of the distance.

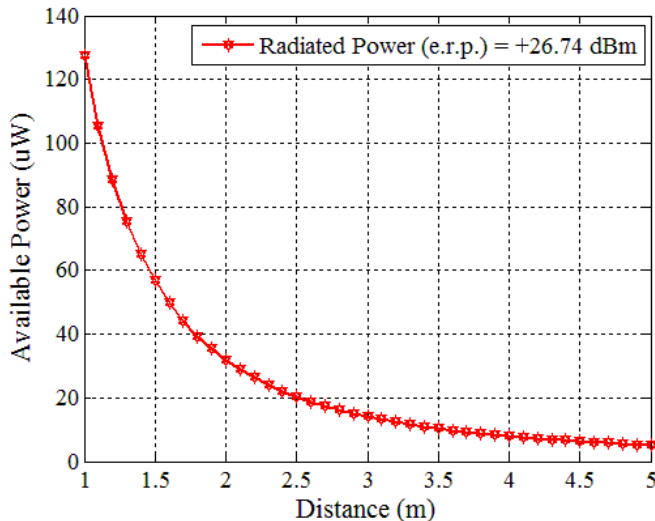


Figure 58: P_{AV} of the UWB spiral as harvester antenna at 2.45 GHz as a function of the distance.

of 33 dBm (covering the band 865.6 - 867.6 MHz [151]) is able to provide rectified powers greater than 100 mW. With the lower RF transmitted power levels these amounts of DC power are reached at distances lower than 3 m.

In the previous results a reference transmitting antenna consisting of an ideal electromagnetic half-wavelength dipole is used .

Similar plots are considered in Fig. 58 and Fig. 59 for the solution adopting a unique antenna for energy harvesting and for UWB communication (UWB Archimedean spiral antenna , see Section 3.8.2). In this case we refer to the 500-mW (27 dBm) maximum Effective Radiated Power (ERP) for indoor 2.45 GHz-RFID standard [152]:

These results clearly show the great impact of the operating frequency on the system performance: only few mWs of P_{DC} are retrieved at 3 m distance. This put into evidence that the choice of combining power harvesting and power management subsystems is mandatory for truly energy-autonomous sensor nodes.

For this purpose representative simulation results are shown in Fig. 59 for the 868 MHz RF link, and in Fig. 59 for the 2.45 GHz link, where we predict the time needed to reach the maximum stored energy in the output capacitor of the PMU. This is carried out by transient simulations of the entire system including the dynamic switch converter described in Section 3.2. The two possible solutions for

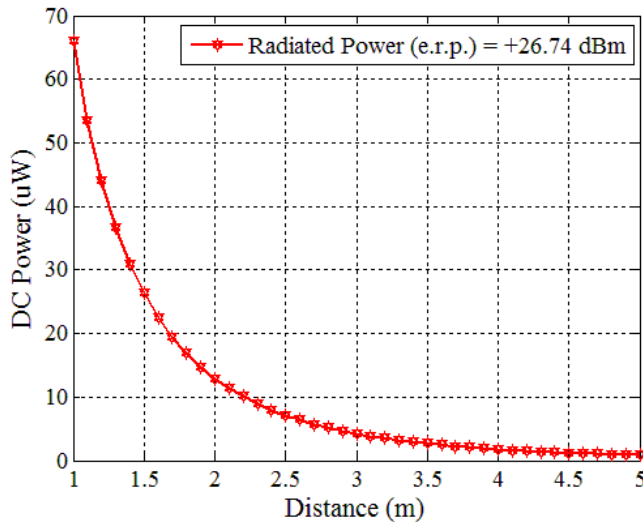


Figure 59: P_{DC} of the UWB spiral as harvester antenna at 2.45 GHz as a function of the distance.

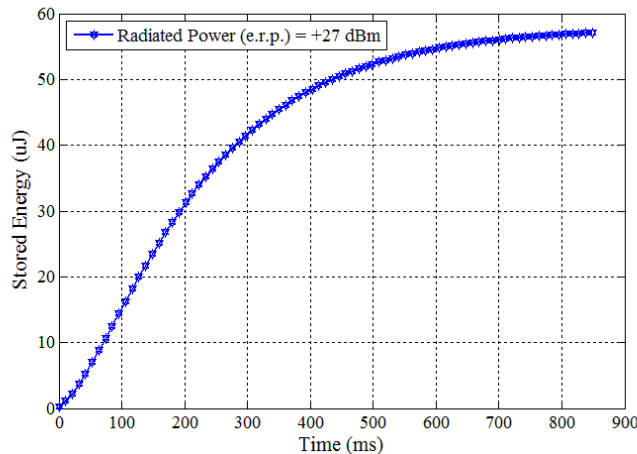


Figure 60: Waveform of the energy stored on the boost converter output capacitance, due to a transmitting dipole resonating at 868 MHz, placed at 3 m far from the dipole harvester antenna.

the rectenna sections are considered. The link distance and the RF transmitted power considered in these cases are 3 m and 27 dBm, respectively. The DC excitations predicted in Fig. 57 and Fig. 59 are used.

The saturated value of the stored energy is reached in 0.5 s for the 868 MHz link and in 4 ms in the 2.45 GHz case. For this first prediction the same components are used, included the output storage capacitor, whose value is 0.1 μ F. A proper architecture will be considered for the future subsystem design.

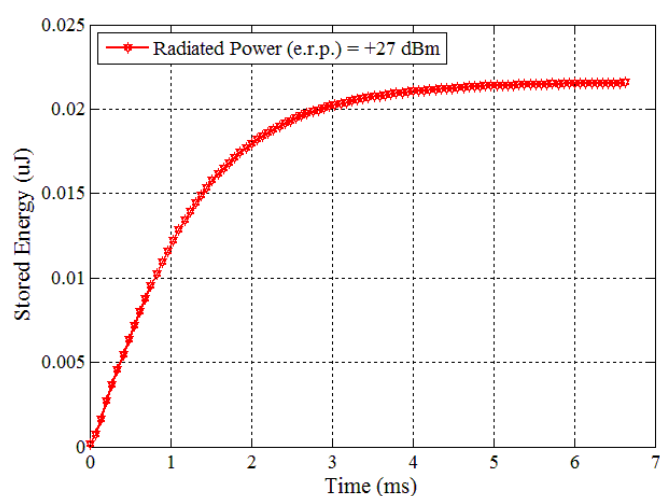


Figure 61: Waveform of the energy stored on the boost converter output capacitance, due to a transmitting dipole resonating at 2.45 GHz, placed at 3 m far from the spiral harvester antenna.

5 DEMONSTRATOR DEFINITION

The case-of-study chosen in the project GRETA for the development and fabrication of the demonstrator is the *smart band-aid* (or the *blood bags tracker*) for eHealth applications, described in section 2.1.

The *smart band-aid* (or the *blood bags tracker*) is based on RFID tag, able to monitor the temperature of the patient (or of the blood bags) by means of a sensor in direct contact with him (or it). The tag transmits to the reader the identification data (and other information) and the data acquired by the on-board sensor. The reader performs the processing of the acquired data. The RFID system, and therefore the demonstrator must be able to **monitor the temperature**, to **localize** and to **track** the tag (three operations are performed).

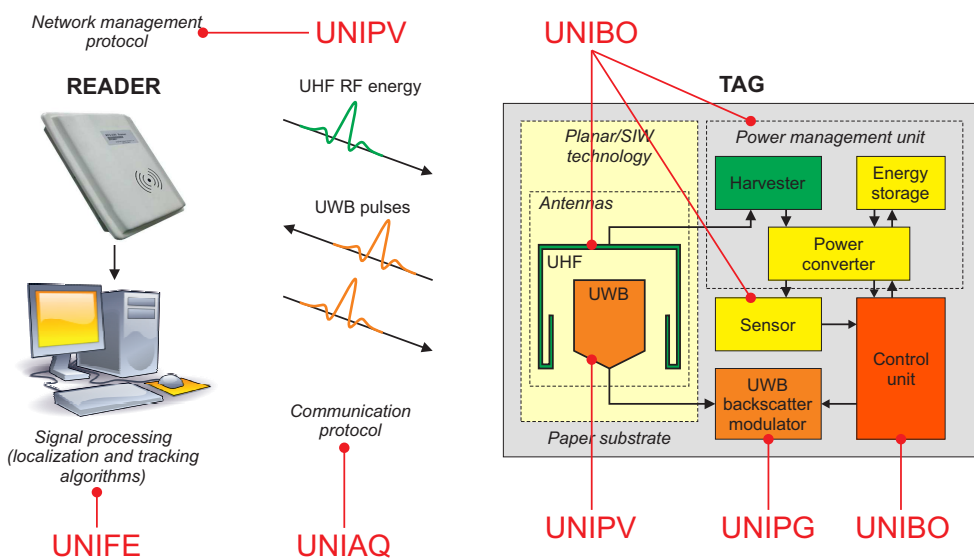


Figure 62: RFID system with tag architecture and units contributions.

The tag architecture chosen is the semi-passive one, Fig. 62, for this reason it must be energized and activated by EM waves from out-side sources. The RF power used to supply the tag is provided by the reader (or energy shower) at UHF, meanwhile the communication between tag and reader is performed by means of UWB signals. The advantages of the semi-passive architecture is the low complexity of the transceiver and the absence of battery, replaced by a power management unit that performs power conversion and storage reducing the tag size and the environmental impact. Organic substrate based on cellulose is chosen for the tag. The fundamental aspects emphasized by this architecture, in agreement with the project criteria, are the **low-power technology**, the **energy harvesting** and the use of **organic materials**.

Each unit of the GRETA project will contribute to the design and the implementation of the demonstrator with its knowledge and background. The various contributions are resumed in Table 2 and are highlighted in Fig. 62. The tag is made of various blocks: the power management and energy harvesting unit is described in section 3.2; the sensor module is defined in section 3.3; the low power microcontroller is shown in section 3.4; the antenna for UWB communication and the UHF antenna for the energy harvesting are described in the sections 3.8; the UWB backscatter modulator is shown in section 3.5. System integration techniques for the assembly of the various tag blocks are described in section 3.7. The UWB communications techniques, protocols and requirements for the reader-tag communications are described in the sections 2.3 and 3.10. The algorithms for the localization and the tracking of the tags are defined in the sections 2.3 and 2.4. A preliminary study about link and power budget is performed in section 4.

Table 2: Units Contributions.

Units	Contributes
UNIAQ	<ul style="list-style-type: none"> •protocols and requirements for UWB communications •data synchronization architectures
UNIBO	<ul style="list-style-type: none"> •sensor architecture •energy harvester architecture •low-power microcontroller •harvesting antenna •UWB backscattering communication techniques
UNIFE	<ul style="list-style-type: none"> •localization techniques •localization and tracking algorithms
UNIPG	<ul style="list-style-type: none"> •tag architecture integration •UWB backscatter modulator architecture
UNIPV	<ul style="list-style-type: none"> •UWB antenna •network management protocol

6 DISSEMINATION PLAN

In this section the preliminary dissemination plans proposed by the research units are reported.

6.1 University of Bologna

The University of Bologna intends to submit papers to the following conferences and workshops:
Conferences: ICC 2013, GLOBECOM 2013, ICC 2014, ICUWB 2014, RFID-TA 2014
Journal papers: IEEE Trans. on Wireless Communications, IEEE Trans. on Communications, EURASIP UNIBO is organizing the IEEE Workshop on Advances in Network Localization and Navigation (ANLN) at ICC 2013, Budapest, June 9-13 (<http://icc2013.spsc.tugraz.at/>).

6.2 University of Ferrara

Researchers at UNIFE will provide invited talks on passive localization within a distinguished lecture program of the IEEE with the possibility of advertising GRETA project. They also intends to submit papers to the main journals and conferences of the field. UNIFE group is organizing the IEEE Workshop on Advances in Network Localization and Navigation (ANLN) at ICC 2013, Budapest, Hungary (<http://icc2013.spsc.tugraz.at/>).

6.3 University of L'Aquila

The University of L'Aquila has planned to submit papers to major journals and conferences in the area of wireless communications for the whole duration of the project: IEEE Transactions on Communications, IEEE Transactions on Wireless Communications and IEEE Transactions on Vehicular Technology are retained as major archival journals, while IEEE ICC, IEEE Globecom, IEEE WCNC and IEEE ICUWB are considered major conferences for disseminating our results. Papers have already appeared in ICC'2013, WCNC'2013, and in the IEEE Trans. on Comm. Nevertheless, other journals and conferences/workshops might be targeted for specific dissemination actions (e.g. special issues or special sessions devoted to GRETA or one of its topics, and in cooperation with GRETA partners). We believe that one journal submission and three conferences/workshops per year are a minimum requirement to be satisfied. Furthermore, specific dissemination actions are likely to be planned in cooperation with other national or international initiatives: one example is represented by the NoE HYCON2 in the area of networked embedded systems, other examples are ERC VISION and ITN GREENET. Finally, a close cooperation with Thales Italia (that officially endorsed GRETA) involves an industry targeted project that also includes RFID as a key technology component in scenarios similar to those envisaged by GRETA: this might lead to other dissemination activities as this new project is going to start in a few months. A newly recruited Ph.D. student is already involved in GRETA, and RFID systems are already part of graduate programs at master and Ph.D. levels. UAQ is of course interested in promoting joint initiatives for international programs (e.g. summer schools) on specific GRETA topics. Furthermore, involvement of students and faculties in international mobility programs (e.g. ERASMUS and ERASMUS Placement for students, cooperation within european projects for faculties) is a natural extension of our current mobility initiatives: as an example, our partners KTH and CNRS have already committed to cooperate on GRETA topics.

6.4 University of Pavia

The MG of the University of Pavia intends to submit papers at the following conferences and journals: IMS2014, EuMW2014, IEEE Transactions on Microwave Theory and Techniques, IEEE Transactions on Antennas and Propagation.

In addition, the MG has organized a Special Session on "Paper-based Microwave Circuits and Antennas" at PIERS2013 conference in Stockholm, Sweden (August 12-15, 2013), and a Focused Session

on "Microwaves in Agriculture, Environment and Earth Observation (MAGEO)" at EuMC2013 conference in Nuremberg, Germany (October 6-11, 2013).

The TLC and RS group of the University of Pavia intends to submit papers to the following conferences and journals: ICC 2014 and/or GLOBECOM 2014, IEEE Trans. on Wireless Communications and/or IEEE Trans. on Communications.

6.5 University of Perugia

The main focus of the University of Perugia research team is the design of the backscatter modulator described in section 3.5. The results expected from this activity research are the design and the measures performed on the on-chip prototype.

The dissemination plan will be the following: submission of journal paper to IEEE Journal of Solid-State Circuits and/or IEEE Microwave and Wireless Components Letters; submission of conference paper to IEEE International Microwave Symposium 2014 and/or IEEE RFID-Technologies and Applications 2014.

REFERENCES

- [1] B. Murmann. Adc performance survey 1997-2013.
- [2] B. E. Jonsson. In *IEEE ADC Forum*, 2011.
- [3] K. Finkenzeller. In *RFID Handbook: Fundamentals and Applications in Contactless Smart Cards and Identification. Second Edition*. Wiley, 2004.
- [4] E.W.T. Ngai, Karen K.L. Moon, Frederick J. Riggins, and Candace Y. Yi. RFID research: An academic literature review (1995-2005) and future research directions. *International Journal of Production Economics*, 112(2):510 – 520, 2008. Special Section on RFID: Technology, Applications, and Impact on Business Operations.
- [5] V. Chawla and D. S. Ha. An overview of passive RFID. *IEEE Applications & Practice*, pages 11–17, Sep 2007.
- [6] R. Das and P. Harrop. RFID forecast, players and opportunities 2007-2017. *available online at <http://www.idtechex.com.>*, 2007.
- [7] D. Dardari, E. Falletti, and M. Luise. In *Satellite and Terrestrial Radio Positioning Techniques - A signal processing perspective*. Elsevier Ltd, London, 2011.
- [8] Davide Dardari, Raffaele D'Errico, Christophe Roblin, Alain Sibille, and Moe Z. Win. Ultrawide bandwidth RFID: The next generation? *Proceedings of the IEEE, Special Issue on RFID - A Unique Radio Innovation for the 21st Century.*, 98(9):1570 –1582, Sep 2010.
- [9] R. Verdone, D. Dardari, G. Mazzini, and A. Conti. In *Wireless Sensor and Actuator Networks: technologies, analysis and design*. Elsevier Ltd, London, 2008.
- [10] M. Z. Win, D. Dardari, A. F. Molisch, W. Wiesbeck, and Z. Jinyun. History and applications of UWB. *Proc. of IEEE, Special Issue on UWB Technology & Emerging Applications*, 97(2):198–204, Feb 2009.
- [11] Davide Dardari, Francesco Guidi, Christophe Roblin, and Alain Sibille. Ultra-wide bandwidth backscatter modulation: Processing schemes and performance. *EURASIP Journal on Wireless Communications and Networking*, 2011:47(1), 2011.
- [12] Moe Z. Win and Robert A. Scholtz. Impulse radio: How it works. *IEEE Commun. Lett.*, 2(2):36–38, February 1998.
- [13] Z. Sahinoglu, S. Gezici, and I. Guvenc. In *Ultra-wideband Positioning Systems: theoretical limits, ranging algorithms, and protocols*. Cambridge University Press, 2008.
- [14] Enrico Paolini, Andrea Giorgetti, Marco Chiani, Riccardo Minutolo, and Mauro Montanari. Localization capability of cooperative anti-intruder radar systems. *EURASIP Journal on Advances in Signal Processing, Special Issue on Cooperative Localization in Wireless Ad Hoc and Sensor Networks*, 2008(Article ID 726854):14 pages, 2008.
- [15] *Proc. of IEEE, Special Issue on UWB Technology & Emerging Applications*, Feb 2009.
- [16] Federal Communications Commission. Revision of part 15 of the commission's rules regarding ultra-wideband transmission systems, first report and order (ET Docket 98-153), Adopted Feb. 14, 2002, Released Apr. 22, 2002.
- [17] European Commission. Commission decision of 21 february 2007 on allowing the use of the radio spectrum for equipment using ultra-wideband technology in a harmonised manner in the community. *Official Journal of the European Union*, C(2007) 522, February 2007.

- [18] European Commission. Amendment to ecc decision to include daa: Ecc/dec/(06)12 amended, October 2008.
- [19] European Commission. Draft ECC report 170 in ECC consultation "ECC report on specific UWB applications in the bands 3.4 - 4.8 GHz and 6 - 8.5 GHz location tracking applications for emergency services (LAES), location tracking applications type 2 (LT2) and location tracking and sensor applications for automotive and transportation environments (LTA)".
- [20] European Commission. Draft ECC recommendation (11)09 UWB location tracking systems type 2 (LT2). Recommendation adopted by the Working Group Frequency Management (WG FM), 2009.
- [21] WiMedia Alliance. Wimeda. 2005.
- [22] IEEE standard for information technology - telecommunications and information exchange between systems - local and metropolitan area networks - specific requirement part 15.4: Wireless medium access control (MAC) and physical layer (PHY) specifications for low-rate wireless personal area networks (WPANs). *IEEE Std 802.15.4a-2007 (Amendment to IEEE Std 802.15.4-2006)*, pages 1–203, 2007.
- [23] IEEE 802.15.4f Draft. IEEE Standard for Information Technology - Telecommunications and Information Exchange Between Systems - Local and Metropolitan Area Networks - Specific Requirements - Part 15.4: Wireless Medium Access Control (MAC) and Physical Layer (PHY) Specifications for Low Rate Wireless Personal Area Networks (WPANs) - Amendment: Active RFID System PHY. 2011.
- [24] M. Baghaei-Nejad, Zhuo Zou, Hannu Tenhunen, and Li-Rong Zheng. A novel passive tag with asymmetric wireless link for RFID and WSN applications. *Circuits and Systems, 2007. ISCAS 2007. IEEE International Symposium on*, pages 1593–1596, May 2007.
- [25] Dajana Cassioli, Moe Z. Win, and Andreas F. Molisch. The ultra-wide bandwidth indoor channel: from statistical model to simulations. *IEEE J. Select. Areas Commun.*, 20(6):1247–1257, August 2002.
- [26] Andreas F. Molisch, Dajana Cassioli, Chia-Chin Chong, Shahriar Emami, Andrew Fort, Balakrishnan Kannan, Johan Karedal, Juergen Kunisch, Hans Schantz, Kai Siwiak, and Moe Z. Win. A comprehensive standardized model for ultrawideband propagation channels. *IEEE Trans. Antennas Propagat.*, 54(11):3151–3166, November 2006. Special Issue on Wireless Communications.
- [27] Moe Z. Win and Robert A. Scholtz. Characterization of ultra-wide bandwidth wireless indoor communications channel: A communication theoretic view. *IEEE J. Select. Areas Commun.*, 20(9):1613–1627, December 2002.
- [28] Marco Chiani and Andrea Giorgetti. Coexistence between UWB and narrowband wireless communication systems. *Proc. IEEE*, 97(2):231–254, February 2009. Special Issue on UWB.
- [29] Davide Dardari, Andrea Conti, Ulric Ferner, Andrea Giorgetti, and Moe Z. Win. Ranging with ultrawide bandwidth signals in multipath environments. *Proc. of IEEE, Special Issue on UWB Technology & Emerging Applications*, 97(2):404–426, Feb 2009.
- [30] Andrea Giorgetti and Marco Chiani. Time-of-arrival estimation based on information theoretic criteria. *IEEE Trans. Signal Processing*, 61(8):1869–1879, 2013.
- [31] Davide Dardari. Pseudo-random active UWB reflectors for accurate ranging. *IEEE Commun. Lett.*, 8(10):608–610, Oct 2004.

- [32] L. Stoica, A. Rabbachin, H. O. Repo, T. S. Tiuraniemi, and I. Oppermann. An ultrawideband system architecture for tag based wireless sensor networks. *IEEE Trans. Veh. Technol.*, 54(5):1632–1645, September 2005.
- [33] Z. Zou, M. Baghaei-Nejad, H. Tenhunen, and L-R. Zheng. An efficient passive RFID system for ubiquitous identification and sensing using impulse UWB radio. *e & i Elektrotechnik und Informationstechnik, Springer Wien*, 124(11):397–403, November 2007.
- [34] Robert J. Fontana and Steven J. Gunderson. Ultra-wideband precision asset location system. *Proc. of IEEE Conf. on Ultra Wideband Systems and Technologies (UWBST)*, 21(1):147–150, May 2002.
- [35] Time domain corporation. www.timedomain.com.
- [36] Ubisense limited. www.ubisense.net.
- [37] Zebra enterprise solutions. zes.zebra.com.
- [38] J. A. Paradiso and T. Starner. Energy scavenging for mobile and wireless electronics. *IEEE Pervasive Computing*, pages 18–26, Jan-Mar 2005.
- [39] K. Pahlaven and H. Eskafi. Radio frequency tag and reader with asymmetric communication bandwidth, February 2007.
- [40] A. Muchkaev. Carrierless RFID system, June 2008.
- [41] J. Jantunen, A. Lappetelainen, J. Arponen, A. Parssinen, M. Pelissier, B. Gomez, and J. Keignart. A new symmetric transceiver architecture for pulsed short-range communication. In *IEEE Global Communications Conference (GLOBECOM 2008)*, New Orelans, LA, USA, November 2008.
- [42] R. Vauche, E. Bergeret, J. Gaubert, S. Bourdel, O. Fourquin, and N. Dehaese. A remotely UHF powered UWB transmitter for high precision localization of RFID tag. In *Proc. of the 2011 IEEE International Conference on Ultra-Wideband (ICUWB 2011)*, pages 494 –498, sept. 2011.
- [43] Stevan Preradovic and Nemai Chandra Karmakar. Chipless rfid: Bar code of the future. *IEEE microwave magazine*, 11(7):87 –97, december 2010.
- [44] Linlin Zheng, S. Rodriguez, Lu Zhang, Botao Shao, and Li-Rong Zheng. Design and implementation of a fully reconfigurable chipless RFID tag using inkjet printing technology. In *IEEE International Symposium on Circuits and Systems, 2008 (ISCAS 2008)*, pages 1524 –1527, may 2008.
- [45] Prasanna Kalansuriya and Nemai Karmakar. Time domain analysis of a backscattering frequency signature based chipless rfid tag. In *Proceedings of the Asia-Pacific Microwave Conference 2011*, pages 183 –186, december 2011.
- [46] S. Preradovic, I. Balbin, N.C. Karmakar, and G.F. Swiegers. Multiresonator-based chipless RFID system for low-cost item tracking. *IEEE Trans. Microwave Theory Tech.*, 57(5):1411 –1419, may 2009.
- [47] Federico Alimenti and Luca Roselli. Theory of zero-power rfid sensors based on harmonic generation and orthogonally polarized antennas. *Progress in Electromagnetics Research*, 134:337 –357, 2013.
- [48] Yuan Shen and Moe Z. Win. Fundamental limits of wideband localization – Part I: A general framework. *IEEE Trans. Inform. Theory*, 56(10):4956–4980, October 2010.

- [49] Chonggang Wang, M. Daneshmand, K. Sohraby, and Bo Li. Performance analysis of RFID generation-2 protocol. *IEEE Transactions on Wireless Communications*, 8(5):2592–2601, 2009.
- [50] ISO 18000 Part 6. Information technology automatic identification and data capture - radio frequency identification for item management air interface. 2003.
- [51] G. De Vita and G. Iannaccone. Design criteria for the rf section of uhf and microwave passive rfid transponders. *Microwave Theory and Techniques, IEEE Transactions on*, 53(9):2978–2990, 2005.
- [52] A. Costanzo, A. Romani, D. Masotti, N. Arbizzani, and V. Rizzoli. Rf/baseband co-design of switching receivers for multiband microwave energy harvesting. *Elsevier Journal on Sensors and Actuators*, 179(1):158 – 168, march 2012.
- [53] A. Romani, M. Filippi, and M. Tartagni. Micro-power design of a fully autonomous energy harvesting circuit for arrays of piezoelectric transducers. *IEEE Trans. Power Electron.*, in press.
- [54] M. Dini, M. Filippi, A. Romani, V. Bottarel, G. Ricotti, and M. Tartagni. A nano-power energy harvesting ic for arrays of piezoelectric transducers. SPIE Microtechnologies 2013.
- [55] M. Del Prete. An alternative rectenna design approach for wirelessly powered energy autonomous systems. In *International Microwave Symposium*, 2013.
- [56] Cymbet. Enerchip smart solid state batteries.
- [57] P. et al. Harpe. A 30 fJ/conversion-step 8b 0-to-10ms/s asynchronous sar adc in 90 nm cmos. In *Proceedings of the IEEE Int. Solid-State Circ. Conf.*, pages 388 –389, 2010.
- [58] Z. et al. Fu. Nano-watt silicon-on-sapphire adc using 2c-1c capacitor chain. *Electronics Letters*, 42(6), 2006.
- [59] Texas Instruments Web Site, MSP430 16 bit microcontroller family.
- [60] Texas Instruments, MSP430FR58xx and MSP430FR59xx Family UserâŽs Guide.
- [61] Microchip, PIC Microcontrollers with eXtreme Low Power technology.
- [62] S. et al. Hanson. A low-voltage processor for sensing applications with picowatt standby mode. *IEEE J. Solid-State Circuits*, 44(4), april 2009.
- [63] F. Fuschini, C. Piersanti, F. Paolazzi, and G. Falciasecca. Analytical approach to the backscattering from uhf rfid transponder. *Antennas and Wireless Propagation Letters, IEEE*, 7:33–35, 2008.
- [64] J.D. Griffin and G.D. Durgin. Complete link budgets for backscatter-radio and rfid systems. *Antennas and Propagation Magazine, IEEE*, 51(2):11–25, 2009.
- [65] A. De Angelis, M. Dionigi, R. Giglietti, and P. Carbone. Experimental comparison of low-cost sub-nanosecond pulse generators. *Instrumentation and Measurement, IEEE Transactions on*, 60(1):310–318, 2011.
- [66] D. Dardari, R. D'Errico, C. Roblin, A. Sibille, and M.Z. Win. Ultrawide bandwidth rfid: The next generation? *Proceedings of the IEEE*, 98(9):1570–1582, 2010.
- [67] B. Gomez, G. Masson, P. Villard, G. Robert, F. Dehmas, and J. Reverdy. A 3.4mb/s rfid front-end for proximity applications based on a delta-modulator. In *Solid-State Circuits Conference, 2006. ISSCC 2006. Digest of Technical Papers. IEEE International*, pages 1211–1217, 2006.

- [68] A. Vaz, H. Solar, I. Rebollo, I. Gutierrez, and R. Berenguer. Long range, low power uhf rfid analog front-end suitable for batteryless wireless sensors. In *Microwave Symposium Digest (MTT), 2010 IEEE MTT-S International*, pages 836–839, 2010.
- [69] J. Meyer, Quang Huy Dao, and B. Geck. Design of an analog frontend for a 5.8 ghz rfid transponder. In *Microwave Conference Proceedings (APMC), 2012 Asia-Pacific*, pages 1043–1045, 2012.
- [70] U. Karthaus and M. Fischer. Fully integrated passive uhf rfid transponder ic with 16.7- mu;w minimum rf input power. *Solid-State Circuits, IEEE Journal of*, 38(10):1602–1608, 2003.
- [71] G. De Vita, F. Bellatalla, and G. Iannaccone. Ultra-low power {PSK} backscatter modulator for {UHF} and microwave {RFID} transponders. *Microelectronics Journal*, 37(7):627 – 629, 2006.
- [72] Y. Yao, Jie Wu, Yin Shi, and F.F. Dai. A fully integrated 900-mhz passive rfid transponder front end with novel zero-threshold rf-dc rectifier. *Industrial Electronics, IEEE Transactions on*, 56(7):2317–2325, 2009.
- [73] D. Vinko, T. Svedek, and D. Zagar. Rectifier and modulator architecture in passive rfid transponders. In *Circuits and Systems for Communications (ECCSC), 2010 5th European Conference on*, pages 169–172, 2010.
- [74] Jong-Wook Lee, Duong Huynh Thai Vo, Quoc-Hung Huynh, and Sang-Hoon Hong. A fully integrated hf-band passive rfid tag ic using 0.18- cmos technology for low-cost security applications. *Industrial Electronics, IEEE Transactions on*, 58(6):2531–2540, 2011.
- [75] S.J. Thomas, E. Wheeler, J. Teizer, and M.S. Reynolds. Quadrature amplitude modulated backscatter in passive and semipassive uhf rfid systems. *Microwave Theory and Techniques, IEEE Transactions on*, 60(4):1175–1182, 2012.
- [76] Chi Xu and ChoiL Law. Toa estimator for uwb backscattering rfid system with clutter suppression capability. *EURASIP Journal on Wireless Communications and Networking*, 2010(1):753129, 2010.
- [77] D. Deslandes and Ke Wu. Integrated microstrip and rectangular waveguide in planar form. *IEEE Microwave and Wireless Components Letters*, 11(2):68–70, 2001.
- [78] D. Deslandes, M. Bozzi, P. Arcioni, and Ke Wu. Substrate integrated slab waveguide (sisw) for wideband microwave applications. In *Microwave Symposium Digest, 2003 IEEE MTT-S International*, volume 2, pages 1103–1106 vol.2, 2003.
- [79] Feng Xu and Ke Wu. Guided-wave and leakage characteristics of substrate integrated waveguide. *IEEE Transactions on Microwave Theory and Techniques*, 53(1):66–73, 2005.
- [80] D. Deslandes and Ke Wu. High isolation substrate integrated waveguide passive front-end for millimeter-wave systems. In *Microwave Symposium Digest, 2006. IEEE MTT-S International*, pages 982–985, 2006.
- [81] M. Bozzi, A. Georgiadis, and K. Wu. Review of substrate-integrated waveguide circuits and antennas. *Microwaves, Antennas Propagation, IET*, 5(8):909–920, 2011.
- [82] Ramesh Garg, Inder Bahl, and Maurizio Bozzi. *Microstrip Lines and Slotlines, Third Edition*. Artech House, 2013.
- [83] M. Bozzi, M. Pasian, L. Perregini, and Ke Wu. On the losses in substrate integrated waveguides. In *European Microwave Conference 2007*, pages 384–387, 2007.

- [84] M. Bozzi, L. Perregrini, and Ke Wu. Modeling of conductor, dielectric, and radiation losses in substrate integrated waveguide by the boundary integral-resonant mode expansion method. *IEEE Transactions on Microwave Theory and Techniques*, 56(12):3153–3161, 2008.
- [85] Ke Wu. Towards system-on-substrate approach for future millimeter-wave and photonic wireless applications. In *Asia-Pacific Microwave Conference 2006 (APMC 2006)*, pages 1895–1900, 2006.
- [86] Zhaolong Li and Ke Wu. 24-ghz frequency-modulation continuous-wave radar front-end system-on-substrate. *IEEE Transactions on Microwave Theory and Techniques*, 56(2):278–285, 2008.
- [87] Maurizio Bozzi, Dominic Deslandes, Paolo Arcioni, Luca Perregrini, Ke Wu, and Giuseppe Conciauro. Efficient analysis and experimental verification of substrate-integrated slab waveguides for wideband microwave applications. *International Journal of RF and Microwave Computer-Aided Engineering*, 15(3):296–306, 2005.
- [88] M. Bozzi, S. A. Winkler, and K. Wu. Broadband and compact ridge substrate-integrated waveguides. *Microwaves, Antennas Propagation, IET*, 4(11):1965–1973, 2010.
- [89] D. Harrison, E. Billett, and J. Billingsley. Novel circuit fabrication techniques for reduced environmental impact. In *International Conference on Clean Electronics Products and Technology 1995 (CONCEPT)*, pages 174–175, 1995.
- [90] D.E. Anagnostou, A.A. Gheethan, T. Amert, and K.W. Whites. A low-cost wlan green pifa antenna on eco-friendly paper substrate. In *IEEE Antennas and Propagation Society International Symposium 2009 (APSURSI '09)*, pages 1–4, 2009.
- [91] D.E. Anagnostou, A.A. Gheethan, A.K. Amert, and K.W. Whites. A direct-write printed antenna on paper-based organic substrate for flexible displays and wlan applications. *Journal of Display Technology*, 6(11):558–564, 2010.
- [92] J.C. Batchelor, E.A. Parker, J.A. Miller, V. Sanchez-Romaguera, and S. G. Yeates. Inkjet printing of frequency selective surfaces. *Electronics Letters*, 45(1):7–8, 2009.
- [93] J. Siden, M. K. Fein, A. Koptyug, and H.-E. Nilsson. Printed antennas with variable conductive ink layer thickness. *IET Microwaves, Antennas Propagation*, 1(2):401–407, 2007.
- [94] Li Yang and M.M. Tentzeris. 3d multilayer integration and packaging on organic/paper low-cost substrates for rf and wireless applications. In *International Symposium on Signals, Systems and Electronics 2007 (ISSSE '07)*, pages 267–270, 2007.
- [95] M.M. Tentzeris. Novel paper-based inkjet-printed antennas and wireless sensor modules. In *IEEE International Conference on Microwaves, Communications, Antennas and Electronic Systems, 2008. COMCAS 2008*, pages 1–8, 2008.
- [96] A. Rida, Li Yang, R. Vyas, and M.M. Tentzeris. Conductive inkjet-printed antennas on flexible low-cost paper-based substrates for rfid and wsn applications. *IEEE Antennas and Propagation Magazine*, 51(3):13–23, 2009.
- [97] V. Lakafosis, A. Rida, R. Vyas, Li Yang, S. Nikolaou, and M.M. Tentzeris. Progress towards the first wireless sensor networks consisting of inkjet-printed, paper-based rfid-enabled sensor tags. *Proceedings of the IEEE*, 98(9):1601–1609, 2010.
- [98] G. Shaker, Safieddin Safavi-Naeini, N. Sangary, and M.M. Tentzeris. Inkjet printing of ultrawide-band (uwb) antennas on paper-based substrates. *IEEE Antennas and Wireless Propagation Letters*, 10:111–114, 2011.

- [99] Li Yang, G. Orecchini, G. Shaker, Ho-Seon Lee, and M.M. Tentzeris. Battery-free rfid-enabled wireless sensors. In *2010 IEEE MTT-S International Microwave Symposium Digest (MTT)*, pages 1528–1531, 2010.
- [100] R. Vyas, V. Lakafosis, A. Rida, N. Chaisilwattana, S. Travis, J. Pan, and M.M. Tentzeris. Paper-based rfid-enabled wireless platforms for sensing applications. *IEEE Transactions on Microwave Theory and Techniques*, 57(5):1370–1382, 2009.
- [101] Li Yang, A. Rida, R. Vyas, and M.M. Tentzeris. Rfid tag and rf structures on a paper substrate using inkjet-printing technology. *IEEE Transactions on Microwave Theory and Techniques*, 55(12):2894–2901, 2007.
- [102] M.M. Tentzeris. Inkjet-printed paper-based rfid and nanotechnology-based ultrasensitive sensors: The green ultimate solution for an ever improving life quality and safety? In *2010 IEEE Radio and Wireless Symposium (RWS)*, pages 120–123, 2010.
- [103] A. Traillé, L. Yang, A. Rida, V. Lakafossis, and M.M. Tentzeris. Novel miniaturized antennas for rfid-enabled sensors. In *2009 IEEE Sensors*, pages 912–915, 2009.
- [104] T. Bjoérninen, S. Merilampi, L. Ukkonen, P. Ruuskanen, and L. Sydanheimo. Performance comparison of silver ink and copper conductors for microwave applications. *IET Microwaves, Antennas Propagation*, 4(9):1224–1231, 2010.
- [105] R. Moro, M. Bozzi, Sangkil Kim, and M. Tentzeris. Novel inkjet-printed substrate integrated waveguide (siw) structures on low-cost materials for wearable applications. In *Microwave Conference (EuMC), 2012 42nd European*, pages 72–75, 2012.
- [106] R. Moro, M. Bozzi, Sangkil Kim, and M. Tentzeris. Inkjet-printed paper-based substrate integrated waveguide (siw) components and antennas. *International Journal of Microwave and Wireless Technologies*, 2013.
- [107] S. Kim B. Cook T. Le J. Cooper H. Lee V. Lakafosis R. Vyas R. Moro M. Bozzi A. Georgiadis A. Collado and M. Tentzeris. Inkjet-printed antennas, sensors and circuits on paper substrate. *IET Microwaves, Antennas and Propagation*, 2013.
- [108] Li Yan, Wei Hong, Guang Hua, Jixin Chen, Ke Wu, and Tie-Jun Cui. Simulation and experiment on siw slot array antennas. *IEEE Microwave and Wireless Components Letters*, 14(9):446–448, 2004.
- [109] R.S. Elliott. An improved design procedure for small arrays of shunt slots. *IEEE Transactions on Antennas and Propagation*, 31(1):48–53, 1983.
- [110] D. Deslandes and Ke Wu. Substrate integrated waveguide leaky-wave antenna: Concept and design considerations. In *Proc. Asia-Pacific Microwave Conference 2005*, pages 346–349, 2005.
- [111] Guo Qing Luo, Zhi Fang Hu, Lin Xi Dong, and Ling-Ling Sun. Planar slot antenna backed by substrate integrated waveguide cavity. *IEEE Antennas and Wireless Propagation Letters*, 7:236–239, 2008.
- [112] J.C. Bohorquez, H.A.F. Pedraza, I.C.H. Pinzon, J.A. Castiblanco, N. Pena, and H.F. Guarnizo. Planar substrate integrated waveguide cavity-backed antenna. *IEEE Antennas and Wireless Propagation Letters*, 8:1139–1142, 2009.
- [113] M.H. Awida and A.E. Fathy. Substrate-integrated waveguide ku-band cavity-backed 2x2 microstrip patch array antenna. *IEEE Antennas and Wireless Propagation Letters*, 8:1054–1056, 2009.

- [114] F. Giuppi, A. Georgiadis, A. Collado, M. Bozzi, and L. Perregrini. Tunable siw cavity backed active antenna oscillator. *Electronics Letters*, 46(15):1053–1055, 2010.
- [115] F. Giuppi, A. Georgiadis, A. Collado, and M. Bozzi. A compact, single-layer substrate integrated waveguide (siw) cavity-backed active antenna oscillator. *Antennas and Wireless Propagation Letters, IEEE*, 11:431–433, 2012.
- [116] Hao Wang, Da-Gang Fang, Bing Zhang, and Wen-Quan Che. Dielectric loaded substrate integrated waveguide (siw) h-plane horn antennas. *IEEE Transactions on Antennas and Propagation*, 58(3):640–647, 2010.
- [117] X. Y. Wu and P.S. Hall. Substrate integrated waveguide yagi-uda antenna. *Electronics Letters*, 46(23):1541–1542, 2010.
- [118] O. Kramer, T. Djerafi, and Ke Wu. Very small footprint 60 ghz stacked yagi antenna array. *IEEE Transactions on Antennas and Propagation*, 59(9):3204–3210, 2011.
- [119] Yu Jian Cheng, Wei Hong, and Ke Wu. Design of a monopulse antenna using a dual v-type linearly tapered slot antenna (dvltsa). *IEEE Transactions on Antennas and Propagation*, 56(9):2903–2909, 2008.
- [120] Alessandra Costanzo. Energy autonomous systems: future trends in devices, technologies and systems. In *RF MST workshop, Otranto*, june 2010.
- [121] J. A. Hagerty, F. B. Helmbrecht, W. H. McCalpin, R. Zane, and Z. B. Popovic. Recycling ambient microwave energy with broad-band rectenna arrays. *IEEE Trans. Microwave Theory Tech.*, 52(3):1014 –1024, march 2004.
- [122] H. J. Visser and R. J. M. Vullers. Wireless sensors remotely powered by rf energy. In *Proc. 6th EUCAP*, pages 1 –4, march 2012.
- [123] Kin-Lu Wong. *Planar Antennas for Wireless Communications*. january 2003.
- [124] B. Wang and A. Chen. Design of an archimedean spiral antenna. In *8th International Symposium on Propagation and EM Theory*, pages 348 –351, november 2008.
- [125] W. Wiesbeck, G. Adamiuk, and C. Sturm. Basic properties and design principles of uwb antennas. *Proceedings of the IEEE*, 97(2):372 –385, february 2009.
- [126] V. Rizzoli and D. Masotti. *Lezioni di Sistemi d'Antenna*. november 2011.
- [127] M. C. Buck and D. S. Filipovic. Spiral cavity backing effects on pattern symmetry and modal contamination. *IEEE Antennas Wireless Propagat. Lett.*, 5(1):243 –246, December 2006.
- [128] F. Yang and Y. Rahmat-Samii. Reflection phase characterizations of the ebg ground plane for low profile wire antenna applications. *IEEE Trans. Antennas Propagat.*, 51(10):2691 –2703, october 2003.
- [129] H. Nakano, K. Kikkawai, N. Kondo, Y. Iitsuka, and J. Yamauchi. Low-profile equiangular spiral antenna backed by an ebg reflector. *IEEE Trans. Antennas Propagat.*, 57(5):1309 – 1318, may 2009.
- [130] A. E. Yilmaz and M. Kuzuoglu. Design of the square loop frequency selective surfaces with particle swarm optimization via the equivalent circuit model. *Radioengineering*, 18(2):95 – 102, June 2009.

- [131] Harry L. Van Trees. *Detection, Estimation, and Modulation Theory*. John Wiley & Sons, Inc., New York, NY 10158-0012, first edition, 1968.
- [132] Moe Z. Win, Andrea Conti, Santiago Mazuelas, Yuan Shen, Wesley M. Gifford, Davide Dardari, and Marco Chiani. Network localization and navigation via cooperation. *IEEE Commun. Mag.*, 49(5):56–62, May 2011.
- [133] F. Gustafsson, F. Gunnarsson, N. Bergman, U. Forssell, J. Jansson, R. Karlsson, and P.-J. Nordlund. Particle filters for positioning, navigation, and tracking. *IEEE Trans. Signal Processing*, 50:425–437, February 2002.
- [134] M.S. Arulampalam, S. Maskell, N. Gordon, and T. Clapp. A tutorial on particle filters for online nonlinear/non-gaussian bayesian tracking. *IEEE Trans. Signal Processing*, 50:174–188, February 2002.
- [135] K. Ito and Kaiqi Xiong. Gaussian filters for nonlinear filtering problems. *IEEE Trans. Automat. Contr.*, pages 910–927, August 2002.
- [136] S.J. Julier and J.K. Uhlmann. Unscented filtering and nonlinear estimation. *Proc. IEEE*, 92:401 – 422, March 2004.
- [137] A. Gning, B. Ristic, L. Mihaylova, and F. Abdallah. An introduction to box particle filtering [lecture notes]. *Signal Processing Magazine, IEEE*, 30(4):166–171, 2013.
- [138] M.S.I.M. Zin and Martin Hope. A review of uwb mac protocols. In *Telecommunications (AICT), 2010 Sixth Advanced International Conference on*, pages 526–534, 2010.
- [139] A. Bachir, M. Dohler, T. Watteyne, and K.K. Leung. Mac essentials for wireless sensor networks. *Communications Surveys Tutorials, IEEE*, 12(2):222–248, 2010.
- [140] Guner D. Celik, Gil Zussman, Wajahat F. Khan, and Eytan Modiano. Mac for networks with multipacket reception capability and spatially distributed nodes. *IEEE Transactions on Mobile Computing*, 9(2):226–240, 2010.
- [141] N. Riaz and M. Ghavami. Analytical performance evaluation of ultra-wideband multiple access schemes for different wireless sensor network application environments. *Communications, IET*, 3(9):1473–1487, 2009.
- [142] Jue Wang, Haitham Hassanieh, Dina Katabi, and Piotr Indyk. Efficient and reliable low-power backscatter networks. In *Proceedings of the ACM SIGCOMM 2012 conference on Applications, technologies, architectures, and protocols for computer communication*, SIGCOMM ’12, pages 61–72, New York, NY, USA, 2012. ACM.
- [143] Qing Ling, Gang Wu, and Zhi Tian. Denoising and error correction in wireless sensor networks. In *Information Fusion (FUSION), 2010 13th Conference on*, pages 1–8, 2010.
- [144] YuKai Li, Yan Bai, Jian Zhang, and Yanbo Cui. A reliable delivery protocol based on competition and cooperation for wireless sensor networks. In *Advanced Computer Control (ICACC), 2010 2nd International Conference on*, volume 4, pages 194–198, 2010.
- [145] P. Mary, I. Fijalkow, and C. Pouliat. Time slot allocation for tdma/cdma th-uwb ad-hoc networks. In *Signal Processing Advances in Wireless Communications (SPAWC), 2010 IEEE Eleventh International Workshop on*, pages 1–5, 2010.
- [146] Fang Bao, Rong Hu, Ruigai Li, and Lianglun Cheng. Principles and implementation challenges of cooperative transmission for realistic wsn. In *Signal Processing Systems (ICSPS), 2010 2nd International Conference on*, volume 2, pages V2–334–V2–338, 2010.

- [147] Christian Floerkemeier and Matthias Lampe. Rfid middleware design: addressing application requirements and rfid constraints. In *Proceedings of the 2005 joint conference on Smart objects and ambient intelligence: innovative context-aware services: usages and technologies*, sOc-EUSAI '05, pages 219–224, New York, NY, USA, 2005. ACM.
- [148] Emanuele Goldoni and Paolo Gamba. Prism: a novel protocol for real-time synchronous acquisitions in wsns. *International Journal of Sensors, Wireless Communications and Control (JSWCC)*, 1(2):1–8, 2011.
- [149] J. Essel, D. Brenk, J. Heidrich, and R. Weigel. A highly efficient uhf rfid frontend approach. In *IEEE MTT-S Int. Microw. Workshop on Wireless Sensing, Local Positioning, and RFID, Croatia*, june 2009.
- [150] V. Rizzoli, A. Costanzo, and G. Monti. General electromagnetic compatibility analysis for nonlinear microwave integrated circuits. In *IEEE MTT-S Int. Microwave Symp. Digest, Fort Worth*, june 2004.
- [151] ETSI EN 302 208-1 V1.1.2. Electromagnetic compatibility and radio spectrum matters (erm); radio frequency identification equipment operating in the band 865 mhz to 868 mhz with power levels up to 2 w. In *European standard*, march 2006.
- [152] ETSI EN 300 440-1 V1.5.1. Electromagnetic compatibility and radio spectrum matters (erm); short range devices; radio equipment to be used in the 1 ghz to 40 ghz frequency range. In *European standard*, march 2009.